IN -71

P. 92

NASA Contractor Report 4695

Airframe Noise Prediction Evaluation

Kingo J. Yamamoto, Michael J. Donelson, Shumei C. Huang, and Mahendra C. Joshi

October 1995

NASA Contractor Report 4695

Airframe Noise Prediction Evaluation

Kingo J. Yamamoto, Michael J. Donelson, Shumei C. Huang, and Mahendra C. Joshi
McDonnell Douglas Aerospace • Long Beach, California

TABLE OF CONTENTS

Abstract

The objective of this study is to evaluate the accuracy and adequacy of current airframe noise prediction methods using available airframe noise measurements from tests of a narrow body transport (DC-9) and a wide body transport (DC-10) in addition to scale model test data. General features of the airframe noise from these aircraft and models are outlined. The results of the assessment of two airframe prediction methods, Fink's and Munson's methods, against flight test data of these aircraft and scale model wind tunnel test data are presented. These methods were extensively evaluated against measured data from several configurations including clean, slat deployed, landing gear deployed, flap deployed, and landing configurations of both DC-9 and DC-10. They were also assessed against a limited number of configurations of scale models. The evaluation was conducted in terms of overall sound pressure level (OASPL), tone corrected perceived noise level (PNLT), and one-third-octave band sound pressure level (SPL).

Introduction

Inlet fan and airframe have been known to be dominant noise sources of aircraft in landing approach. However, with advances in fan noise control through low noise fan design, advanced acoustic liners or active noise control, reducing airframe noise is projected to be increasingly important.

The relative importance of airframe noise is more significant for larger aircraft. The NASA Advanced Subsonic Technology - Noise Reduction Program has established a goal of 4 dB reduction in airframe noise.

Among several components which contribute to airframe noise generation, flap trailing edge, flap side edge, slat trailing edge, and main gear assembly are regarded as the most important noise sources. Since most of the noise from these sources is basically of a diffracted dipole type whose intensity is proportional to the fifth power of the air speed, it is obvious that reducing aircraft speed at approach is the most effective way to mitigate airframe noise. This reduction in aircraft approach speed can be realized by use of advanced high-lift devices and improved wing designs. However, this approach represents a major design change to the existing aircraft configuration, so additional reduction techniques must be developed.

Existing airframe noise prediction models, a key design tool for developing noise reduction techniques, are still immature. Those prediction models are heavily dependent upon the empiricism, and therefore, inherently subject to the Reynolds number issue, unless the models are developed exclusively based on full scale flight test data. In addition, none of them explicitly addresses the flap side edge noise which is believed to be one of the most important airframe noise components. Another area of airframe noise whose noise generation mechanism is not well established is interaction between components. Interaction of main gear with trailing flaps is one example.

The objective of the present study is to evaluate the accuracy and adequacy of current airframe noise prediction methods using available airframe noise measurements from tests of a narrow body transport (DC-9) and a wide body transport (DC-10), in addition to the scale model tests as documented in literature.

This report first outlines the DC-9/DC-10 flight test programs and the major characteristics of airframe noise from these aircraft, followed by a brief discussion on the scale model test data. Then, the methodologies of two airframe noise prediction models are discussed. An extensive evaluation of those prediction models against full-size and scale model test data is presented in the following section. Finally, accuracy and limitations of the models are summarized in the conclusion section. Figure 1.1 shows a sketch of the DC-9 and DC-10 flap systems.

2. Flight Test Data

In the present study two flight test data bases of airframe noise were employed - DC-10-10 flight test data and DC-9-31 flight test data. In this section a brief discussion on the flight test programs and acoustic characteristics of the airframe noise from these aircraft will be presented.

2.1 DC-9-31 Flight Test Data

The airframe noise flight test with a DC-9-31 was conducted in December 1975 at Yuma, Arizona. Flyover noise measurements were made for several combinations of flap deflection, landing gear position, slat position and aircraft speed with the aircraft at flight idle-power settings. The configurations and flight conditions are given in Table 2. A series of microphones were located under the flight path. The acoustic data used for the analysis of the present study were recorded with a flush-mounted ground microphone located under the flight path.

The DC-9 airframe noise data presented here are corrected for engine noise. The contributions of the fan and turbine blade passing frequency (BPF) and its higher harmonics are removed from the one-third-octave band spectra. However, its subharmonics are not removed. Since the data are extensively evaluated in terms of tone corrected perceived noise level (PNLT) in the present study, presence of any extraneous noise of high frequencies in the data would lead us to erroneous conclusions. A more detailed description of the test program can be found in Reference 1.

The data were analyzed in terms of OASPL and PNLT directivities, and one-third-octave SPL. The data were normalized with respect to airspeed, aircraft height and air absorption. For aircraft height, the certification approach height of 394 ft was selected, and the air absorption was calculated based on the standard weather conditions using ARP 866. The reference speed was arbitrarily selected from the measured airspeeds of the runs in concern. For the normalization of airspeed, a 50 LOG scaling law was used. The validity of this scaling law was confirmed with an entire set of DC-9 data as is shown in Figure 2.1.

Acoustic Data Repeatability: Before analyzing the data, its repeatability was determined to evaluate data quality. Figures 2.2 through 2.4 illustrate the data repeatability for the clean configuration. It is noted that the data for Runs 7 and 11 are close to each other, but Run 9 is as much as 4 dB higher than these two runs in the aft quadrant. As noted in Figure 2.4, the SPL for Run 9 is higher than that for Runs 7 or 11 over a wide range of frequency. The airspeed for Run 9 was 203 kts, lowest among the three. The RPM of the first stage fan was almost equal among these runs, approximately 3880, corresponding blade passing frequency (BPF) being 800 Hz. The spectra shown in Figure 2.4 (90°) have local peaks at 800 Hz (BPF) and 400 Hz (first subharmonic).

Airframe Noise Characteristics: In this subsection, some features of the airframe noise from DC-9 are discussed. Figure 2.5 through 2.7 illustrate angle of attack (α) effects on airframe noise for landing (approach) configurations in which slat, landing gears and 50° flap were deployed. The angle of attack effects were investigated in OASPL

and PNLT directivities as well as in one-third-octave band spectra at 60°, 90° and 120°. The angle of attack varies for these runs as -3.8 <α< -1.7. Since the range of variation in α is not large, it may not be possible to identify any systematic trend of angle of attack effect. However, it may be said, based on the results of these figures, that the lowest SPL corresponds to the smallest α.

Next, how deployment of slat affects noise for the clean configuration is investigated. Figures 2.8 through 2.10 illustrate a comparison of airframe noise between clean and slat deployed configurations. In those figures, Run 9 is for clean configuration, while Run 10 corresponds to slat-only-deployed configuration. The airspeed is almost identical for these runs - 203 kts. We note here a significant noise increase due to the deployment of slat. The noise increase is particularly significant in the forward quadrant in both OASPL and PNLT directivities, showing a typical half-baffled dipole directivity pattern. The spectra given in Figure 2.10 (60°) show that Run 10 has much higher SPL over the entire frequency range depicted in this figure.

Next, slat and gear effect on the airframe noise for flaps retracted and the landing gear deployed configuration is studied in Figures 2.11 through 2.13. In these figures, three configurations are shown: clean (Run 11), landing gear deployed (Run 16), and slat and landing gear deployed (Run 22) configurations. It is interesting to note that deployment of slat does not change the noise level for the landing gear deployed configuration except in the aft quadrant where slat deployment somehow reduces noise over a wide range of frequency by 2-3 dB as seen in Figure 2.13 (120°).

Figures 2.14 through 2.16 illustrate landing gear effect on the airframe noise for the flap deployed configuration. Run 27 is for the slat and 50° flap deployed configuration, while Run 20 is for the slat, landing gear and 50° flap deployed configuration. As is illustrated in Figure 2.14, there seems no difference between these runs when compared in terms of OASPL. However, when compared in terms of PNLT, a significant difference is noted as seen in Figure 2.15. As will be discussed in a later section, the identical trend prevails with DC-10 data. -

How the deployment of the trailing edge flap affects airframe noise from the slat deployed configuration is next investigated in Figures 2.17 through 2.19. Run 10 is for the slat-only-deployed configuration, whereas Run 23 is for the slat and 40° flap deployed configuration. It is noted that the deployment of flap and/or slat significantly increases airframe noise in terms of OASPL over the entire emission angle as indicated in Figure 2.17. However, in terms of PNLT, flap does not increase noise in the forward quadrant. This can be checked with Figure 2.19 (60°).

In this figure, SPL spectra measured at 60° are compared for these configurations. It is noted that for mid-to-high frequencies the difference is negligibly small. This fact is reflected upon the PNLT directivity at this emission angle. In the aft quadrant, however, effect of flap deployment is remarkably high. The SPL spectrum for Run 23 is as much as 3 to 5 dB higher then Run 10 over the entire frequency range of interest, and 10-20 dB above the clean configuration.

In Figures 2.20 through 2.22 the effect of flap deflection angle on airframe noise is illustrated. In those figures, Run 15 is for the slat and 20° flap deployed configuration,

and Run 27 is for the slat and 50° flap deployed configuration. Increasing flap deflection angle increases noise nearly equally over the wide range of emission angle in terms of OASPL. However, PNLT for Run 27 is much higher at certain emission angles of either forward or aft quadrant than at flyover direction. At 120°, for example, Run 27 is approximately 8 PNdB higher than Run 15.

Finally, order of magnitude of noise levels from several source components is investigated in Figures 2.23 through 2.25. The configurations considered in these figures include clean, slat only, landing gear only, slat plus landing gear plus 40° flap, and slat plus landing gear plus 50° flap configurations. In terms of OASPL, as noted in Figure 2.23, the landing configuration with 50° flap is the nosiest followed by the landing configuration with 40° flat. Gear noise is higher than slat noise for the emission angles less than 140°. When plotted in terms of PNLT, the order has changed. Now, the landing configuration with 40° flap is noisier than the landing configuration with 50° flap at shallow emission angles. At this point, no explanation is available to address this unexpected result.

2.2 DC-10-10 Flight Test Data:

The flight test with a DC-10-10 was conducted in November, 1973 at the test site in Yuma, Arizona. The engine nacelles of the aircraft was specially treated for this test to reduce propulsive noise as much as possible. The test consisted of 17 flyovers recorded on 8 microphones located at various distances from the flight path. The test was conducted for several configurations including clean, flaps down and gear up, and flaps and gear both down. The leading edge slat was automatically deployed when flaps were deflected. Flight speed was varied from approximately 280 ft/s (166 kts) to approximately 320 ft/s (190 kts). Most tests were conducted with engines at flight idle setting. Table 2 summarizes the test conditions. All the acoustic data used for the analysis of the present study were recorded by a flush-mounted ground microphone located under the flight path.

The DC-10 airframe noise data presented here are corrected as was done for DC-9 data, for engine noise. The contributions of the fan and turbine blade passing frequency (BPF) and its higher harmonics are removed from the one-third-octave band spectra. However, its subharmonics are not removed. A more detailed description of this test program is found in Reference 2.

All the data presented in this section were normalized, unless otherwise mentioned, for airspeed, height and air absorption in he same manner as for DC-9 data. The 5th power law was used for the velocity dependence and the inverse square law was applied for the height.

Acoustic Data Repeatability: Figures 2.26 through 2.31 are presented to illustrate data repeatability of DC-10 airframe noise flight test data. Figures 2.26 through 2.28 are for the clean configuration, while Figures 2.29 through 2.31 correspond to the landing configuration. As noted in these figures, data repeatability is excellent with the exception of the very high frequency bands. Both directional and spectral characteristics are well repeated though the aircraft-to-microphone distance varies significantly among the runs depicted in those figures.

5

<u>Airframe Noise Characteristics:</u> The noise characteristics from two major airframe noise sources - gear and flap - are briefly discussed here. A more detailed discussion on the noise characteristics of DC-10 data will be given in a later section. Figure 2.32 through 2.34 illustrate effects of flap deflection angle on airframe noise. The selected configurations for this investigation were slat, landing gear and 35° flap deployed configuration, and slat, landing gear and 50° flap deployed configuration. As noted in Figure 2.32, Run 4 for 50° flap has higher OASPL than Run 3 for 35° flap over the emission angle range less than approximately 120°. However, plotted in terms of PNLT, as seen in Figure 2.33, it may not be possible to identify correlation, if any, between flap deflection angle and corresponding noise level. Based on the PNLT directivities for Run 3 and Run 4 shown in this figure, we can assume EPNL being almost identical for these two runs. If we take a look at corresponding SPL spectra shown in Figures 2.34, we note that Run 4 has generally higher SPL than Run 3 for low to mid frequencies. However, in the PNL calculation a few dB difference in SPL of this frequency range does not change its value. This is the reason why we don't see any noteworthy difference in PNLT directivity between these two runs.

Figures 2.35 through 2.37 illustrates contributions of landing gear to the total airframe noise. In these figures, Run 7 is for the configuration with 35° flap and slat deployed, while Run 14 corresponds to the configuration with 35° flap, slat and landing gear deployed. Figure 2.35 presents OASPL directivities for these runs. We would be tempted to think from this figure that Run 14 with landing gear deployed is noisier than Run 7 with landing gear up. However, the PNLT directivities presented in Figure 2.36 give an opposite result. Apparently, EPNL calculated based on these PNLT directivities is higher for Run 7 with landing gear up than that for Run 14 with landing gear deployed. A similar trend is noted in the DC-9 data (see Figures 2.14 through 2.16). If this is due to a favorable interaction between landing gear and flap, the implication of using PNLT directivity in airframe noise analysis would be significant. With only OASPL directivity available, we would be misled to think that the gear-down configuration is noisier than gear-up configuration. It should be noted that DC-10-10 has two flaps, and the inboard flap is positioned right behind the four-wheeled main gear. When the gear is deployed, deflected inboard flap is generally in the wakes caused by cavity and gear. It has been believed that this wake-flap interaction generally increases noise (Ref. 3). This conclusion is mostly based on laboratory tests with isolated models. However, actual flow field for such a large transport aircraft could be significantly different from that for an idealized, simple, isolated model. Therefore, the conclusions based on laboratory tests may not always be applied to full-size airplanes. It could be said that, if this favorable interaction is real, the inboard flap is a more important noise source than the outboard counterpart for DC-10; while for DC-9, the portion of flap right behind the main landing gear is a more important source of airframe noise.

3. Scale Model Test Data

Airframe noise data from the scale models are very limited in open literature. Furthermore, important configuration information is often missing in the literature. Because of this, quantitative assessment of the data found in open literature is generally not possible. In the present study, data from the B-737 (Ref. 4) and B-747 (Ref. 5) scale model tests were evaluated.

3.1 B-737 Scale Model Test Data

A 5% B-737 scale model was tested in the anechoic flow facility at the Naval Ship Research and Development Center (Ref. 5). Although the tunnel background noise of the facility is reasonably low, because of rather small size of the model, airframe noise for the clean configuration was not measurable. The airframe noise data reported in Ref. 5 are limited, therefore, to the data from the 'dirty' configurations-either flap or gear or both flap and gear deployed. It should be noted that in this test when the main gears were deployed the wheel doors were left open and the wheel cavity was exposed to the flow.

The data evaluated herein were obtained by a microphone located at the flyover position, 3 meters from the model. Figure 3.1 shows the OASPL variation with the tunnel speed. The authors of Ref. 4 reported a V^6 dependency. One-third octave SPL spectra of airframe noise for three configurations are presented in Figure 3.2. We can summarize the features of airframe noise from this model as follows: First, the landing gear generates more noise than the flap. Secondly, gear noise appears to be discrete tones. Thirdly, the peak frequency increases when both gear and flap are deployed. The first feature cannot be compared with either DC-9 or DC-10 data, since in their flight tests slat was always deployed when flap was extended. Regarding to the second feature, the landing gear cavity was always closed for a DC-9 and DC-10 flight test. Therefore, the observed noise for landing gear deployed configuration could be significantly different from each other between the B-737 model and DC-9/DC-10. Third feature again cannot be confirmed with DC-9 or DC-10 data because of deployed slat when flap was extended.

Figure 3.3 represents narrowband SPL spectra supplementing to Figure 3.2. Note that the discrete tones are reduced by the deflection of flap while the broadband noise is increased. Sound radiation from the cavity is considered to be caused either by impingement of flow over the forward edge of a cavity or impingement of separated flow on the aft edge of the cavity or volumetric flow fluctuations across the cavity mouth (Ref. 3). As pointed out in Reference 3, under certain conditions cavities can produce very high intense discrete tones, and these conditions are governed by several factors including cavity's length-depth ratio. To avoid these conditions, the wheel doors should be closed in the landing configuration. The result of Figure 3.3 suggests importance of the narrowband analysis for a better understanding of noise generation mechanism.

3.2 B-747 Scale Model Test Data

Reference 5 presents results from airframe noise measurements of a 3% scale model of B-747 in the same anechoic facility as the B-737 model was tested. As in the case of B-737, airframe noise from the clean configuration of B-747 was not detectable because of rather high background noise levels. In this section, the analysis is, therefore, limited to the 'dirty' configurations.

One-third-octave SPL spectral comparisons are shown in Figure 3.4 for three configurations: flap only, slat only, and both flap and slat. The flap deflection angle was 30°. The tunnel speed was 50 m/s (97 kts). The data was recorded by the microphone at flyover position. From the comparison between flap only and slat only configurations, it is noted in the frequency range lower than approximately 10 kHz (full scale frequency 300 Hz) slat deployed configuration is noisier than 30 flap. In this frequency range, the spectra for both configurations are almost flat. The spectra start to fall off after approximately 6 kHz (full scale frequency 180 Hz). There is no DC-9 or DC-10 data available which can be used for direct comparison with the results of Figure 3.4. In these aircraft, when flaps are deployed, slat is automatically deployed, and, therefore, flap only (no slat deployed) configuration is not possible. When both flap and slat are deployed, according to Figure 3.4, the total noise level generally exceeds the logarithmic sum of flap and slat noise, indicating unfavorable interactions between flap and slat.

Figure 3.5 illustrates SPL spectra for gear noise, slat and flap noise and airframe noise for the landing configuration. First, we note that the gear generates low frequency noise. Secondly, we observe that the noise level for the landing configuration is almost identical to the for the slat and flap configuration. This corresponds to Figure 2.16 for DC-9 where landing gear effects on airframe noise from the flap and slat deployed configuration are illustrated. There, we note no significant difference between Run 20 and Run 27. However, if the data are analyzed in terms of PNLT, we may see some differences between these runs. The analysis presented in this section shows that the interaction effects among the airframe noise sources may be favorable in some cases and unfavorable in others. Because of this rather complicated nature of airframe noise generation mechanism, the component approach to airframe noise prediction must be extended so that the interaction effects are appropriately addressed.

4. Airframe Noise Prediction Models

Several airframe noise prediction models have been developed in the past. Because of complexity of airframe noise generation mechanism, their methodologies are, without exception, heavily dependent on empiricism. These models can be categorized into two groups based on the analysis method: the total noise model and the component noise model. The former does not differentiate the noise sources in an aircraft but regard the entire aircraft as a single source. The models in the latter category, on the other hand, calculate noise contributions from each component source and then add up those contributions on an energy basis to define the total airframe noise for a given aircraft.

In the present study, two airframe noise prediction models were selected for evaluation, one from each category. They are the Munson model and the Fink model. In the following a brief discussion on their methodologies is presented.

4.1 Munson Model

The Munson model (Ref. 2)is a total noise prediction model developed at McDonnell Douglas. It has been generally accepted that the airframe noise is mainly generated by the fluctuating lift acting upon airframe surfaces. This fluctuating lift has a half-baffled dipole directivity, its peak radiation direction being-baffled determined by $\cos^2(\theta/2)$. Together with the convective amplification term, this term gives an OASPL directivity profile which has a peak in the forward quadrant. Munson tested this concept against the DC-10 flight test data, and found that the measured OASPL directivity has an almost symmetrical profile with respect to the overhead direction.

To solve this inconsistency, he introduced a lift and drag dipole concept. He assumed that the Lighthill stress tensor which is responsible for noise generation by unsteady forces consists of both lift and drag fluctuations, and developed the following equation to account for the airframe noise by these unsteady forces:

$$p^2 = \frac{(1 - M\cos\theta)^{-4}}{16\pi a_0^2 R^2}(\cos^2\theta(\frac{\delta F_1}{\delta t})^2 +$$

$$2\sin\theta\cos\theta\frac{\delta F_1}{\delta t}\frac{\delta F_3}{\delta t} + \sin^2\theta(\frac{\delta F_3}{\delta t})^2)$$

where R is the aircraft-to-monitor distance, and F1 and F3 respectively correspond to the lift and drag forces. The flight Mach number is designated as M.

The first term in the braces is a drag dipole and the third term represents a lift dipole. The second term is present only if there is any degree of correlation between the lift forces and the fluctuating drag forces. Upon rewriting this in terms of dB, he derived the following equation which contains three unknown numerical coefficients:

$$OASPL = 10 \log \left(\frac{V^6}{16\pi^2 a_0^2 (1 - M_r)^4 R^2} (K_L \sin^2 \theta + \right.$$

$$\left. K_D \cos^2 \theta + K_{LD} \sin\theta\cos\theta) \right).$$

where Mr = M cosθ. Munson derived an analogous expression for the one-third octave band SPL which can be written as

$$SPL = 10 \text{Log} \left(\frac{V^6}{16\pi^2 a_0^2 (1 - M_r)^4 R^2} (F_L \sin^2 \theta + F_D \cos^2 \theta + F_{LD} \sin\theta\cos\theta) \right)$$

The numerical constants, $K_L, K_D, K_{LD}, F_L, F_D, F_{LD}$ should be determined by means of curve-fitting against measured data. It may now be possible to obtain a symmetric directivity profile by using appropriate numerical coefficients. A major drawback of this model, as Munson admits, is that these coefficients are not universal constants but vary from one configuration to another. Because of this drawback, the applicability of this model may be limited.

4.2 Fink Model:

The most widely used model among the existing airframe noise models is the one developed by Fink (Ref. 6). This model falls in the category of the component method in which wing trailing edge noise, flap trailing edge noise, noise due to the landing gears, and noise from the leading edge slat are independently calculated based on an extensive data base. Cavity (of gear-well) noise and interaction effects between noise generating components are not addressed in this model. ANOPP has adopted this model as AIRFRAME NOISE MODULE (Ref. 7). A brief discussion on the prediction methodology of this model will be given in the following section. The discussion is limited to the wing trailing edge noise and flap trailing edge noise.

4.2.1 Wing Trailing Edge Noise: For the cruise configuration when all the high-lift devices and landing gears are retracted, the wing is the major airframe noise source. This configuration is often called as "clean " configuration. The convection of the turbulent boundary layer past the trailing edge of wing is believed to be responsible for the airframe noise from the clean configuration. In this model, it is assumed that the turbulent length scale which determines the peak frequency is the turbulent boundary

layer thickness. It also assumes that the directivity function incorporated in this model is aligned with the so-called half-baffled dipole.

The equation for the far-field sound pressure level for a given Strouhal frequency, s is given by

$$SPL = C + 10Log\left(\frac{M^5\delta}{R^2}\right)\left(\frac{D(\theta,\phi)}{(1-M\cos\theta)^4}F(s)\right)$$

$$D(\theta,\phi) = 4\cos^2\phi\cos^2\theta/2$$

$$s = \frac{f\delta b}{Mc}(1-M\cos\theta),$$

where C is a numerical constant, M flight mach number, θ polar angle, Φ azimuthal angle, D is a directivity function, δ the boundary layer thickness, and F(s) a spectrum function which is given in Figure 4.1. The boundary layer thickness is computed from the standard flat-plate turbulent boundary layer model and b represents the wing span. Because of the directivity function D and the convective amplification factor, the wing trailing edge noise preferably radiates in the forward quadrant directions. Just as Munson's model, Fink assumes a fifth-power dependency on airspeed. To compute the boundary layer thickness the mean aerodynamic chord (MAC) is used as a representative chord length.

4.2.2. Flap Trailing Edge Noise: In Fink's model, the flap trailing edge noise is assumed to be produced by the lift fluctuations due to the incident turbulence on the flaps. The model also assumes that the noise is aligned with the lift dipole of the deflected flap. As in the case of the wing trailing edge noise, the boundary layer thickness at the trailing edge is assumed to determine its frequency characteristics.

The equation for the far-field sound pressure level for a given frequency, s is, then, given by

$$SPL = C + 10Log\,(M^6 A\frac{Sin^2\delta}{b^2})(\frac{D(\theta,\phi)}{R^2(1-Mcos\theta)})F(s)$$

$$D(\theta,\phi) = 3(\sin\delta\cos\theta + \cos\delta\sin\theta\cos\phi)^2$$

$$s = \frac{fA}{Mbc}(1-Mcos\theta)$$

In the first equation, A is flap area, δ flap deflection angle, b flap span, R aircraft-to-monitor distance, C numerical constant. The directivity function $D(\theta, \Phi)$ is defined in the second equation. F(s) is the spectrum function which is empirically determined and given in Figure 4.2. The Strouhal number, s for the flap trailing edge noise is defined using the flap chord as the reference length as shown in the third equation.

We note several major differences between the wing and flap trailing edge noise. First, the fifth power law is applied to the wing, while the flap trailing edge noise is assumed to increase in proportion to the sixth power of the airspeed. The directivity of the flap trailing edge noise depends on the flap deflection angle in addition to the polar and azimuth angles. This means that with an increase of the flap deflection the peak radiation angle shifts to larger forward quadrant angles.

5. Assessment of Prediction Models

In this section, the capabilities of two airframe noise prediction models will be assessed against DC-9/DC-10 test data and model test data. Assessment of the prediction models against model test data is presented in Appendix A.

The assessment will be performed in terms of SPL, OASPL and PNLT. The airframe configurations considered in this assessment are: a) clean configuration, b) slat deployed, c) gear deployed, d) flap deployed, and e) landing configuration, wherever corresponding data are available. For part of the illustrations presented in this section, only Fink's model is compared with data. This is because the coefficients factors that appeared in Munson's formulation (see Section 4.1) are defined for only certain configurations.

As discussed in Section 2, DC-9/DC-10 flight test data are to some extent contaminated by tones generated by the inlet fan and turbine. The DC-9/DC-10 data used in this section for comparison, however, are corrected for these tones. This is necessary, since data-to-prediction comparison will be made not only in terms of OASPL but also in terms of PNLT. In the PNLT calculation, high frequency extraneous tones are often highly weighted, and, consequently, resulting PNLT could be entirely different from those for contamination-free airframe noise. However, tones in lower frequencies have not been removed, and, therefore, care should be exercised when those data are interpreted. In some charts, effective perceived noise level (EPNL) is given to show how it varies with the predictions when applied for the certification noise estimate.

5.1 Predictions Versus DC-9 Data

Clean configuration: In Fink's model, the wing trailing edge is regarded as a major noise source for the clean configuration. As previously discussed, the convection of the turbulent boundary layer past the wing trailing edge is assumed to be the generation mechanism of the trailing edge noise. The noise intensity is assumed to be proportional to the turbulent boundary layer thickness which is, in turn, proportional to the 0.8th power of the wing chord. It also assumes the half-baffled dipole directivity for the radiation of this type of noise. The airframe noise for the clean configuration is usually very difficult to measure with a small scale model in wind tunnel, mainly because of a poor signal to noise ratio. At this point, no reliable laboratory test data for the clean configuration is available. Because of this reason, the flight test data such as DC-9/DC-10 data are very valuable.

As was discussed in Section 4.2, Munson's method includes several numerical coefficients which are to be empirically determined. The coefficients of the Munson model which is evaluated here have been defined using the DC-10 (wide-body) airframe noise flight test data (Ref. 2). Accordingly, it is logical to expect a good agreement between data and Munson's prediction when applied to DC-10 data. Therefore, our main interest in this section is to determine how the model agrees with the DC-9 (narrow-body) airframe noise data.

Figure 5.1 illustrates an OASPL directivity comparison between DC-9 data and prediction. Apparently, the data has a symmetric directivity profile with respect to the

flyover direction (θ=90°), while the prediction by Fink has a peak in the forward quadrant. This is due to the half-baffled dipole directivity characterized by square of $\cos(\theta/2)$ and the convective amplification. Prediction by Munson has a better agreement, since it includes the drag dipole directivity in addition to the lift dipole. However, the prediction by Munson is approximately 3 dB higher at flyover direction. Figure 5.2 shows corresponding PNLT directivities for data and predictions. Here, it is noted that Fink is better in the forward quadrant than Munson. But discrepancy of Fink's prediction with the data is significant in the aft quadrant, where the predicted level is below the measured level by 10-15 dB aft of 120°. As much as 6 dB overprediction by Munson is observed at 90°. This can be explained from the results of Figure 5.3 where SPL spectra are compared between data and predictions. As noted in the figure for 90°, the agreement between Munson and data is fairly good for mid to high frequencies where noise is heavily weighted in PNL calculations. It is ironical that EPNL for Fink's prediction is very close to the measured value in spite of large discrepancy in the aft quadrant as noted in Figure 5.2. This should be, however, regarded as fortuitous. The local peak at 400 Hz in Figure 5.3 is for the first sub-harmonic of the BPF of fan noise. If we remove this tone, SPL spectral profile would become virtually flat in the low-to-mid frequency range. So, it is hard to locate the peak for airframe noise from the measured data. We also note a Doppler-shift for this tone in Figure 5.3.

We may summarize the assessment of Fink and Munson models against clean configuration as follows: Fink tends to overpredict in low-to-mid frequency range and underpredict the high frequency, while Munson model overpredicts the entire frequency range. Although both models predict a local peak, the measured data virtually doesn't have a peak and its spectral profile is fairly flat. What is needed for a better prediction, therefore, is correlation of frequency where spectrum begins to fall off, and the fall-off slope, with the key flow and geometric parameters. An accurate prediction in the 1 - 4 KHz range is most important as it relates to aircraft noise certification metrics (i.e. PNLT/EPNL).

Slat Deployed Configuration:

Figures 5.4 through 5.6 illustrate prediction versus data comparisons for the slat deployed configuration of DC-9. In these comparisons, only Fink's model is evaluated. In Fink's model the slat is assumed to produce noise in the same manner as the wing trailing edge. As discussed in the previous section, the slat noise is assumed to consist of enhanced wing trailing edge noise and slat trailing edge noise. Fink also assumed that the noise intensity is the same for both noise components. As noted in Figure 2.10, slat deployment increased noise over a wide range of frequency. The slat has a much smaller length scale associated with the slat noise generation, and, therefore, slat noise should be higher in high frequencies as compared with that for clean configuration.

Figure 5.4 illustrates an OASPL directivity comparison. It is noted that predicted OASPL directivity is much lower than measured counterpart over the entire emission angle, the discrepancy being larger with increasing emission angle.

14

Corresponding PNLT directivity comparison presented in Figure 5.5, however, is somewhat different. Here, we note a good agreement in the forward quadrant; with agreement in the aft quadrant being as poor as in that in Figure 5.4. Just as in Figure 5.2, EPNL predicted by Fink is very close to that measured as shown in Figure 5.5. However, as indicated in the spectra of Figure 5.6, this is fortuitous.

In Fink's model the slat trailing edge noise is assumed to have a higher peak frequency than the "added" wing trailing edge noise; this is because that the slat is assumed to have a chord which is 15% of that of wing. Therefore, the combined spectrum for the slat deployed configuration has a higher peak frequency than that for the clean configuration (see Figure 5 of Reference 7).

Figure 5.6 illustrates spectral comparisons for Fink's model. As noted in this figure, Fink underpredicts for the frequencies lower than approximately 1250 Hz at θ =60°, and the dividing frequency shifts to higher frequencies with increasing emission angle.

The normalized spectrum used in Fink's model for slat deployed noise is about 2 dB higher than that for clean configuration up to the peak and then the difference drastically increases with frequency (see Figure 20 of Reference 6). However, as noted in Figure 2.10 (θ=90°) where noise from the slat deployed configuration is compared with the clean configuration, the trend is just opposite; difference between slat and clean configurations decreases with frequency.

We can summarize the results from prediction vs. data comparisons for the slat deployed configuration as follows:

- Fink model significantly underpredicts slat noise, the discrepancy being larger in the aft quadrant. This trend is noted in both OASPL and PNLT directivities.

- The normalized spectrum for slat noise assumed in the model appears to be inadequate.

Landing Gear Deployed Configuration:

Figures 5.7 through 5.9 presents prediction versus data comparisons for the landing gear deployed configuration. Again, only Fink's prediction is available. Figure 5.7 illustrates an OASPL directivity comparison. We note overprediction by 3 to 6 dB by Fink over the entire emission angle range, though the general directivity profile is well predicted. Figure 5.8 shows a similar comparison for PNLT directivity. Here, we note a better agreement between prediction and data. It may be useful to examine the reason for this by checking spectra presented in Figure 5.9. It appears that Fink overpredicts for low-to-mid frequencies but agreement is fairly good for higher frequencies. This results in the more accurate correlation with PNLT directivity.

In Fink's model, the landing gear noise is predicted separately for wheel noise and strut noise. However, the strut noise is not significant at the monitor under the flight path because of its directivity which is strongest in the plane normal to the strut axis. Since the DC-9 data used in the present study were recorded by a flash-mounted

ground microphone located under the flight path, we may think that the data shown here consist of only wheel produced noise.

The directivity function assumed in Fink's model has a typical dipole directivity which is symmetric with respect to $\theta =90°$. As noted in Figure 5.7, however, the peak OASPL is slightly off from the flyover direction, indicating convective amplification. One of the reasons which may explain the overestimate by Fink's model is that while the DC-9 data are normalized for airspeed by a 5th-power law, the prediction assumes a 6th-power dependence (Eq. 20 of Ref. 7). As illustrated in Figure 2.11, the landing gear deployed configuration is almost 8 to 10 dB noisier than the clean configuration, indicating gear noise dominance over wing trailing edge noise. Then, one is tempted to use the 6th-power law, which is empirically derived based on isolated lading gear tests, to address the characteristics of airframe noise for the landing gear deployed configuration. However, since the acoustic environment in the vicinity of the landing gear system of full size aircraft, especially large transport aircraft, is much more complex than that for the landing gear system usually employed in laboratory tests, scaling of the laboratory data to full size configuration may not always simulate the real situation with an acceptable accuracy.

The results of the assessment of the landing gear noise prediction model can be summarized as follows:

- The predicted OASPL directivity profile agrees with the measured one, but Fink over predicts the level over the entire emission angle. This may be related to the sixth-power dependence on airspeed implemented in the model.

- Predicted spectrum agrees well for higher frequencies; this contributes to a fairly reasonable PNLT directivity prediction.

Figures 5.10 through 5.12 illustrate Fink versus data comparison against the landing gear and slat deployed configuration. Only difference form Figures 5.7 through 5.9 is the slat deployment. As shown in Section 2, the deployment of slat does not change the noise characteristics of landing gear noise (see Figures 2.11 through 2.13). Predicted OASPL in Figure 5.10 is almost identical to that in Figure 5.7. However, there is slight difference in the PNLT directivity; the discrepancy between Fink and data is larger for the slat and landing gear deployed configuration in the forward quadrant than the gear only deployed configuration. This is due to the poor prediction for high frequencies as indicated in Figure 5.12.

Flap and Slat Deployed Configuration:

The DC-9 and DC-10 flap/slat system is designed to have the slat automatically deployed when the flap is deployed. For this reason, flap-only configuration comparisons are not possible. In this section, we will evaluate Fink and Munson models against the flap and slat deployed configuration of the DC-9. These comparisons have the landing gear retracted.

Figures 5.13 through 5.15 present prediction versus data comparisons for the slat and 20° flap deployed configuration. Figure 5.13 illustrates an OASPL directivity comparison between data and two predictions. We see that the measured directivity is

almost symmetrical; this is correctly predicted by Munson. Fink, on the other hand, gives a typical half-baffled dipole directivity pattern. In Fink's model, the OASPL directivity is assumed to be determined by the directivity factor of

$$D(\theta,\delta) = 3(\sin\delta\cos\theta + \cos\delta\sin\theta)^2,$$

where δ is the flap deflection angle and θ the polar emission angle. This equation is valid for the monitor located directly under the flight path (azimuthal angle = 90°).

In the case of Figure 5.13, the flap deflection angle is 20°. Then, the directivity factor D has a maximum value near = 50° as noted in this figure.

Because of this directivity, Fink shows a significant discrepancy in the aft quadrant. For Munson, difference between measured and predicted values is 3 to 7 dB over a wide range of emission angle. Corresponding PNLT directivity comparisons are presented in Figure 5.14. Here, we note that Munson shows a good agreement. Prediction by Fink, however, is poor. Spectral comparisons between predictions and data are given in Figure 5.15. Based on the results in this figure, we may characterize the spectrum for this configuration as follows: a) spectrum is flat up to approximately 1000 Hz, b) then, it falls off almost linearly, c) the slope of this fall-off is largest at 90° and becomes smaller for smaller or larger emission angles than 90°.

The predicted spectra by Munson appear to be almost flat up to approximately 2500 Hz for 60° and 90°, and beyond this frequency they fall off much more gradually than data. In the case of θ = 120°, however, a local peak is noted at near 1000 Hz. Munson underpredicts for low-to-mid frequencies and overpredicts for higher frequencies, and, in total, the deficit for lower frequencies is fortuitously compensated by the excess for higher frequencies, resulting in a good agreement in PNLT directivity as noted in Figure 5.14.

The prediction by Fink is somewhat different from that by Munson. The spectrum predicted by Fink has a peak at all emission angles, and the peak frequency shifts to a lower frequency with increasing emission angle. This is apparently due to the directivity factor D mentioned above and the Doppler shift. Overprediction for higher frequencies tends to decrease with emission angle, and in the aft quadrant (θ = 120°) it significantly underpredicts.

Figures 5.16 through 5.18 present similar comparisons for slat and 50° flap deployed configuration. Before getting into the assessment of the prediction models against those data, it may be useful to review Figures 2.20 through 2.22 where noise from the 20° flap and 50° flap is comparatively evaluated. As noted in these figures, the OASPL directivity or SPL spectrum has an identical profile for 20° flap and 50° flap, although noise level for 50° flap is much higher than for 20° flap. If an appropriate constant value is added to the spectrum for 20° flap over the entire frequency range, we would be able to construct a spectrum which is closely matches the spectrum for 50° flap.

Figure 5.16 shows an OASPL directivity comparison for Fink and Munson for the slat and 50° flap deployed configuration. The predicted OASPL directivity by Munson is

almost identical shown in Figure 5.13 for 20° flap. However, the predicted OASPL directivity by Fink now has a peak in the aft quadrant. It is difficult to explain the reason for this feature from Fink's methodology, since, according to the directivity factor D, for a larger flap deflection angle a smaller peak emission angle should correspond. Therefore, its peak angle for 50° flap should be smaller than 50° of Figure 5.13 for 20° flap.

Figure 5.17 represents a PNLT directivity comparison for this configuration. As indicated by EPNL, prediction by either model is poor, being significantly underestimated. If we take a look at the results in Figure 5.18, we will see large discrepancy for higher frequencies which are highly weighted in PNL calculation.

Assessment of Fink and Munson models against airframe noise from the slat and flap deployed configuration can be summarized as follows:

- Both models significantly underpredict one-third-octave SPL over the entire frequency range of interest.

- Because of this, significant discrepancy is noted between predicted and measured OASPL and PNLT directivities.

Landing Configuration:

In this section, data-to-prediction comparison of airframe noise for the landing configuration of DC-9 will be presented along with a brief discussion on the interaction effects between flap and landing gear. This section concludes the assessment of Fink and Munson models against DC-9 airframe noise flight test data.

For large aircraft all high-lift devices and both nose and main landing gears are deployed for landing. The high-lift devices include the slat located at the leading edge of the wing and highly deflected flaps. DC-9-30 series aircraft have one double-slotted flap as illustrated in Figure 1.1. This is the only configuration which matters as far as noise certification is concerned.

Figures 5.19 through 5.21 present prediction versus data comparisons of airframe noise for this type of configuration. The DC-9 configuration addressed in these figures has a 50°-deflected flap. The first two charts illustrate OASPL and PNLT directivity, respectively. Note that the measured directivities in those figures are similar to those depicted in Figures 5.16 and 5.17. The difference in configuration between this section and the previous section is that the landing configuration has deployed landing gears in addition to the deployed slat and 50° flap. As previously pointed out landing gear deployment does not affect airframe noise for already slat and highly-deflected-flap deployed configuration. (see Figures 2.35 through 2.37). This implies that if we are able to accurately predict the airframe noise from the configuration in which slat and flap are deployed, we would also be able to predict with an equal accuracy the airframe noise from the landing configuration noise.

Next, we will assess how prediction fares with Fink's model. Comparing Figure 5.19 with Figure 5.16, we note that Fink predicts better for the landing configuration. Especially, the deficiency noted in the forward quadrant (of Figure 5.16) is significantly

reduced. However, this should be regarded as fortuitous. Since Fink tends to highly overpredict landing gear noise as illustrated in Figure 5.7, the predicted landing gear noise increase the total noise, resulting in a better agreement.

A similarly good but fortuitous agreement is observed for Munson in the PNLT directivity of Figure 5.20. Here we see a virtually perfect agreement with the data. With Munson's model it can happen that prediction for the slat and flap deployed configuration is poor, but that for the landing configuration is good. This is because as mentioned in Section 4.1, the numerical constants in the equations which define OASPL and SPL vary from one configuration to another. In other words, those constants should be determined by a curve-fitting against the configuration of interest. Hence, the constants used for the prediction of the case presented in Figure 5.17 are different from those used for the case of Figure 5.20.

If we take a close look at the predicted spectra by Munson in Figure 5.21, we realize that underprediction for low-to-mid frequencies is compensated by overprediction for higher frequencies, yielding a good agreement with the data. Poor agreement for Fink's prediction observed in the aft quadrant of the PNLT directivity (Figure 5.20) is due to significant underestimate for mid-to-high frequencies as illustrated in Figure 2.21 (θ =90° and 120°).

In this section, a brief discussion on the interaction effects on airframe noise will also be presented. There have been documented studies on the interaction effects on total airframe noise (e.g., Ref. 8, Ref. 9). However, reported results often lack consistency, and, therefore, it is difficult to generalize the findings. Probably, Reynolds number effect plays an important role in airframe noise generation, and this prevents us to apply our findings obtained with a certain type or size of aircraft to another.

One example of interaction effects on airframe noise is the flap noise reduction by the deployment of landing gear. This favorable interaction has already been discussed in Section 2 (see Figure 2.15, Figure 2.36 and related discussions). For DC-9, the distance to the leading edge of the fully deployed flap from the gear strut is approximately 3 ft, and the distance to the trailing edge is 6 ft. It is, therefore, quite obvious the flap is in the wakes of strut and/or wheels. Experience has shown that the flow near the trailing edge of flap always stalls when the flap is fully deployed. It is possible, then, to conjecture that the turbulence in the wakes more or less suppresses flow separation, resulting in reduced flap noise. At any rate, this finding is valuable in that the feature is observed for DC-9 as well as DC-10.

The following is the summary of the assessment of Fink and Munson models against DC-9 airframe noise flight test data:

Clean Configuration:

Fink tends to overpredict in low-to-mid frequency range and underpredict at higher frequencies, while Munson model overpredicts over the entire frequency range tested. Although both models predict a local peak, the measured data virtually does not have a peak, and its spectral profile is flat. What we need for better prediction, therefore, is to be able to correlate the frequency where the spectrum begins to fall off, and the fall-

off slope with the key flow and geometric parameters. From a practical view point, accurate prediction in the most audible frequency rage (1 to 4 kHz) really does matter.

Slat Deployed Configuration: (Fink only):

Fink model significantly underpredicts slat noise, the discrepancy being larger in the aft quadrant. This trend is noted in both OASPL and PNLT directivities.

The normalized spectrum for slat noise assumed in the model appears to be inadequate.

Landing Gear Only Deployed and Landing Gear/Slat Deployed Configurations: (Fink only):

The predicted OASPL directivity profile agrees with measured data, but Fink over-predicts over the entire emission angle. This may be related to the sixth-power dependence on airspeed implemented in the model. Predicted spectrum agrees well for higher frequencies, yielding a fairly reasonably good agreement with PNLT directivity.

Flap and Slat Deployed Configuration:

Both models tend to underpredict one-third-octave SPL over the entire frequency range of interest. Because of this, discrepancy is noted between predicted OASPL and PNLT directivities and measured counterparts.

Landing Configuration:

Fink predicts OASPL directivity relatively well, especially in the forward quadrant. Although the numerical constants implemented in the Munson's prediction method were determined based on DC-10 flight test data, Munson gives a fairly good agreement with DC-9 data in terms of PNLT directivity and EPNL.

It is evident in view of the one-third-octave SPL spectra of DC-9 data that the spectral profile is almost flat to a certain frequency if extraneous tones are removed from the spectrum, and, then, SPL falls off almost linearly. It is, therefore, difficult to locate peak frequency, if any, in the spectrum. This is true for any configuration. Because of this we intentionally avoided assessment of the predictability of peak frequency by the prediction models in this section.

5.2 Predictions Versus DC-10 Data

In this section, Fink and Munson prediction models will be assessed against DC-10 airframe noise flight test data. Data-to-prediction comparison will be limited to the following configurations: clean; slat and flap deployed; slat, flap and landing gear deployed (landing) configurations. The comparisons are made based on one-third-octave SPL normalized in the same manner as for the DC-9 data.

Clean Configuration

Figures 5.22 and 5.24 present prediction versus data comparisons for the clean configuration of DC-10. Measured OASPL and PNLT directivities are compared with the predictions by Fink and Munson models in Figure 5.22 and Figure 5.23, respectively. A good agreement is noted for Munson, while a significant discrepancy is observed for Fink in these figures, where Munson predicts within 0.2 EPN dB off flight data as compared to Fink which predicts 8.3 EPN dB below flight data. Fink's prediction shows a directivity patter which has a peak in the forward quadrant; this is partly due to the half-baffled dipole and partly due to the convective amplification. However, the measured directivity of the clean configuration has a peak in the aft quadrant rather than in the forward quadrant that is slightly off from the overhead as noted in Figure 5.22.

Spectral comparisons illustrated in Figure 5.24 show why Fink's prediction for PNLT directivity is poor in the aft quadrant. Fink significantly underpredicts higher frequencies in the aft quadrant, yielding a significantly low PNLT.

A comparison of Munson's prediction between Figure 5.3 (DC-9) and Figure 5.24 (DC-10) suggests that the numerical coefficients implemented in its prediction equations (see Section 4.1) are geometry dependent or more generally Reynolds number dependent. If, therefore, these coefficients can be defined as a function of Reynolds number using an appropriately selected length scale, Munson's model would predict airframe noise well irrespective of aircraft geometry.

Slat and Flap Deployed:

Figures 5.25 to 5.27 present prediction versus data comparisons for the slat and 35° flap deployed configuration. The measured OASPL and PNLT directivities noted in Figures 5.25 and 5.26 have similar profiles to those corresponding to the clean configuration presented in Figures 5.22 and 5.23. However, the major noise source in this case is no longer the wing trailing edge, but rather the flap trailing edge, or possibly flap side-edge.

It should be noted that Fink's prediction is also pretty much the same as that for the clean configuration, showing a typical half-baffled dipole directivity. The observed discrepancy noted for Fink's prediction is generally smaller as compared with the clean configuration. However, the prediction in the aft quadrant is still poor due to a significant underestimate over the entire frequency range, as evidenced in Figure 5.27.

For this configuration, prediction by Munson's model is not as good as it is for the clean configuration. An underestimate over a wide range of emission angle, as noted in figure 5.26, results in a lower EPNL than the measured data by 3.7 EPN dB.

In figure 5.27 (120°) approximately 3 dB difference between prediction by Munson and data is noted over the entire frequency range of interest.

Landing Configuration:

During landing, all high-lift devices are deployed in addition to the landing gear. In this section, two landing configurations are considered; one w th 35° flaps and one with 50° flaps. It should be noted that DC-10-10 has two flaps. The inboard flap is located right behind the main landing gear.

Figures 5.28 through 5.33 present the results of prediction versus data comparisons with the airframe noise data from these configurations. The measured OASPL directivity has a symmetrical profile with respect to the overhead position for both configurations. This feature is also noted for the measured PNLT directivity. Munson predicts OASPL and PNLT directivity fairly well for both configurations as illustrated in Figures 5.28, 5.29, 5.31 and 5.32, with he resulting EPNL being within 1.2 EPN dB.

The predicted OASPL directivity by Fink for the 35° flap deployed configuration, however, has a peak at approximately 50° as noted in Figure 5.28. The same trend prevails with the PNLT directivity. it is interesting to note that in Fink's prediction increasing flap deflection angle from 35° to 50° shifts the peak from 50° to 80° as evidenced by comparing Figure 5.28 and Figure 5.31. Fink assumed that the flap trailing edge noise is aligned with the lift dipole of the deflected flap. Because of this assumption, a larger flap deflection corresponds to a larger emission angle. This can be confirmed by the directivity function defined in Section 4.2.

The EPNL values shown in Figures 5.29 and 5.32 indicate that Munson predicts better for the 50° flap deployed configuration than for the 35° flap configuration. As noted in Figure 5.29, Munson slightly overestimates over the entire emission angle. This is due to slightly higher SPL by Munson for high frequencies as seen in Figure 5.30. An excellent agreement, however, is noted for Munson in the SPL spectra for the 50° flap deployed configuration illustrated in Figures 5.33.

The predicted EPNL by Fink indicates that Fink overestimates for both 35° flap and 50° flap deployed configurations, slightly larger discrepancy corresponding to the latter. This is due to the overprediction by Fink over the entire frequency range observed in the spectra for the emission angles near overhead. (see Figure 5.33 θ =60° and 90°).

The discussions of this section are summarized as follows:

- Airframe noise prediction by Fink is generally better for 'dirty' configurations than clean configuration. The best results were obtained for the landing configuration.

- Munson's model predicts well both overall and spectral characteristics of airframe noise for any configurations considered in this section.

22

6. Conclusions and Recommendations

Two airframe noise prediction methods were evaluated against measured data from full-size and scale model aircraft. These methods are referred to as Fink's and Munson's models. The former is an aircraft component prediction model, while the latter is a total aircraft prediction model.

The analysis of the present study has shown that Fink's method predicts the spectral characteristics of airframe noise from scale model aircraft reasonably well but its prediction against full size data is poor. Fink fails to address landing gear noise against scale model and full size data. This result may indicate Reynolds number dependence of airframe noise.

Munson's model, which was developed based on the DC-10 airframe noise flight test data by means of curve-fitting, predicts the spectral features of airframe noise quite well for all configurations of DC-10 considered in this study. Some discrepancy is noted in terms of OASPL, however, when compared to the data for DC-9, which has a significantly different geometry than that for DC-10. However, the model predicts airframe noise from the landing configuration fairly well, resulting in an accurate EPNL. it should be noted that the landing configuration is the only configuration that matters for the noise certification. In some cases, a seemingly fortuitous agreement is noted for Munson's prediction. However, this situation is inherent in any total aircraft prediction method, and cannot be avoided, and, therefore, Munson's model provides a good tool for noise certification.

To be useful as a design tool, any noise prediction model should be able to address noise characteristics in terms of PNL. This requires an accurate prediction of higher frequencies which are subject to heavy weighting in PNL calculations. For this reason, airframe noise prediction models were evaluated against PNLT directivities of DC-9 and DC-10 data, as well as against OASPL.

As pointed out in the text, a good agreement of OASPL directivity does not always imply a good prediction of PNLT directivity. Since the noise in the most audible frequency range (1000 to 4000 Hz), is more heavily weighted in terms of perceived noisiness, an accurate prediction of SPL in this frequency range is important.

The analysis presented here also shows that the SPL spectrum of airframe noise for any DC-9 configuration is virtually flat from 50 Hz (lowest frequency measured) up to a certain frequency, if extraneous noise is removed. The SPL, then, falls off almost linearly up to approximately 4000 Hz. Beyond that frequency, SPL decays rapidly. The same trend prevails with DC-10 data, but to a less prominent degree.

There are, therefore, three key elements to be considered in constructing a normalized SPL spectrum: amplitude of the flat portion, the frequency at which a linear fall-off starts, and the slope of the fall-off. The non-linear decay portion may be important, but it is difficult to obtain reliable data in this high frequency range, and, therefore, evaluation of prediction models for such high frequencies is often meaningless.

The amplitude of the flat portion must be a function of source dimension and the length scale associated with the configuration of concern. The frequency at which a linear fall-off begins should be defined by a Strouhal number based on local airspeed and length scale. It should be noted, however, that local airspeed may not always be equal to the aircraft speed. It is a function of aircraft atitude and wing geometry. The slope of the linear fall-off was found to vary from one configuration to another, suggesting its dependency on length scale.

From the above discussion it is evident that identification of length scale is by far the most important in developing a component prediction method. This, of course, requires us a good understanding of airframe noise generation mechanisms. The following questions become important: How should Reynolds number effect be implemented in the prediction methodology? Is flap side-edge noise the most dominate noise source? If so, what is the associated length scale? When flow stalls at the flap trailing edge, how should the length scale for flap trailing edge noise be defined? How should the interaction effect between components be implemented in the prediction methodology?

Until these questions are answered, the empirical total aircraft approach may have to be used. However, since this approach is not appropriate as a design tool, continued effort to upgrade current component prediction methodologies is needed.

References:

1. Bauer, A.B., Munson, .G., "Airframe Noise of the DC-9," AIAA 77-1272, 1977

2. Munson, A.G., "A Modeling Approach to Nonpropulsive Noise," AIAA 76-525,1976

3. Hardin, J.C., "Prediction of Airframe Noise," NASA TN D-7821, 1975

4. Shearin, J.G., Block, P.J., "Airframe Noise Measurements and Transport Model In a Quiet Flow Facility," AIAA 75-509, 1975

5. Shearin, J.G., et al., "Model and Full-Scale Large Transport Airframe Noise," AIAA 76-550,1976

6. Fink, M.R., "Airframe Noise Prediction Method," FAA-RD-77-29, 1977

7. Zorumski, W.E., "Aircraft Noise Prediction Program Theoretical Manual," NASA TM 83199,1982

8. Fink, M.R., Shlinker, R.H., "Airframe Noise Component Interaction Studies," J. Aircraft, Vol. 17, No. 2, 1980

9. Grosche, F.R. et al., "Acoustic Wind-Tunnel Measurements with a Highly Directional Microphone," AIAA Journal, Vol. 15, No. 11, 1977

Appendix

Evaluation of Fink's Model Against 3% B-747 Scale Model Test Data:

The Fink model used to evaluate DC-9/DC-10 data is the McDonnell Douglas version which is slightly different from the ANOPP version. The difference is mainly due to coding; the basic prediction methodology is identical. Difficulties were encountered when extending frequency range for use with model test data. Hence, it was decided to use ANOPP instead for the model study. (see Figure A.1)

The scale model test data used in this study is from a 3% B-747 scale model (Reference 5).

Because of its rather small size, airframe noise levels from this model were not high enough to be detected over the tunnel background noise, and, therefore, available data from this model test was limited. For example, data for the clean configuration is unavailable. The data presented here were recorded by a microphone located at the flyover position. The tunnel speed was maintained at 50 m/s (164 ft/s) for all cases reported herein.

Figure A. 2 illustrates a data-to-prediction comparison for the slat deployed configuration in terms of one-third-octave SPL. ANOPP predicts the spectral profile in the higher frequency range fairly well but fails in the mid-to-low frequency range. It appears that the measured spectrum consists of two segments, one in the high frequency region (3150 Hz and higher) and one in the lower frequency region (3150 Hz and lower). The former may be related to the noise generated by the slat itself (in Fink's model its size is assumed to be 15% of wing chord), while the latter corresponds to the "added" wing trailing edge noise (see Section 5.1). In Fink's model, the noise level for these two noise components is assumed to be identical. This assumption may need to be evaluated against other data base.

Figure A. 3 represents a similar comparison for the 30° flap deployed configuration. As noted in Figure A. 2, the noise level for the slat deployed configuration is lower than 65 dB except in the lower frequency range. Therefore, for the slat and flap deployed configuration, most noise is generated by the deflected flap. As discussed in Section 5, data of this figure must include interaction effects between the slat and flap, and, therefore, the total noise level should be lower than the level of the logarithmic sum of the individual noise. Predicted SPL agree with the data within 2 dB except near 2500 Hz, where a dip is noted. Whether this dip is an intrinsic property of the airframe noise from this model, or facility related, or instrumentation related, is not known.

Final comparison is made in Figure A. 5 for the landing configuration. It is interesting to compare the data in this figure with the data of Figure A. 4. From this comparison it is obvious that the airframe noise for the landing configuration is almost identical to the flap generated noise.

The dip noted near 2500 Hz in Figure A. 4 is now recovered to some extent, from probably due to the noise from the landing gear which generally has a peak in the lower frequency region. On the other hand, from the comparison of the predicted

26

spectra, significant overprediction occurs for the landing configuration. Sine the landing configuration includes the landing gears in addition to the slat and flap, this overestimate can be attributed to the inappropriate prediction of landing gear noise. The same trend is seen in Figure 5.16 for the predicted spectrum for the gear deployed configuration of DC-9.

To summarize the discussions of this section it can be said that agreement between ANOPP and the scale model data (B-747) is generally good except in the case when the landing gear is deployed.

During the development process of his prediction model, Fink extensively analyzed B-747 (full size) data and incorporated the results of the analysis into his prediction methodology. In view of this fact, a good agreement can be expected for this configuration. As stated earlier, the flow condition near the gear system of the full-size aircraft is very complex, and, therefore, to scale up (or scale down) the landing gear noise, detailed information about the real flow field in the vicinity of the landing gear system is essential.
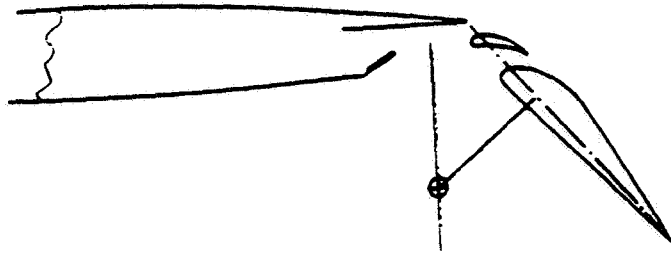
(a)
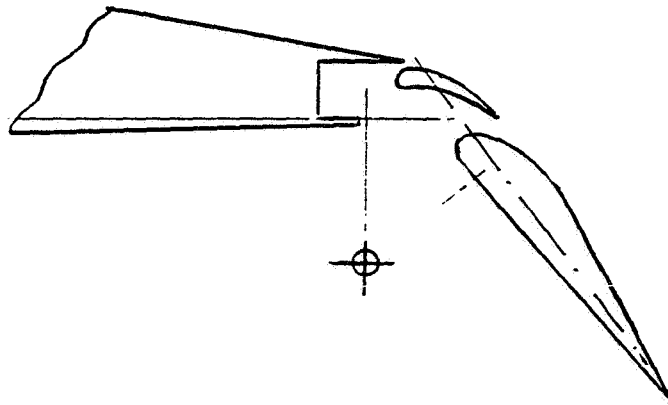
(b)

Figure 1.1   Outboard Flap Section (a) DC-9-31, (b) DC-10-10

28

Table 1   DC-9-31 Flight Test Conditions

RUN	FLIGHT SPEED KTS	GLIDE SLOPE DEGREES	CONFIGURATION		
			SLAT	GEAR	FLAP
3	224	-2.4			
4	223	-2.7			
6	222	-2.6			
7	216	-2.6			
9	211	-3.6			
11	254	-4.4			
17	294	-6.3			
16	215	-6.5		X	
24	290	-12.1		X	
25	295	-13.2		X	
8	175	-3.7	X		
10	208	-4.4	X		
22	251	-8.4	X	X	
13	156	-5.4	X		20
15	182	-7.1	X		20
23	227	-10.7	X		20
26	177	-13.0	X	X	40
27	154	-12.9	X		50
19	177	-13.5	X	X	50
20	157	-12.0	X	X	50
21	159	-13.3	X	X	50

*   'X' indicates deployment of the devise

*   The numbers in the column for flap indicate flap deflection angles

    (from Reference 1)

Table 2   DC-10-10 Flight Test Conditions

RUN	FLIGHT SPEED KTS	GLIDE SLOPE DEGREES	CONFIGURATION		
			SLAT	GEAR	FLAP
1	184	-4.7	X	X	35
2	187	-4.9	X	X	35
3	186	-6.7	X	X	35
4	185	-9.5	X	X	50
5	184	-9.5	X	X	50
7	171	-2.9	X		35
9	169	-3.5	X		35
10	171	-2.8	X		35
11	179	-5.2	X		35
12	178	-5.9	X		35
14	179	-6.4	X	X	35
15	176	-4.9	X	X	35
16	175	-5.0	X	X	35
17	190	-3.3	X		
19	177	-2.7	X		
20	168	-6.2	X	X	50
21	165	-6.1	X	X	50

* 'X' indicates deployment of the devise

* The numbers in the column for flap indicate flap deflection angles

(from Reference 2)
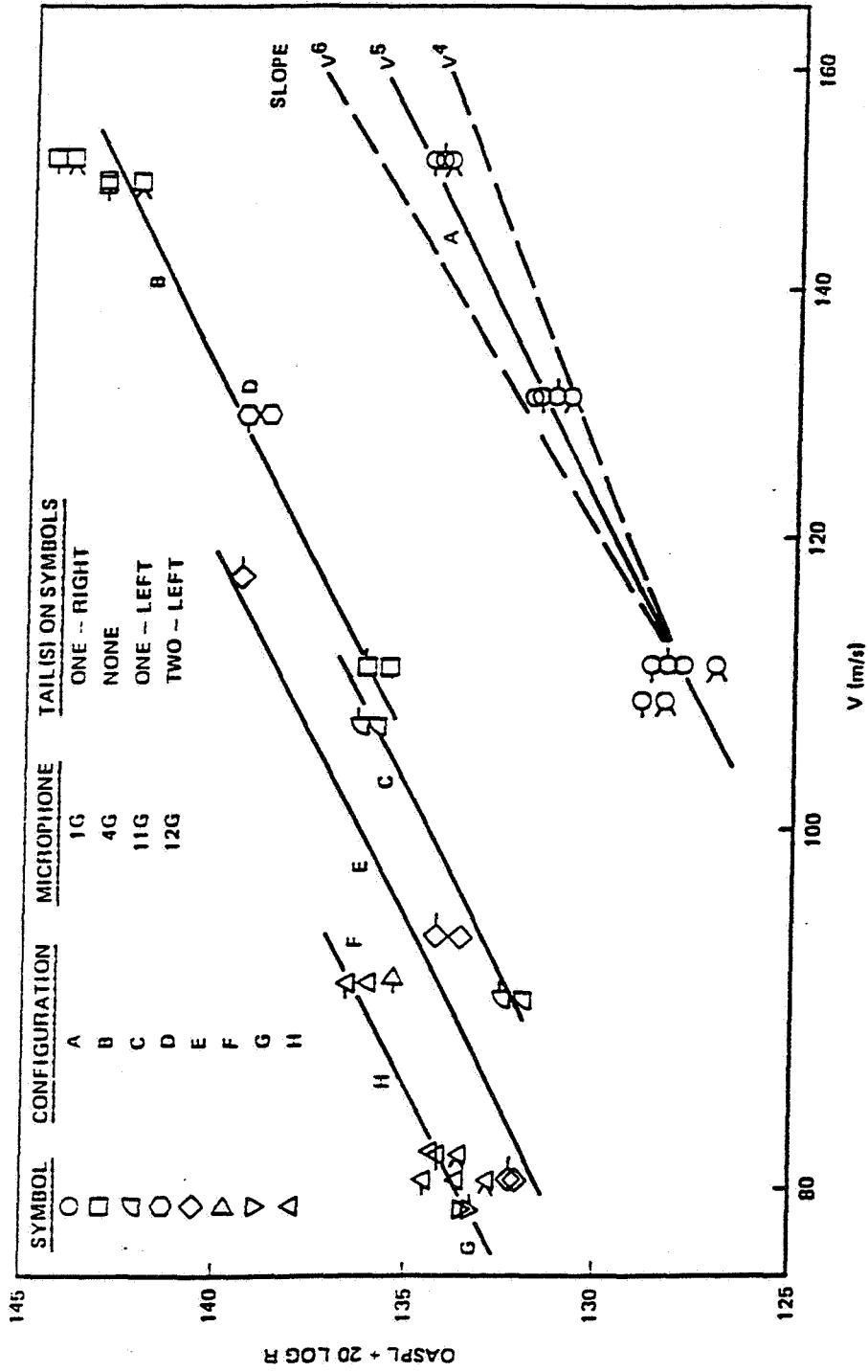
FIGURE 2.1 MEASURED OASPL'S CORRECTED FOR WIND SPEED, ATMOSPHERIC ABSORPTION, AND SPHERICAL DIVERGENCE, AIRPLANE OVERHEAD ($\mu \approx 90$ DEG)

(Bauer, A.B., Munson, A.G., "Airframe Noise of the DC-9," AIAA 77-1272, 1972)

31
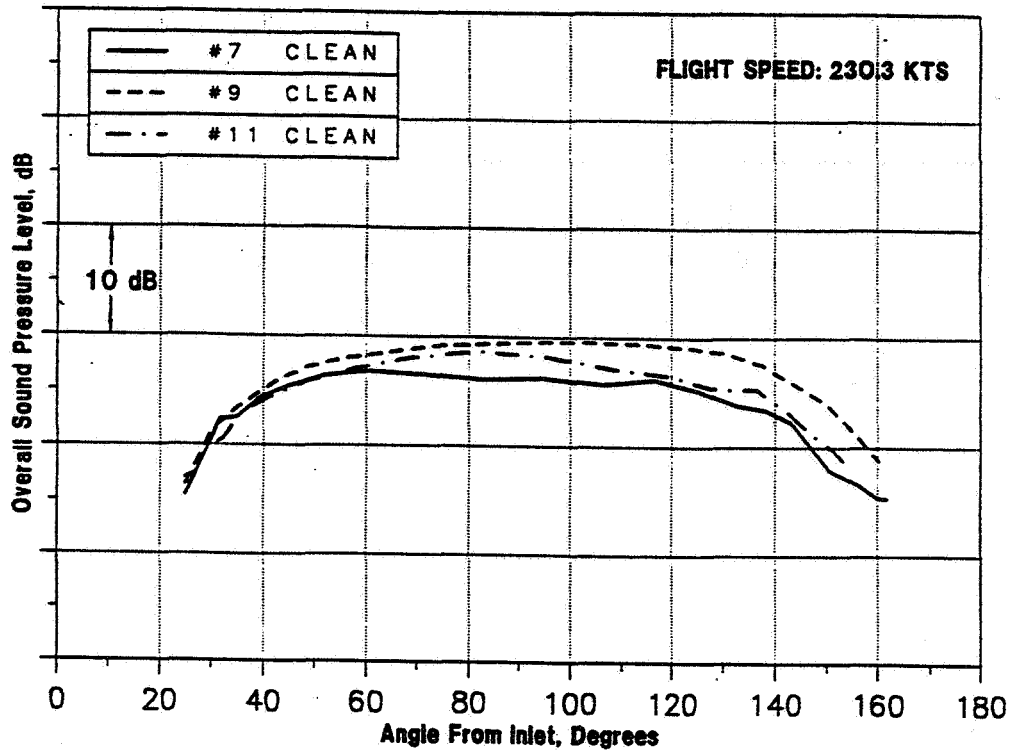
Figure 2.2 DC-9-30 Flight Test: OASPL Directivity to illustrate Data Repeatability: Clean Configuration
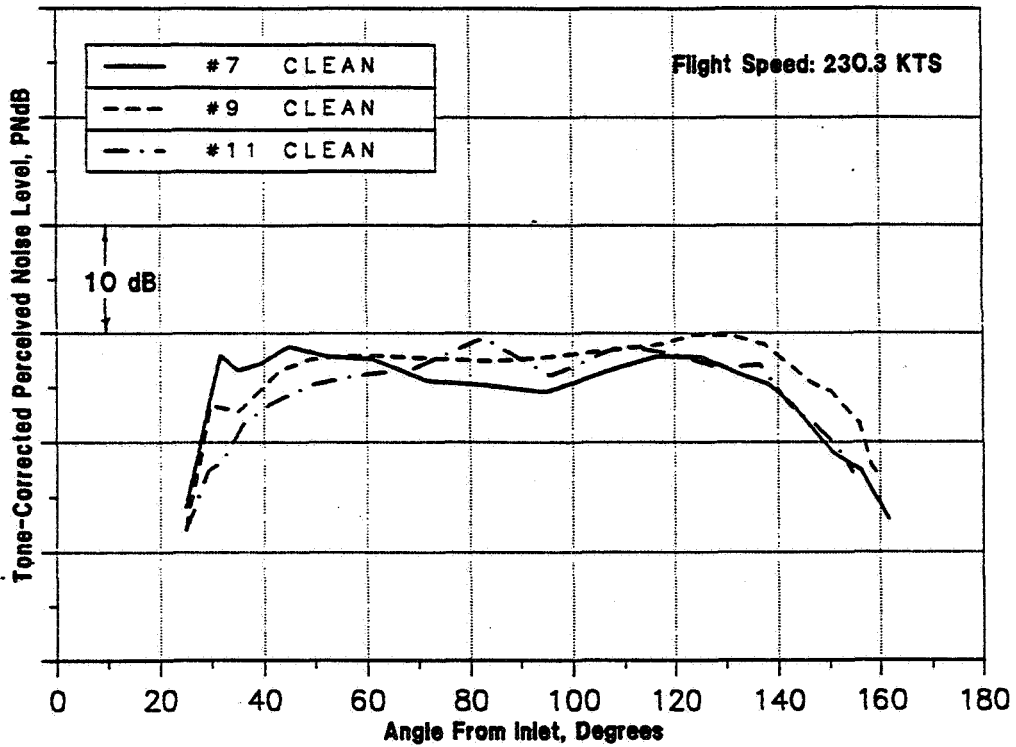
Figure 2.3 DC-9-30 Flight Test: PNLT Directivity to illustrate Data Repeatability: Clean Configuration
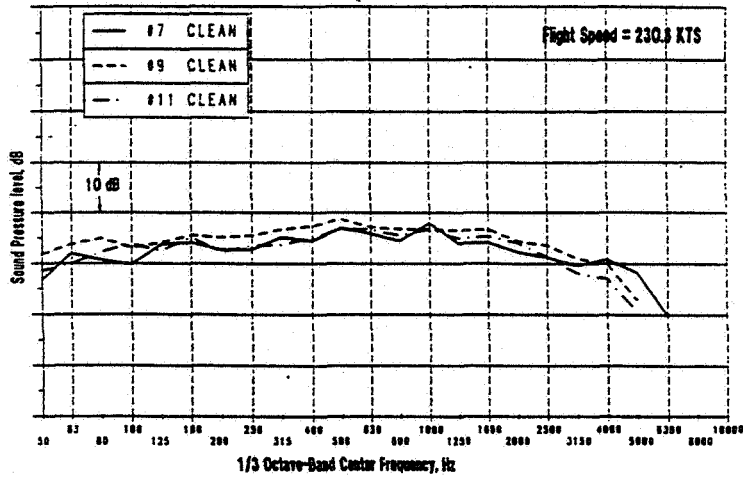
Figure 2.4 DC-9-30 Flight Test: One-Third-Octave SPL To Illustrate Data
Repeatability: Clean Configuration, 60 Degrees
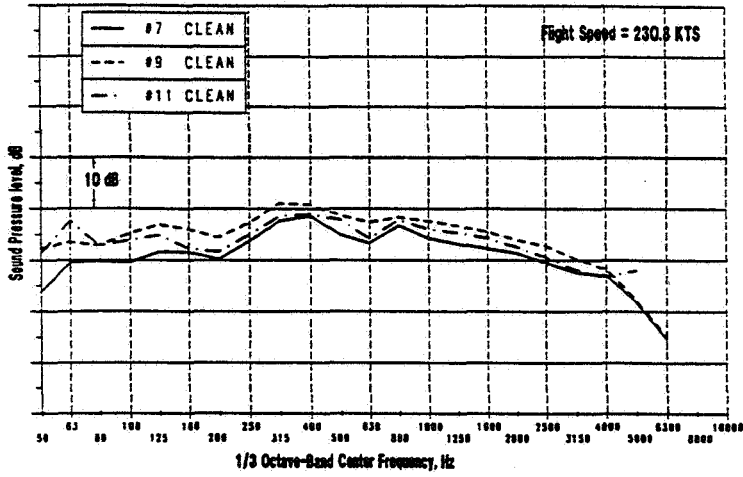
Figure 2.4 (continued) DC-9-30 Flight Test: One-Third-Octave SPL To Illustrate Data
Repeatability: Clean Configuration, 90 Degrees
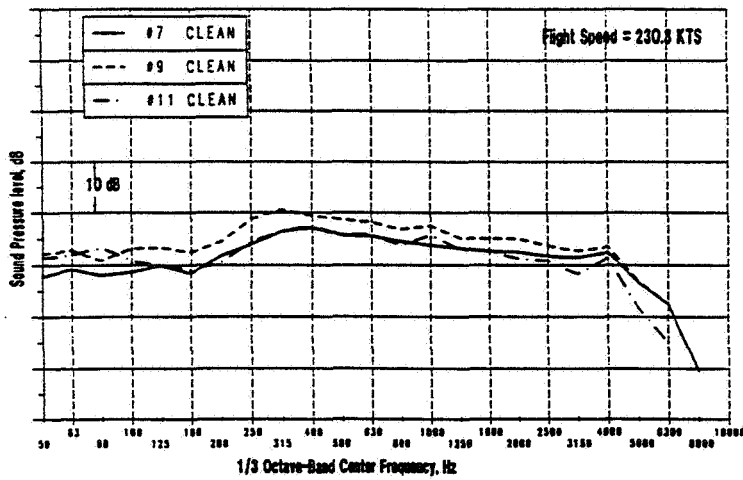
Figure 2.4 (concluded) DC-9-30 Flight Test: One-Third-Octave SPL To Illustrate Data
Repeatability: Clean Configuration, 120 Degrees
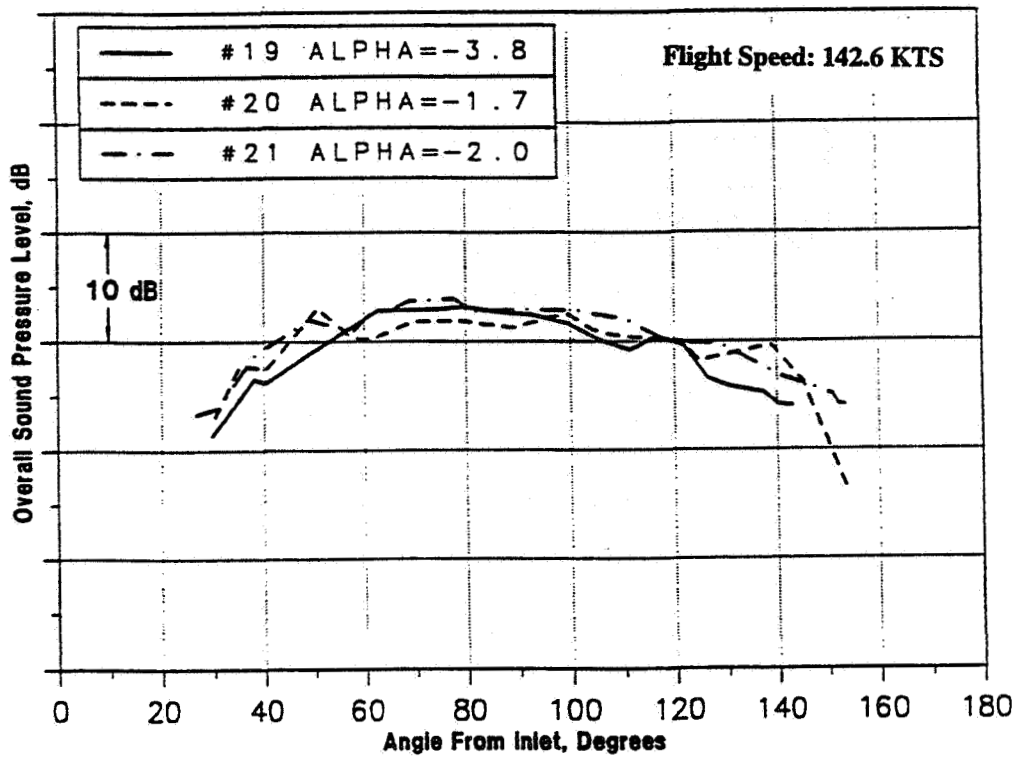
Figure 2.5 DC-9-30 Flight Test: OASPL Directivity To Illustrate Angle Of Attack Effects: Approach Configuration.
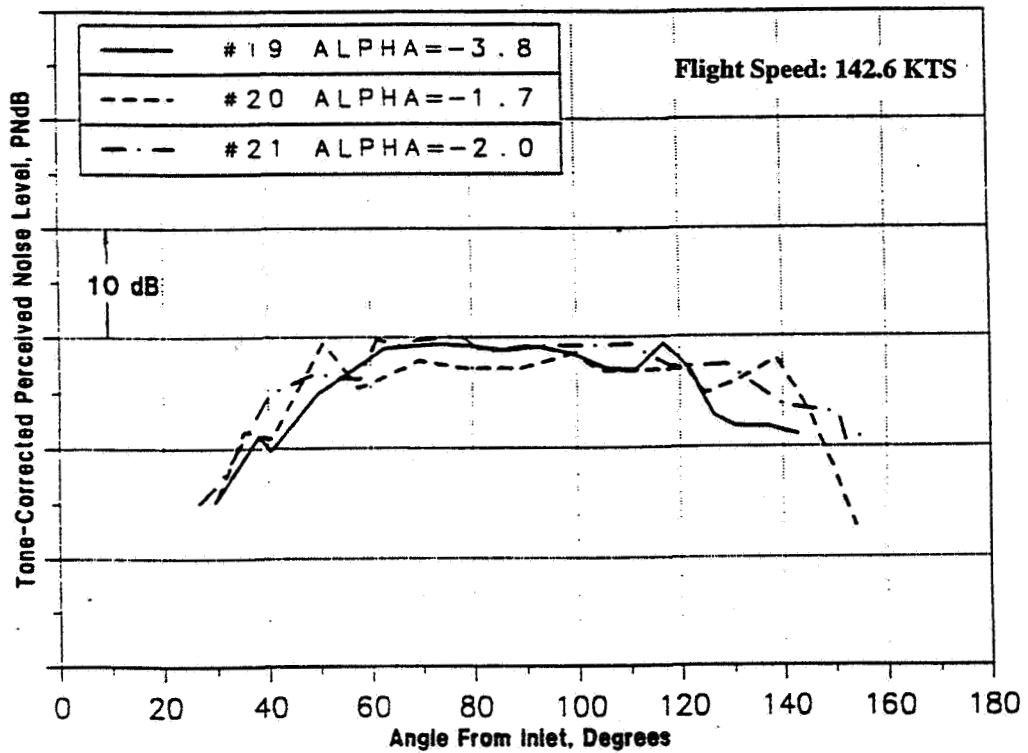
Figure 2.6 DC-9-30 Flight Test: PNLT Directivity To Illustrate Angle Of Attack Effects: Approach Configuration.
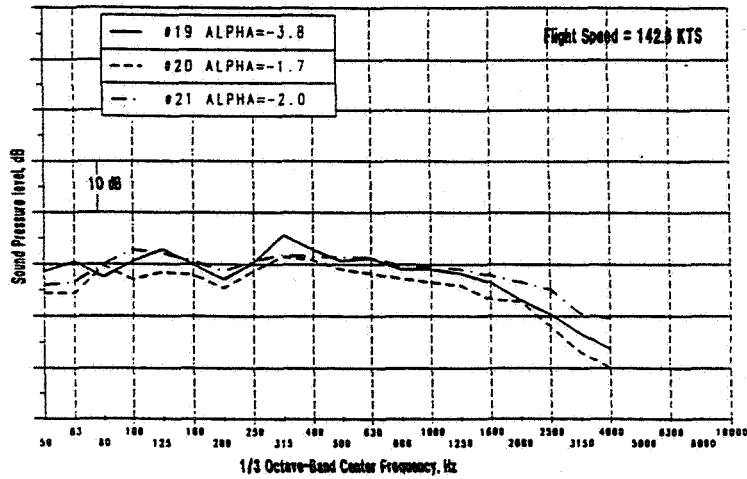
Figure 2.7 DC-9-30 Flight Test: One-Third-Octave SPL To Illustrate
Angle Of Attack Effects: Approach Configuration, 60 Degrees
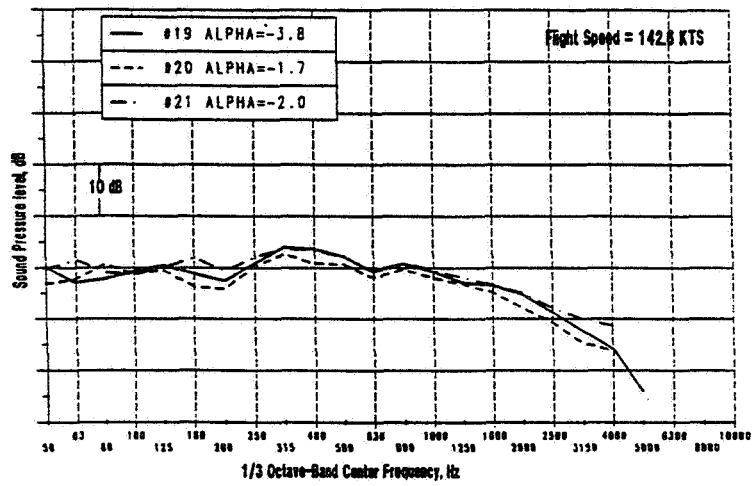
Figure 2.7 (continued) DC-9-30 Flight Test: One-Third-Octave SPL To Illustrate
Angle Of Attack Effects: Approach Configuration, 90 Degrees
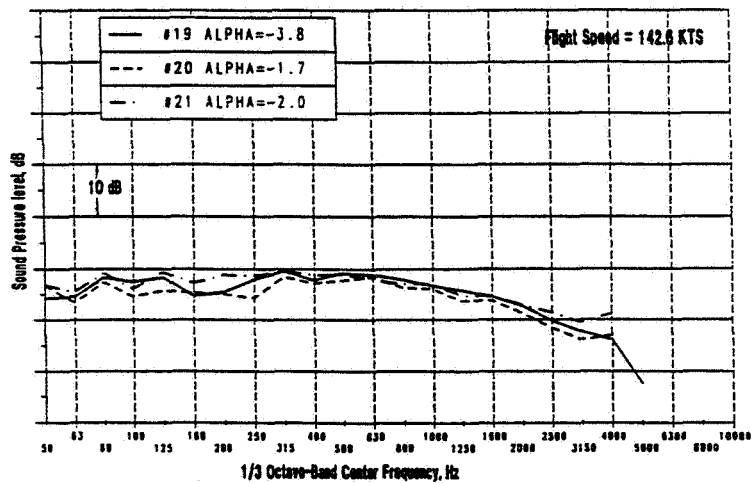
Figure 2.7 (concluded) DC-9-30 Flight Test: One-Third-Octave SPL To Illustrate
Angle Of Attack Effects: Approach Configuration, 120 Degrees

35
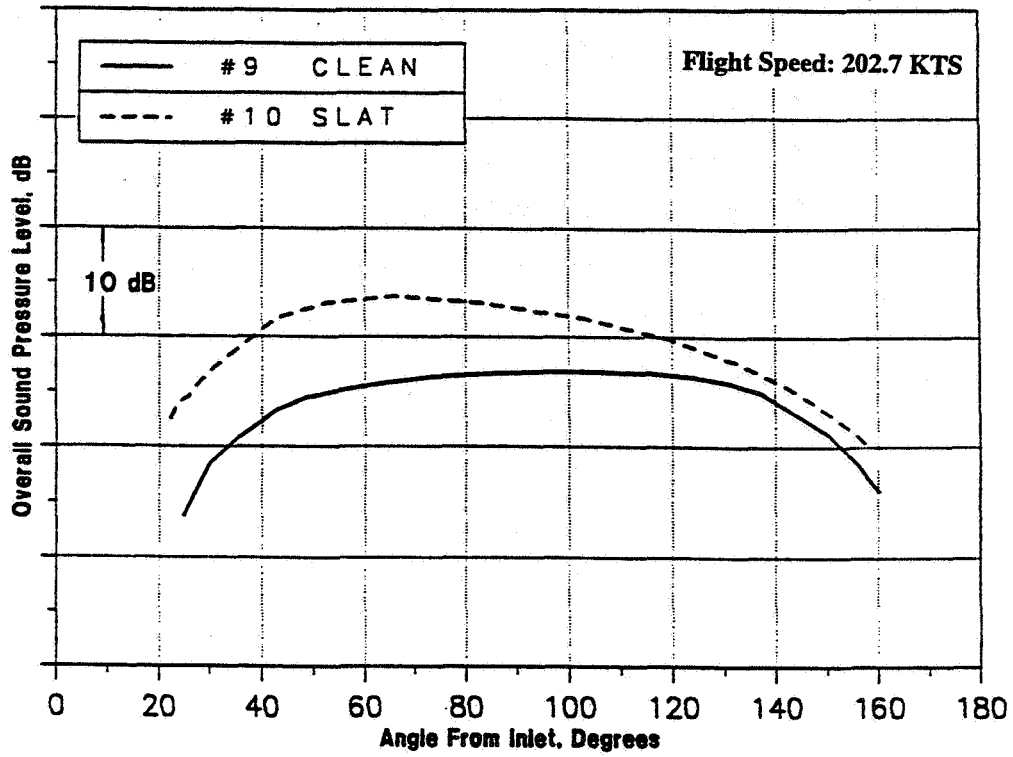
**Figure 2.8 DC-9-30 Flight Test: OASPL Directivity To Illustrate
Slat Effects On Airframe Noise From Clean Configuration.**
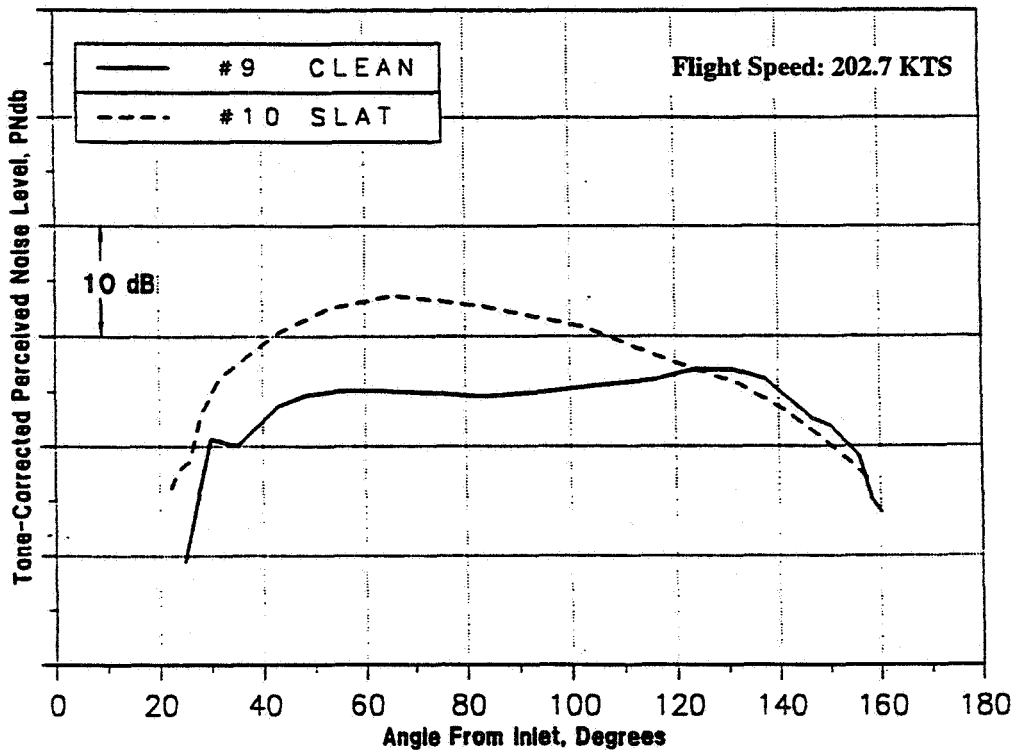
**Figure 2.9 DC-9-30 Flight Test: PNLT Directivity To Illustrate
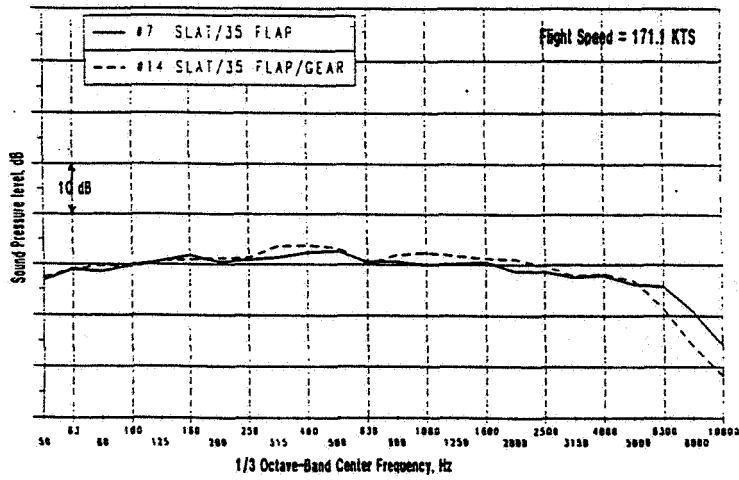Slat Effects On Airframe Noise From Clean Configuration.**
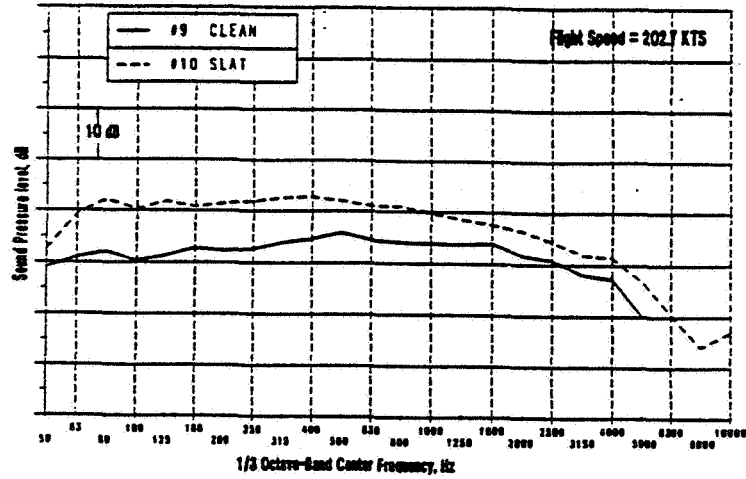
Figure 2.10 DC-9-30 Flight Test: One-Third-Octave SPL To Illustrate
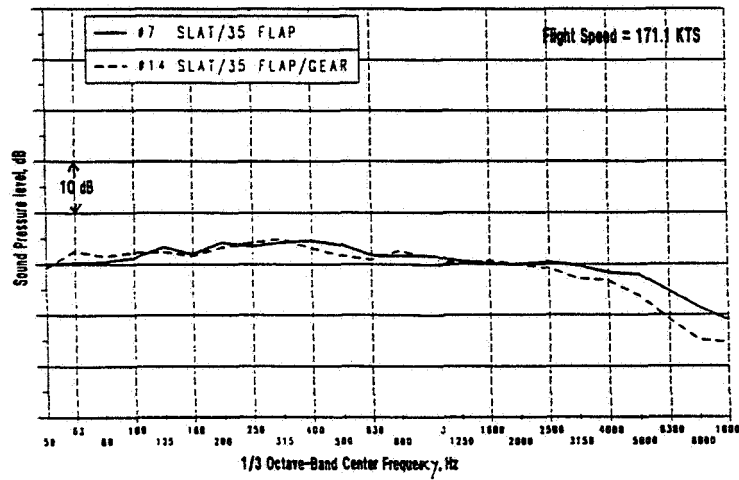Slat Effects On Airframe Noise From Clean Configuration, 60 Degrees
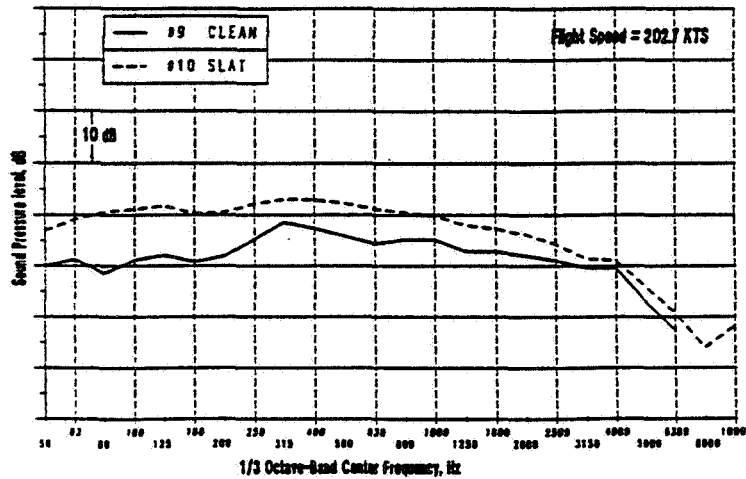
Figure 2.10 (Continued) DC-9-30 Flight Test: One-Third-Octave SPL To Illustrate
Slat Effects On Airframe Noise From Clean Configuration, 90 Degrees
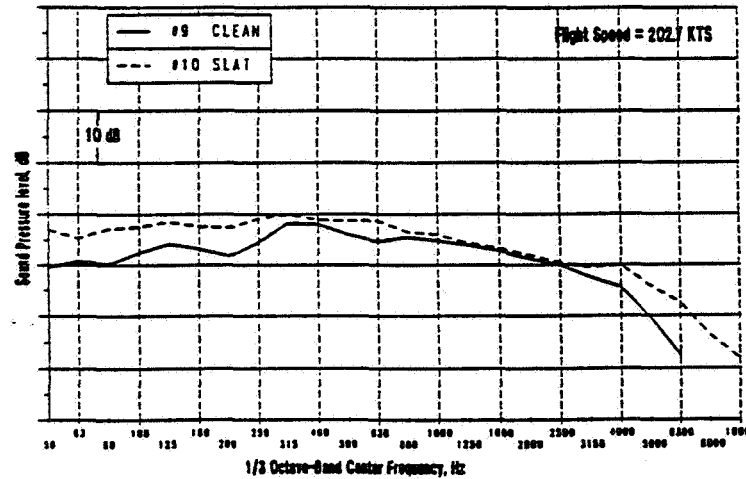
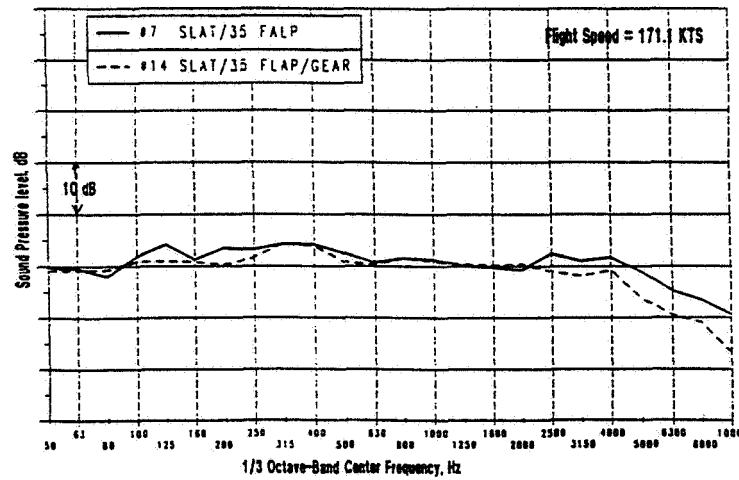Figure 2.10 (Concluded) DC-9-30 Flight Test: One-Third-Octave SPL To Illustrate
Slat Effects On Airframe Noise From Clean Configuration, 120 Degrees

37
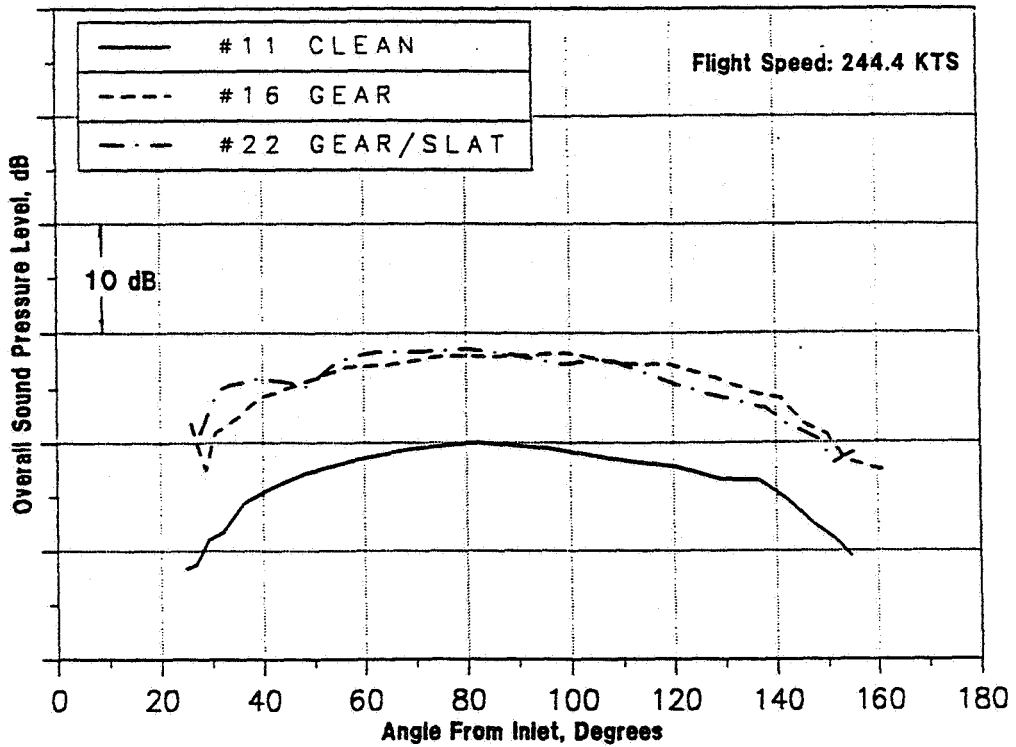
Figure 2.11 DC-9-30 Flight Test: OASPL Directivity To Illustrate Slat
Effects On Airframe Noise From Landing Gear Deployed Configuration.
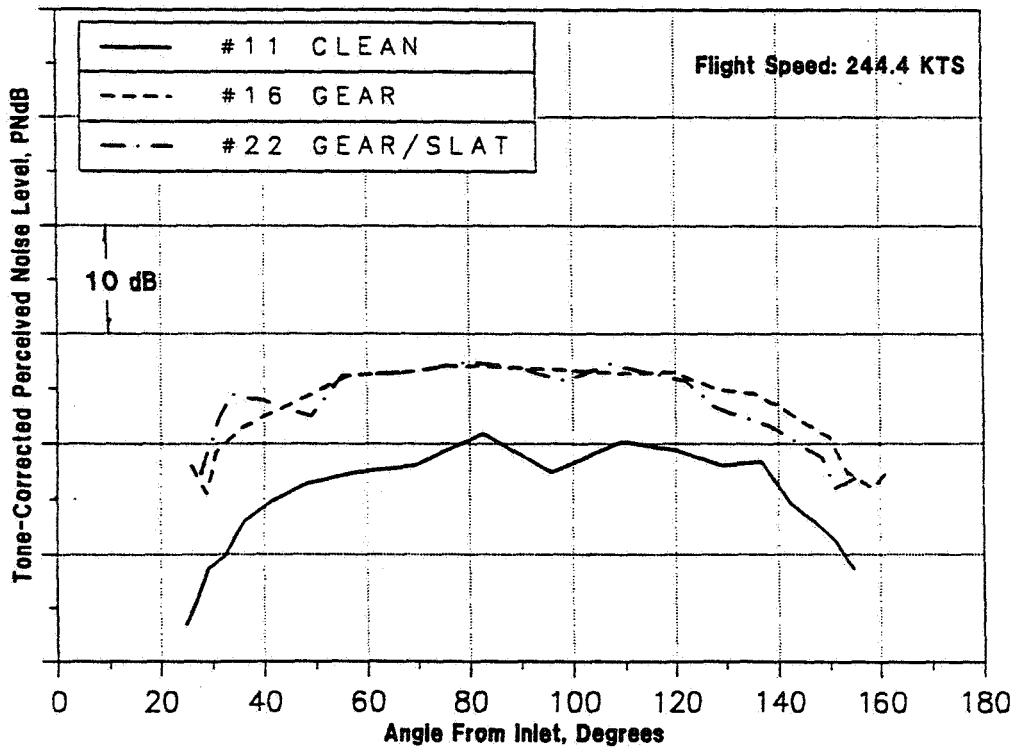
Figure 2.12 DC-9-30 Flight Test: PNLT Directivity To Illustrate Slat
Effects On Airframe Noise From Landing Gear Deployed Configuration.

38
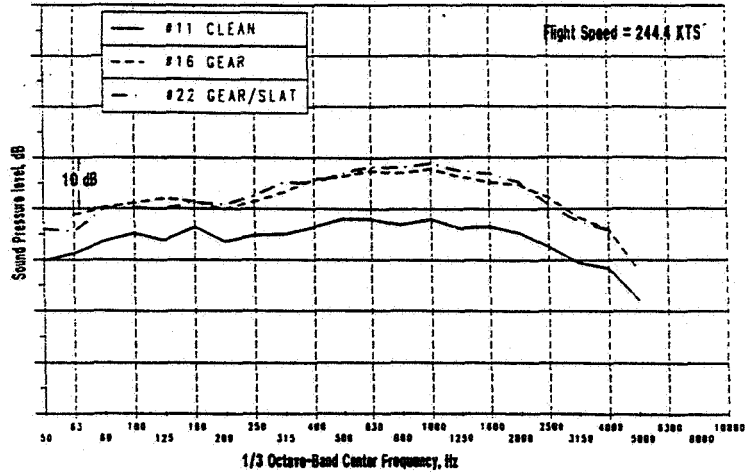
Figure 2.13 DC-9-30 Flight Test: One-Third-Octave SPL To Illustrate Slat Effects On Airframe Noise From Landing Gear Deployed Configuration, 60 Degrees
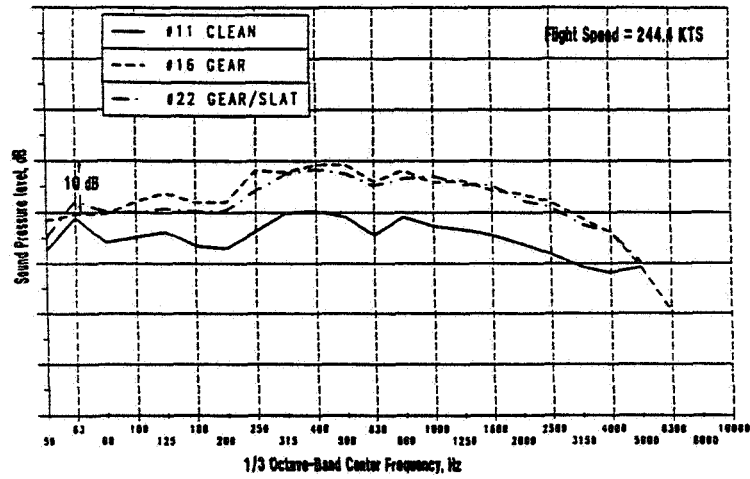
Figure 2.13 (continued) DC-9-30 Flight Test: One-Third-Octave SPL To Illustrate Slat Effects On Airframe Noise From Landing Gear Deployed Configuration, 90 Degrees
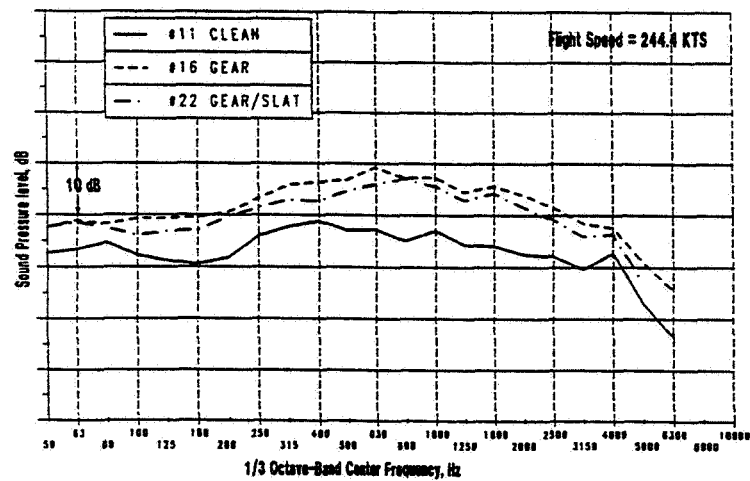
Figure 2.13 (concluded) DC-9-30 Flight Test: One-Third-Octave SPL To Illustrate Slat Effects On Airframe Noise From Landing Gear Deployed Configuration, 120 Degrees

39
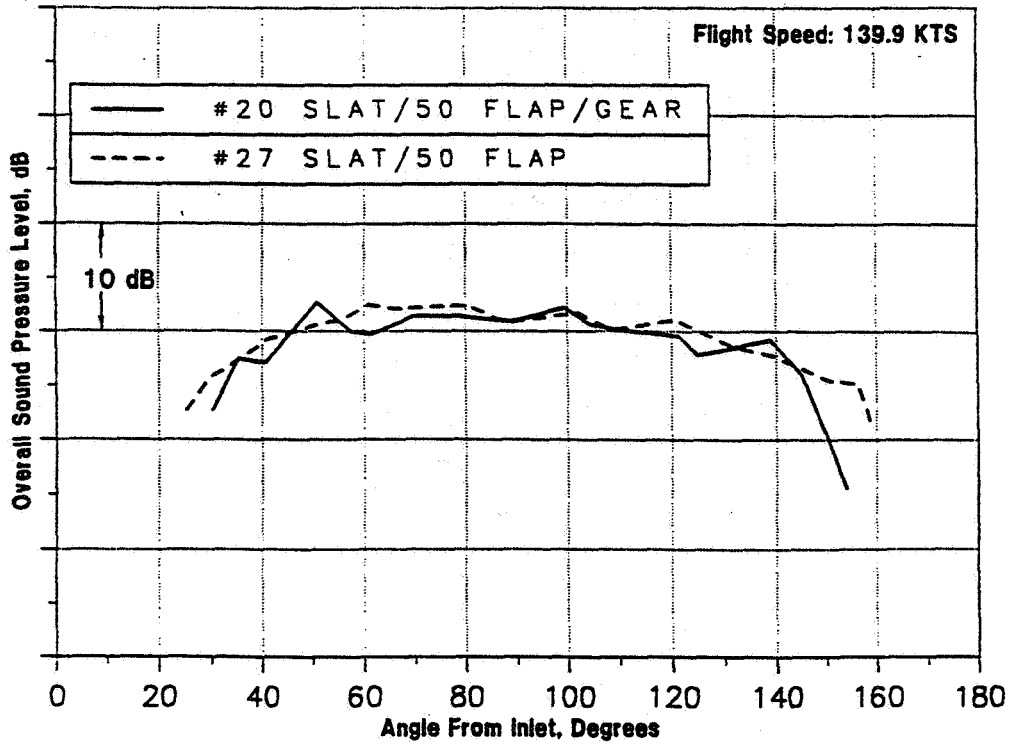
Figure 2.14 DC-9-30 Flight Test: OASPL Directivity To Illustrate Landing Gear Effects On Airframe Noise From Flap Deployed Configuration.
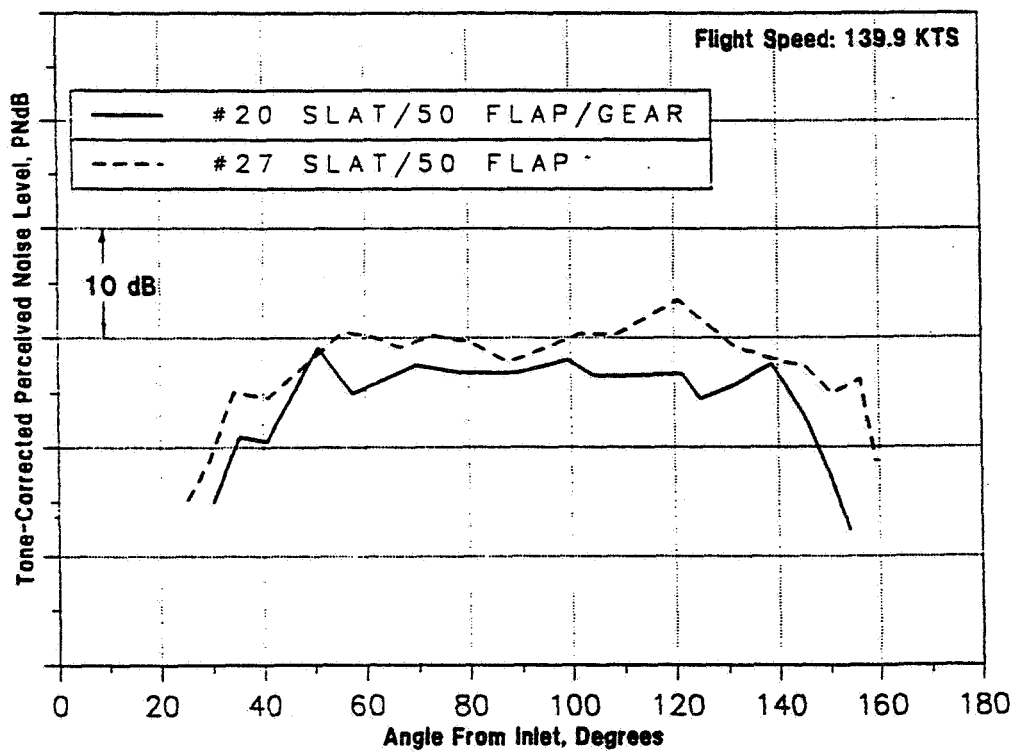
Figure 2.15 DC-9-30 Flight Test: PNLT Directivity To Illustrate Landing Gear Effects On Airframe Noise From Flap Deployed Configuration.

40
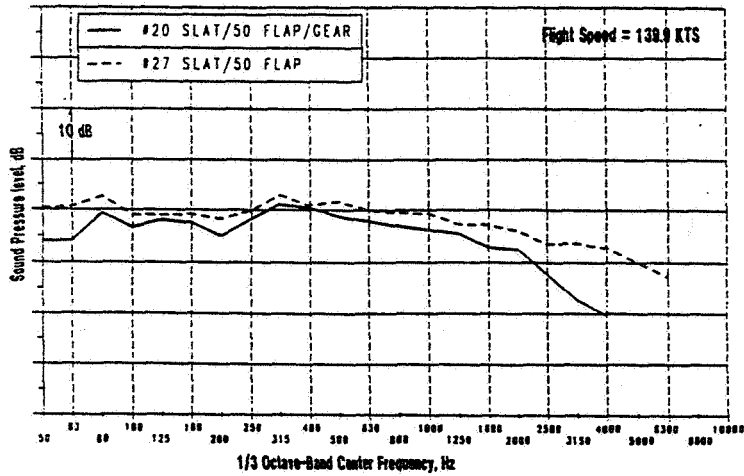
Figure 2.16 DC-9-30 Flight Test: One-Third-Octave SPL To Illustrate Landing Gear
Effects On Airframe Noise From Flap Deployed Configuration, 60 Degrees
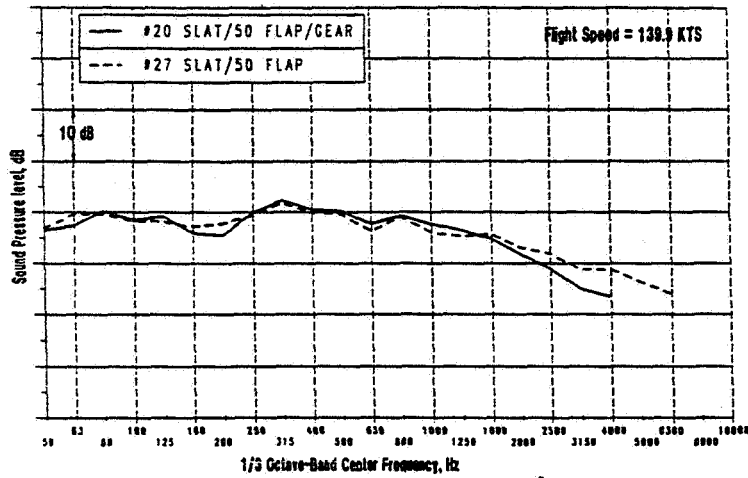
Figure 2.16 (continued) DC-9-30 Flight Test: One-Third-Octave SPL To Illustrate Landing Gear
Effects On Airframe Noise From Flap Deployed Configuration, 90 Degrees
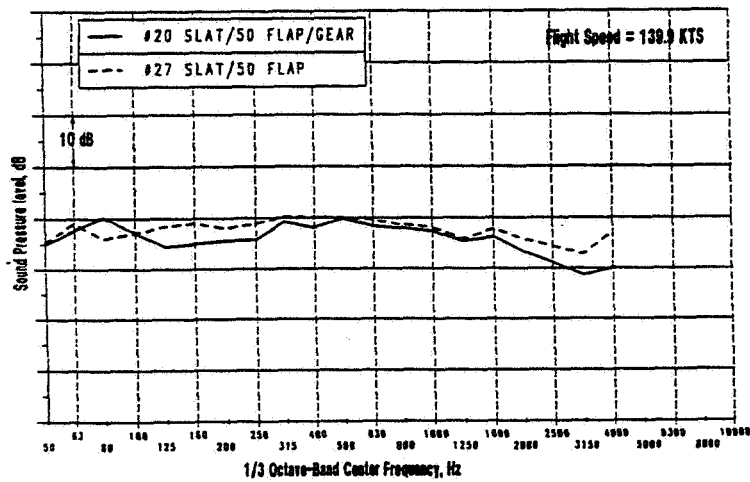
Figure 2.16 (concluded) DC-9-30 Flight Test: One-Third-Octave SPL To Illustrate Landing Gear
Effects On Airframe Noise From Flap Deployed Configuration, 120 Degrees
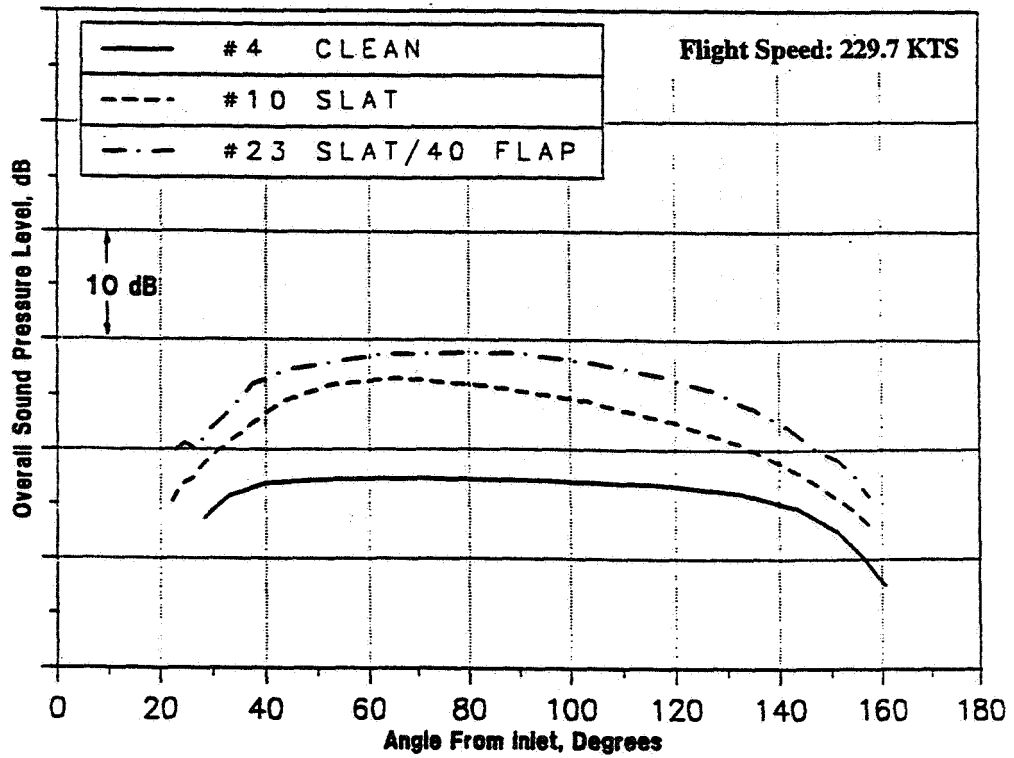
Figure 2.17 DC-9-30 Flight Test: OASPL Directivity To Illustrate
Flap Effects On Airframe Noise From Slat Deployed Configuration.
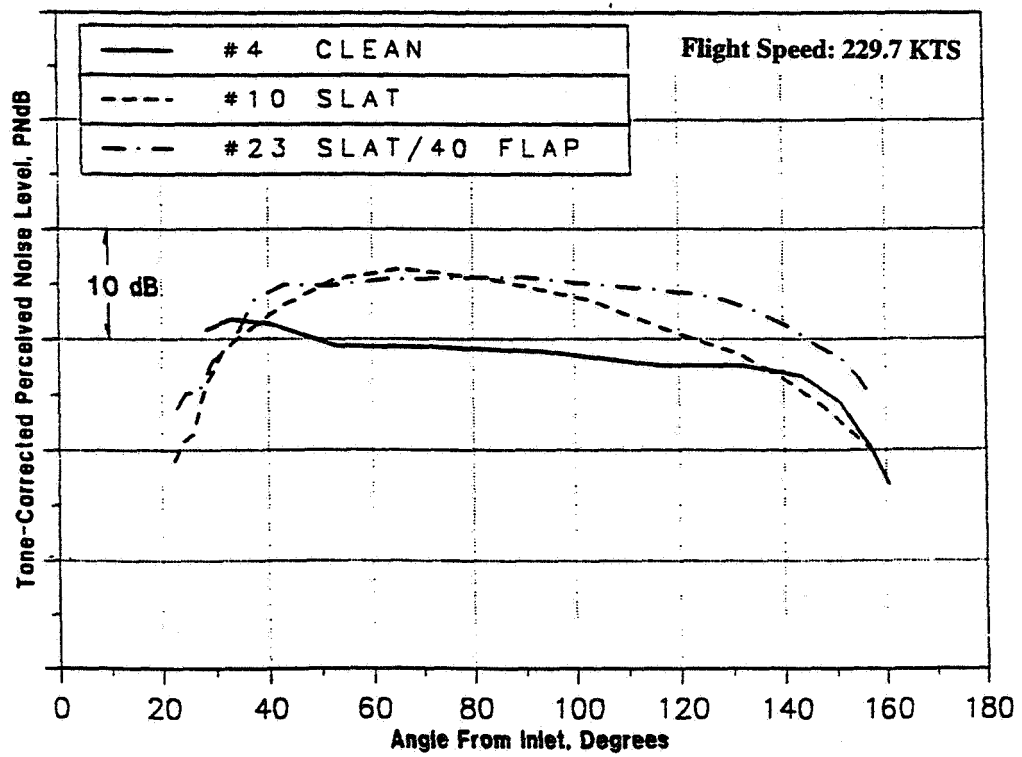
Figure 2.18 DC-9-30 Flight Test: PNLT Directivity To Illustrate
Flap Effects On Airframe Noise From Slat Deployed Configuration.
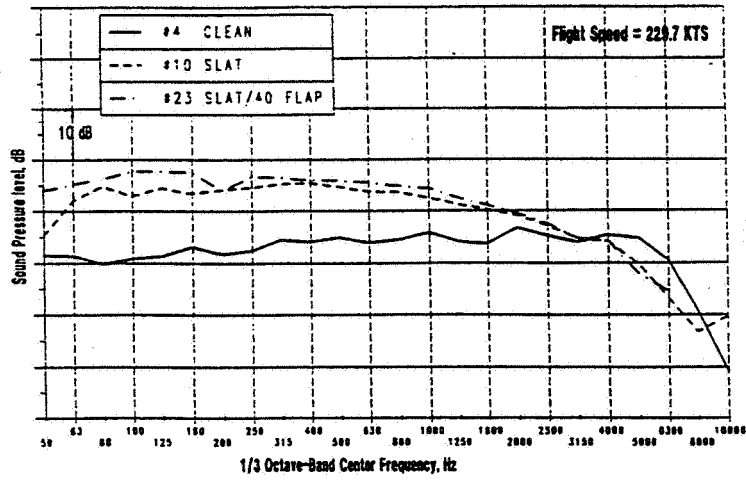
Figure 2.19 DC-9-30 Flight Test: One-Third-Octave SPL To Illustrate
Flap Effects On Airframe Noise From Slat Deployed Configuration, 60 Degrees
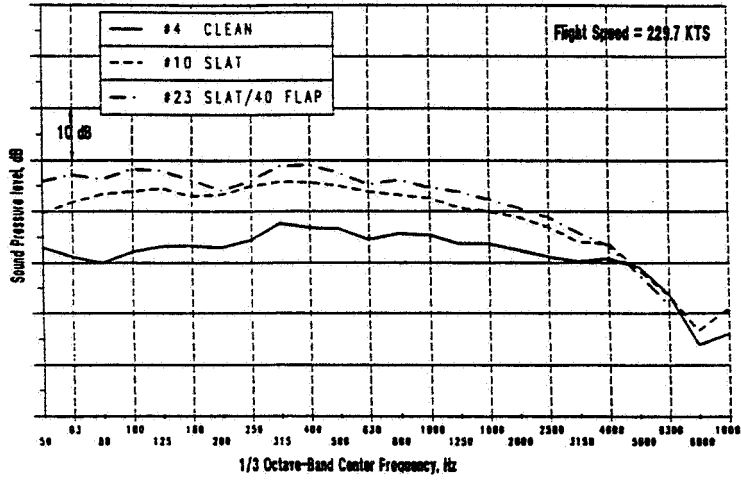
Figure 2.19 (Continued) DC-9-30 Flight Test: One-Third-Octave SPL To Illustrate
Flap Effects On Airframe Noise From Slat Deployed Configuration, 90 Degrees
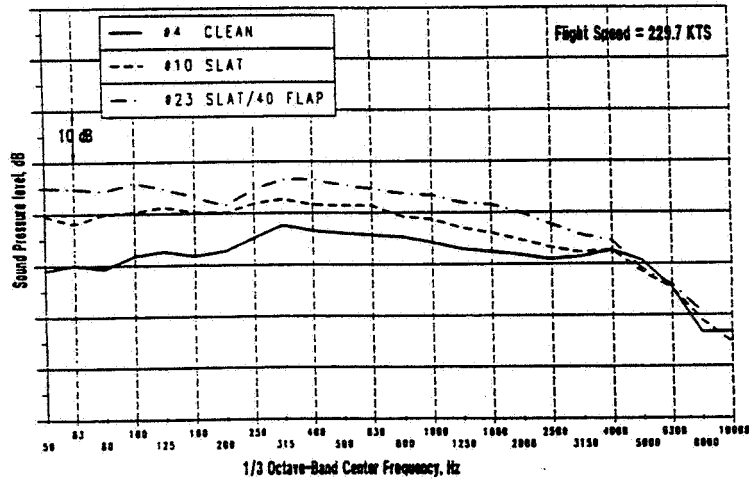
Figure 2.19 (Concluded) DC-9-30 Flight Test: One-Third-Octave SPL To Illustrate
Flap Effects On Airframe Noise From Slat Deployed Configuration, 120 Degrees
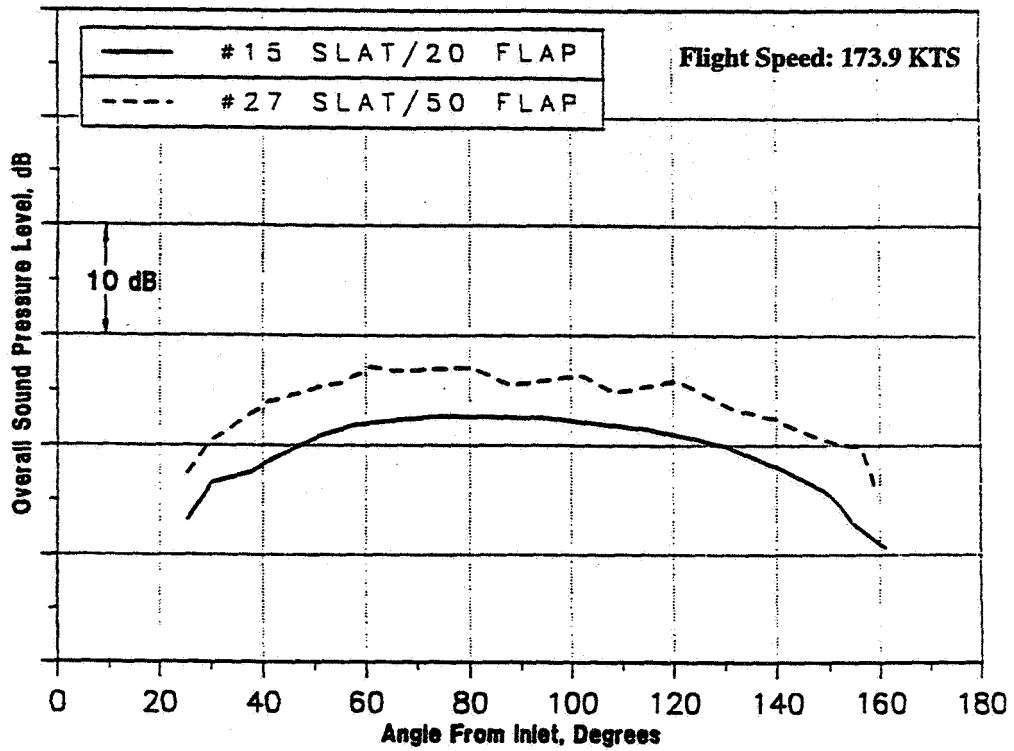
Figure 2.20 DC-9-30 Flight Test: OASPL Directivity To Illustrate Effects Of Flap Deflection Angle On Airframe Noise From Slat Deployed Configuration.
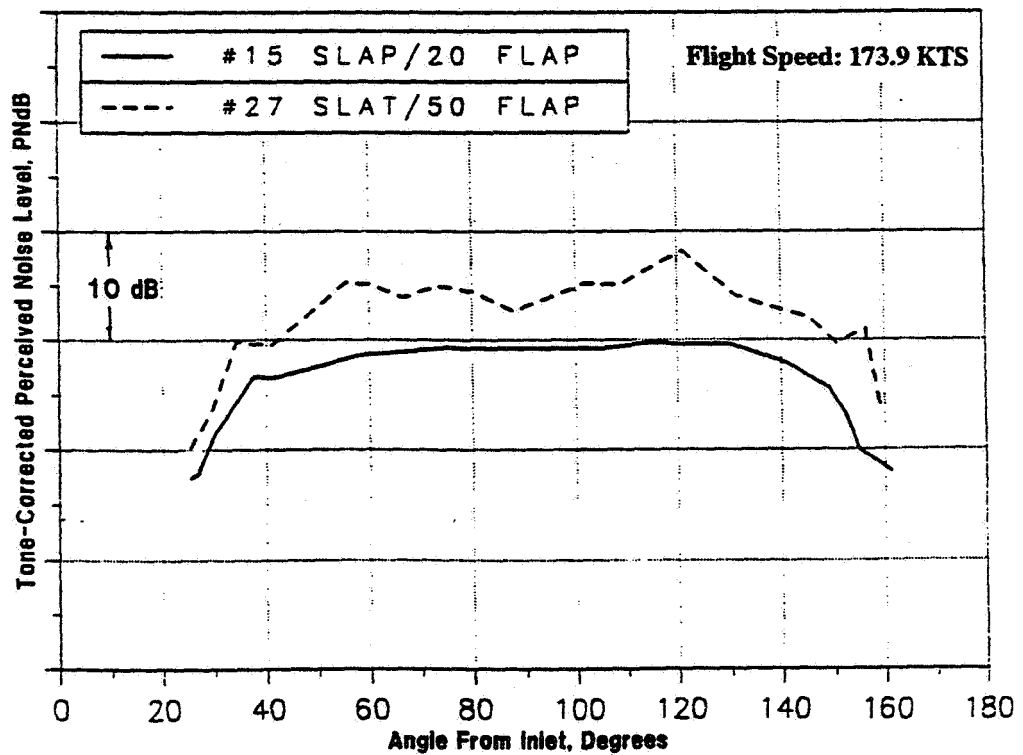
Figure 2.21 DC-9-30 Flight Test: PNLT Directivity To Illustrate Effects Of Flap Deflection Angle On Airframe Noise From Slat Deployed Configuration.

44
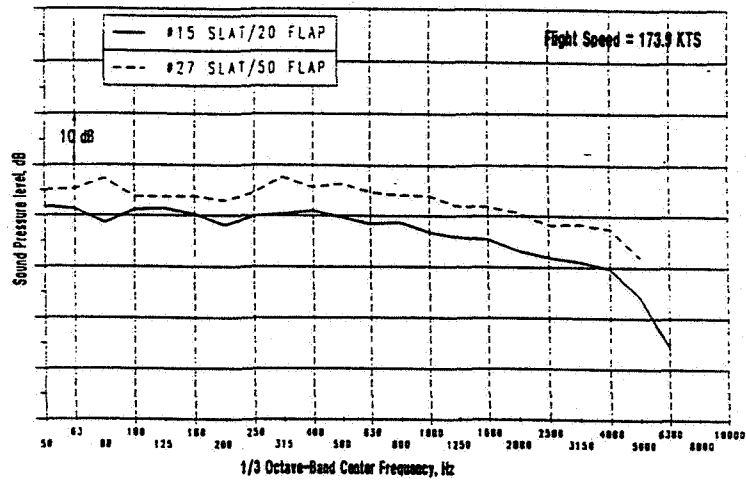
Figure 2.22 DC-9-30 Flight Test: One-Third-Octave SPL To Illustrate Effects Of Flap
Deflection Angle On Airframe Noise From Slat Deployed Configuration. 60 Degrees
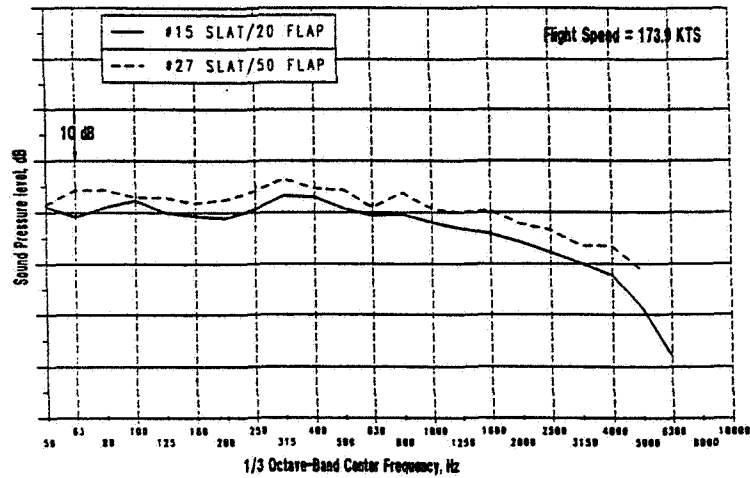
Figure 2.22 (Continued) DC-9-30 Flight Test: One-Third-Octave SPL To Illustrate Effects Of Flap
Deflection Angle On Airframe Noise From Slat Deployed Configuration. 90 Degrees
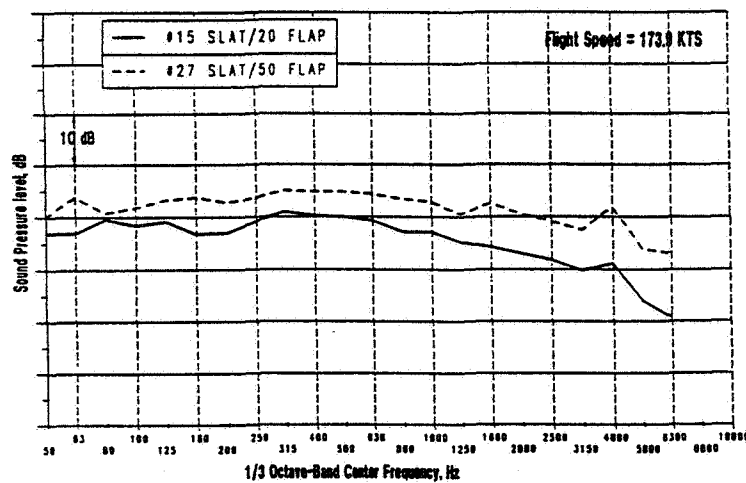
Figurec2.22 (Concluded) DC-9-30 Flight Test: One-Third-Octave SPL To Illustrate Effects Of Flap
Deflection Angle On Airframe Noise From Slat Deployed Configuration. 120 Degrees

45
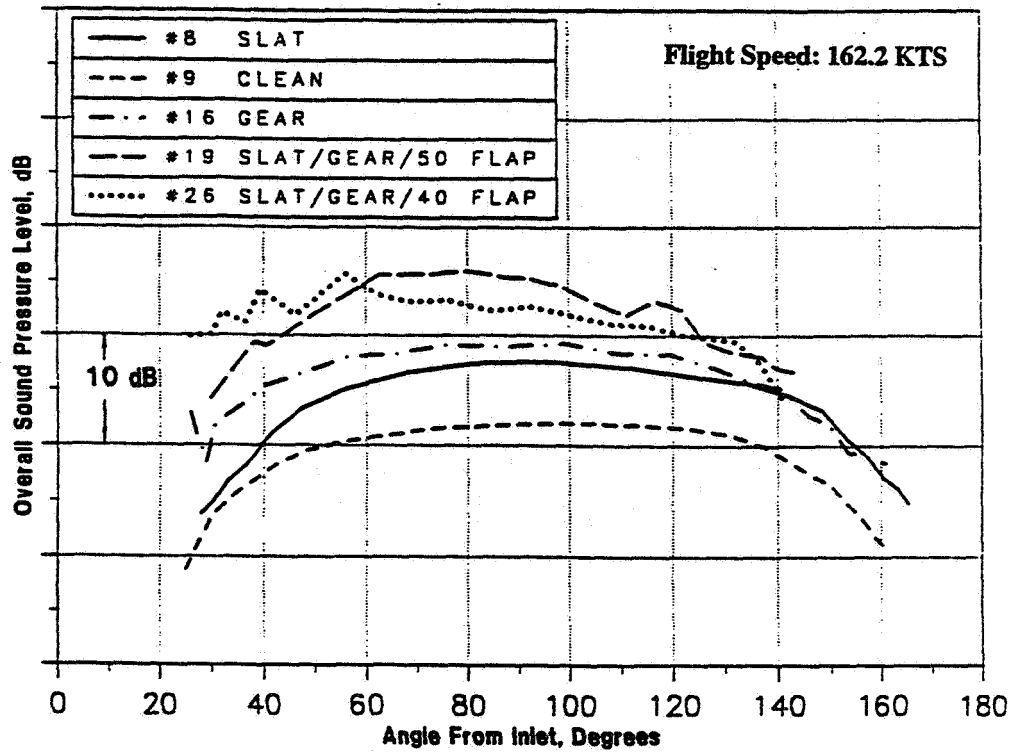
Figure 2.23 DC-9-30 Flight Test: OASPL Directivity To Illustrate Component Contributions Of Airframe Noise
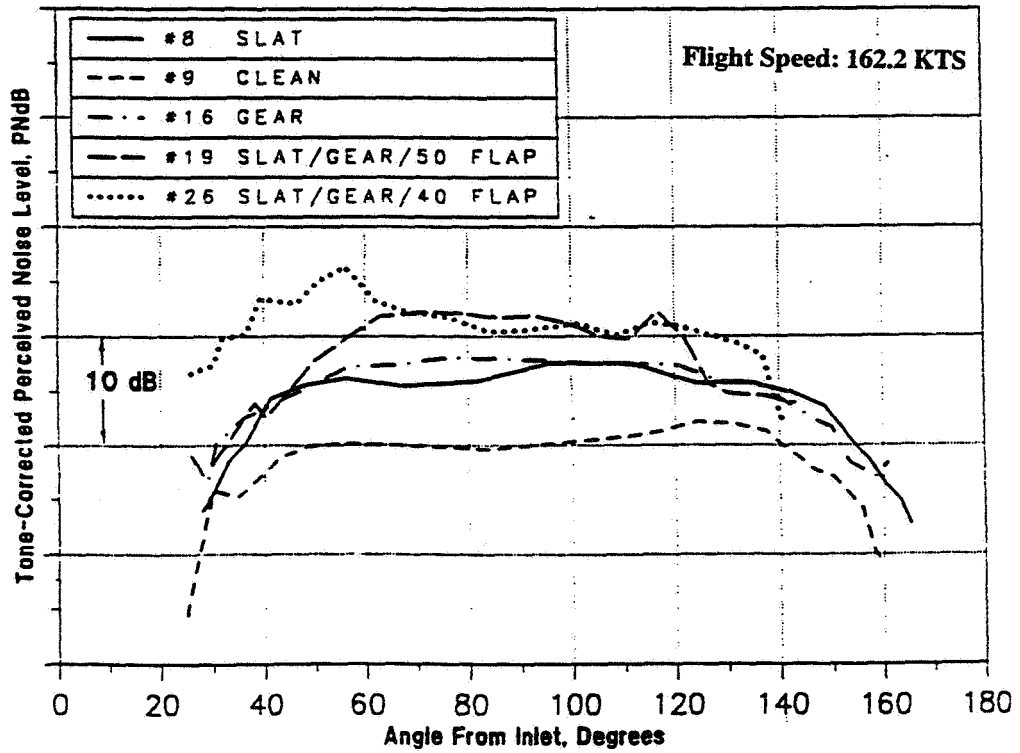
Figure 2.24 DC-9-30 Flight Test: PNLT Directivity To Illustrate Component Contributions Of Airframe Noise
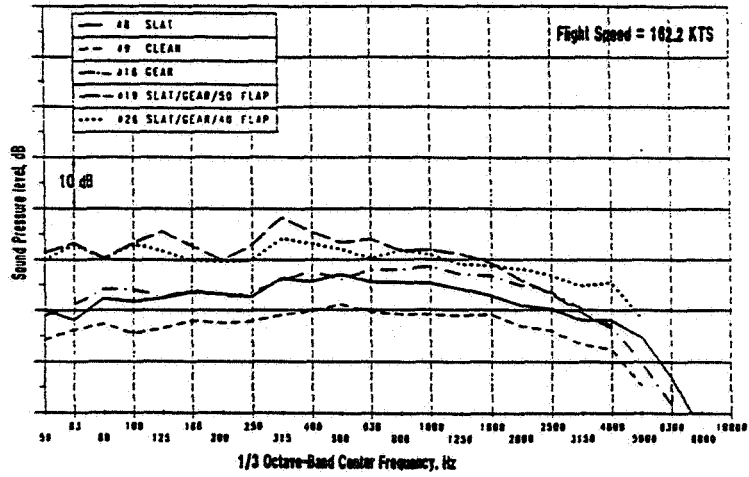
Figure 2.25 DC-9-30 Flight Test: One-Third-Octave SPL To Illustrate Component
Contributions To Airframe Noise, 60 Degrees
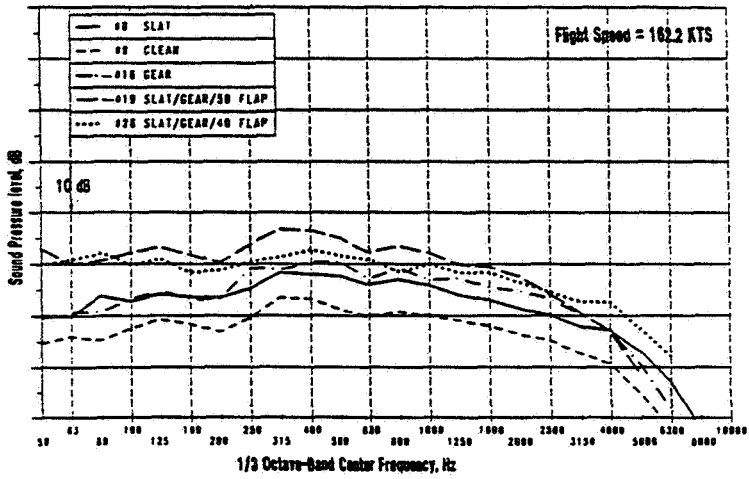
Figure 2.25 (Continued) DC-9-30 Flight Test: One-Third-Octave SPL To Illustrate Component
Contributions To Airframe Noise, 90 Degrees
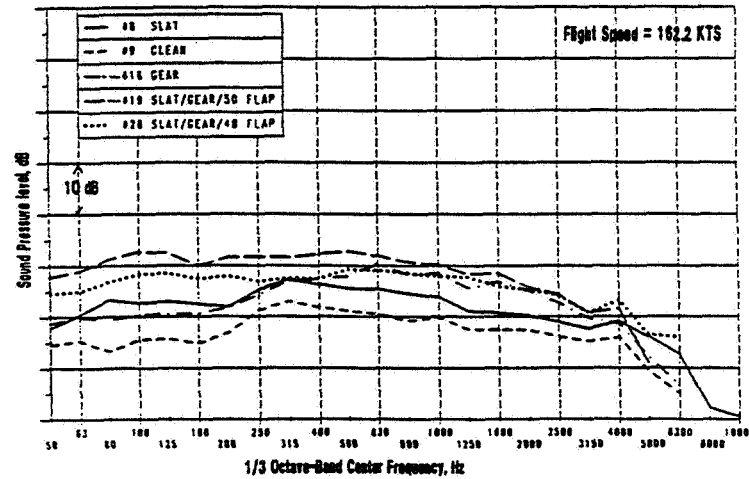
Figure 2.25 (Concluded) DC-9-30 Flight Test: One-Third-Octave SPL To Illustrate Component
Contributions To Airframe Noise, 120 Degrees

47
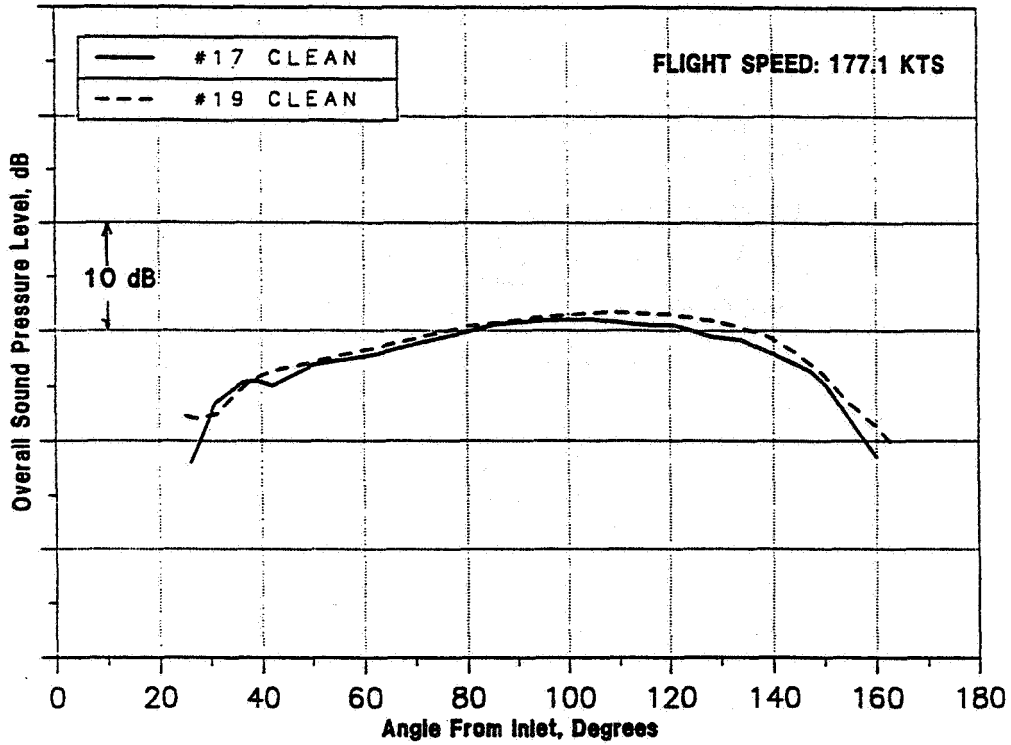
Figure 2.26 DC-10-10 Flight Test: OASPL Directivity to illustrate Data Repeatability: Clean Configuration
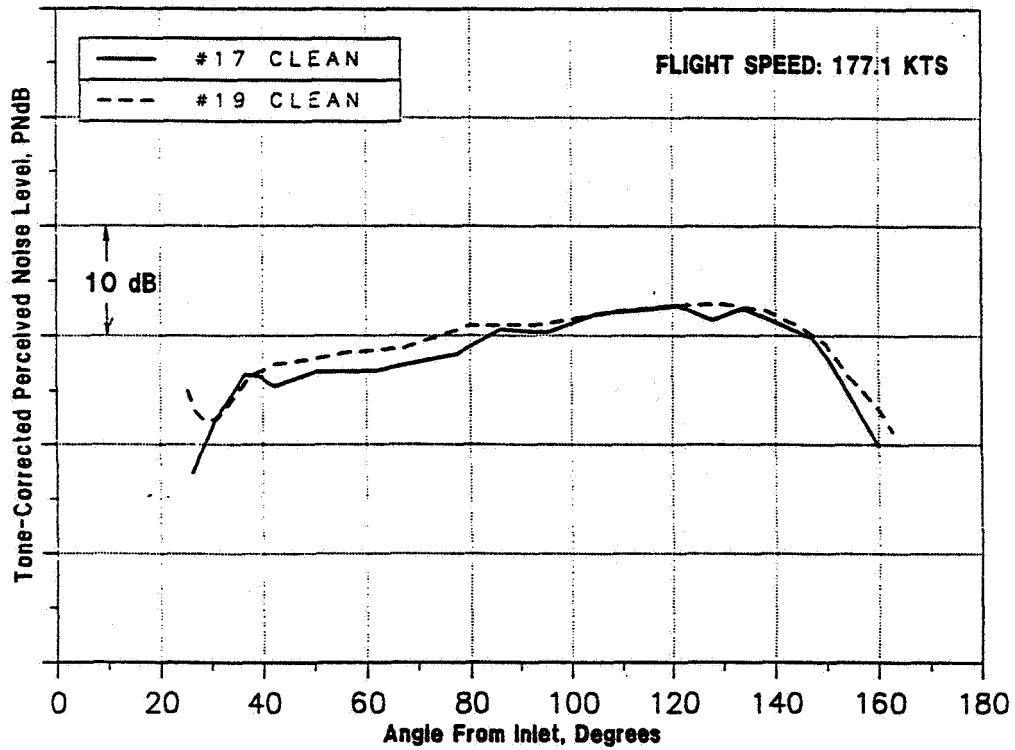
Figure 2.27 DC-10-10 Flight Test: PNLT Directivity to illustrate Data Repeatability: Clean Configuration

48
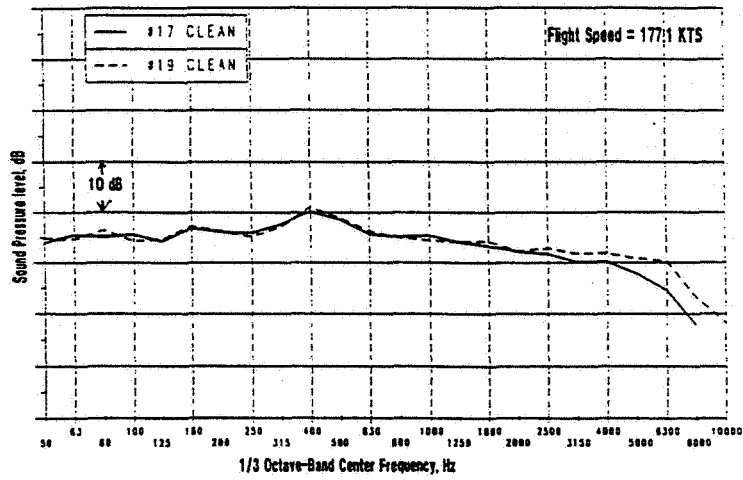
Figure 2.28 DC-10-10 Flight Test: One-Third-Octave SPL To Illustrate Data
Repeatability: Clean Configuration. 60 Degrees
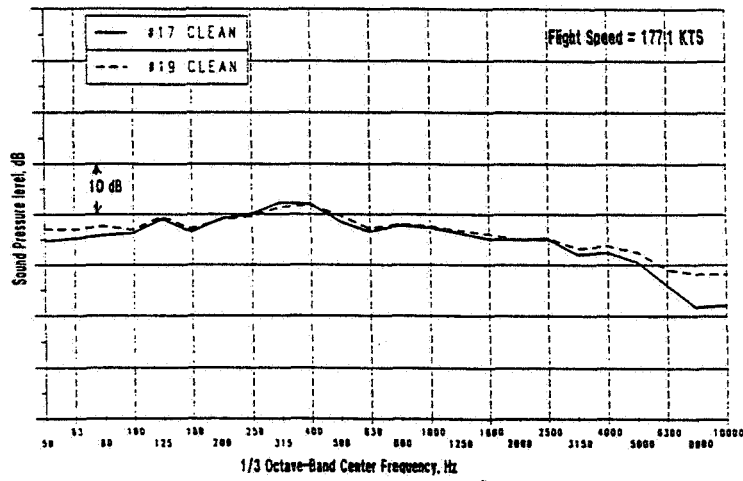
Figure 2.28 (continued) DC-10-10 Flight Test: One-Third-Octave SPL To Illustrate Data
Repeatability: Clean Configuration. 90 Degrees
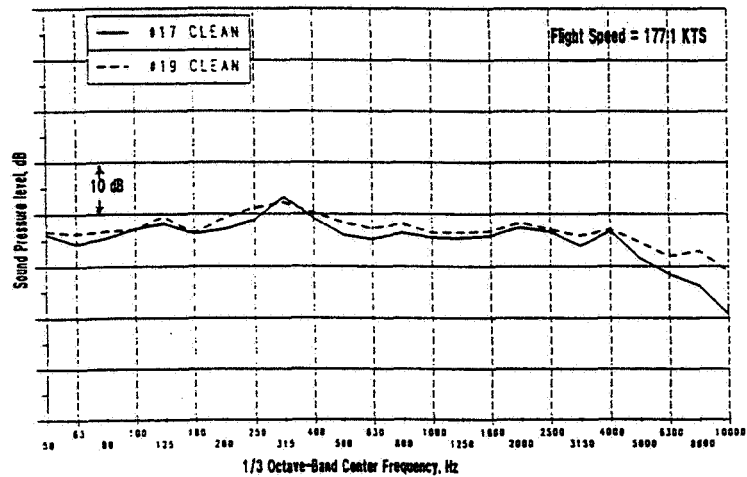
Figure 2.28 (concluded) DC-10-10 Flight Test: One-Third-Octave SPL To Illustrate Data
Repeatability: Clean Configuration, 120 Degrees

49
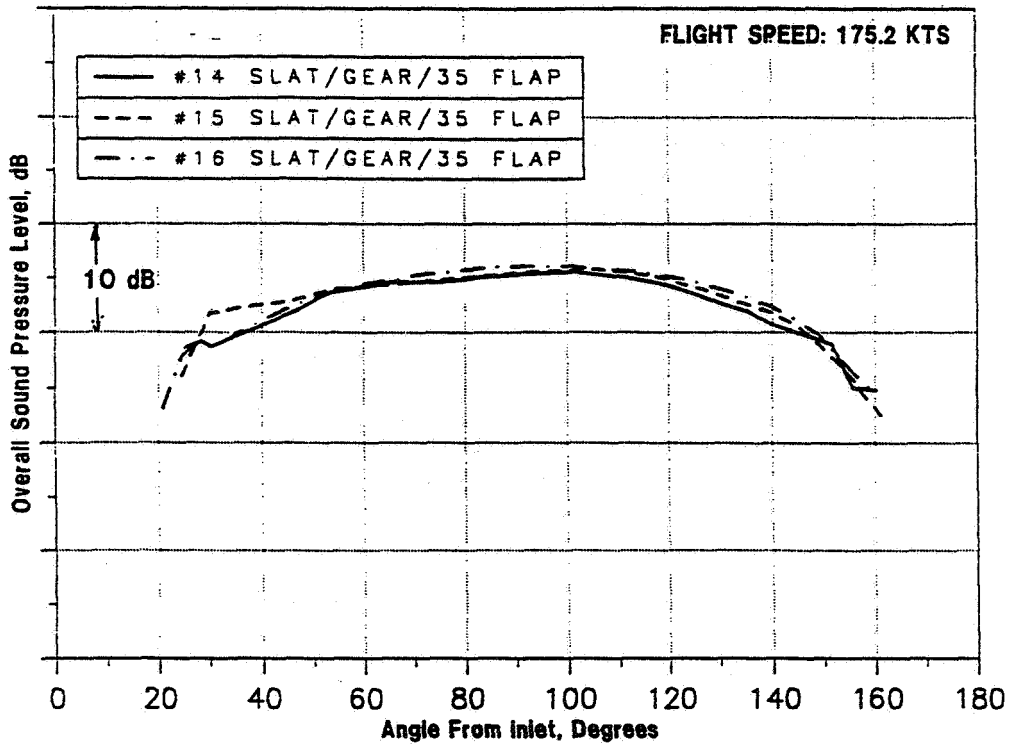
Figure 2.29 DC-10-10 Flight Test: OASPL Directivity to illustrate Data Repeatability: Landing Configuration
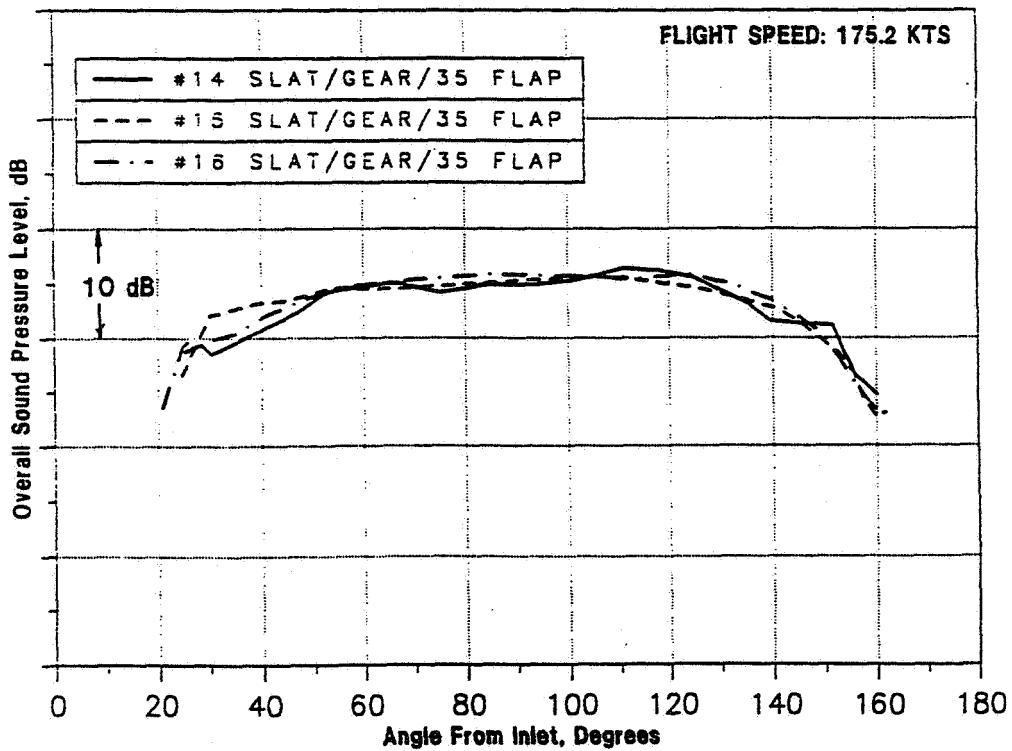
Figure 2.30 DC-10-10 Flight Test: PNLT Directivity to illustrate Data Repeatability: Landing Configuration
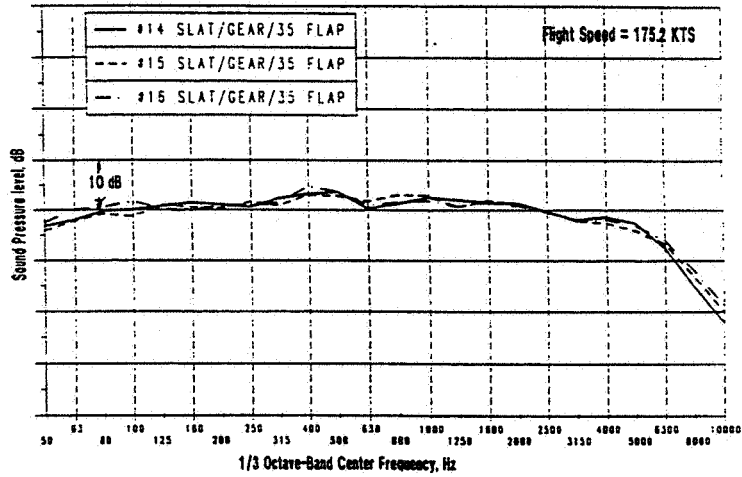
Figure 2.31 DC-9-30 Flight Test: One-Third-Octave SPL To Illustrate Data
Repeatability: Landing Configuration, 60 Degrees
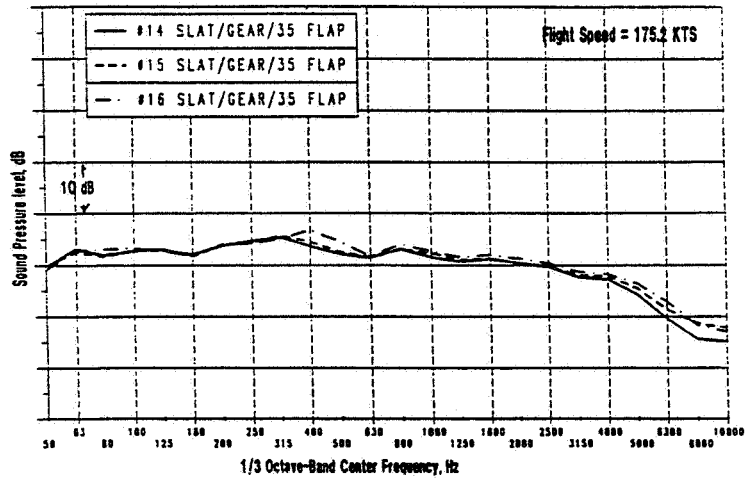
Figure 2.31 (continued) DC-10-10 Flight Test: One-Third-Octave SPL To Illustrate Data
Repeatability: Landing Configuration, 90 Degrees
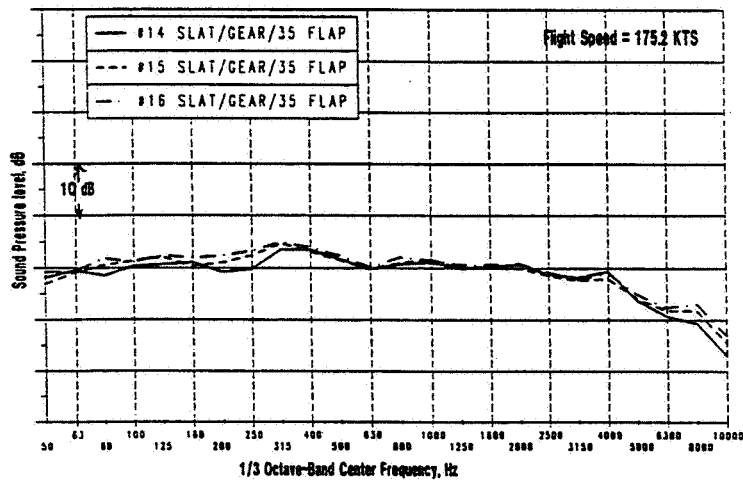
Figure 2.31 (concluded) DC-10-10 Flight Test: One-Third-Octave SPL To Illustrate Data
Repeatability: Landing Configuration, 120 Degrees

51
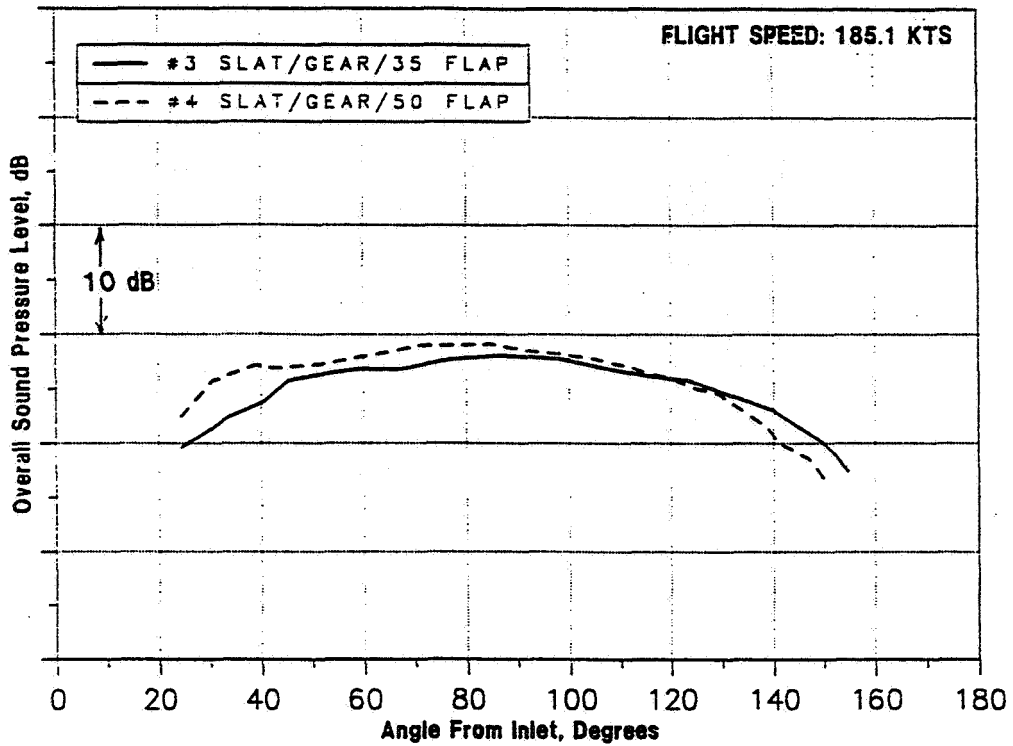
Figure 2.32 DC-10-10 Flight Test: OASPL Directivity to illustrate Effects of Flap
Deflection Angle on Airframe Noise From Landing Configuration.
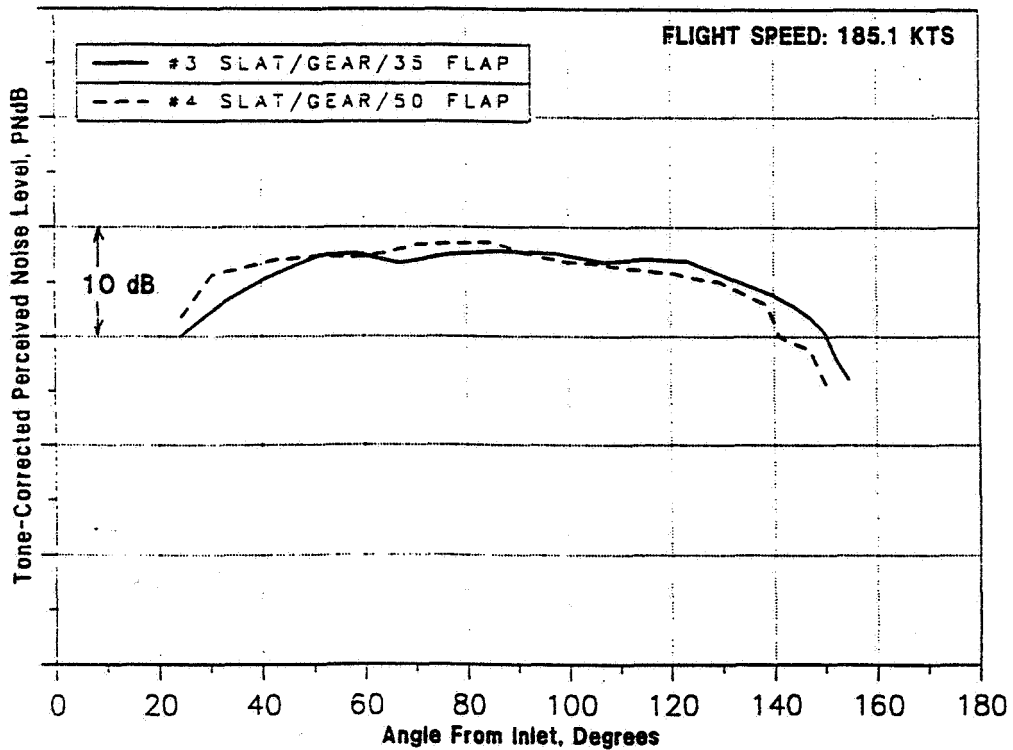
Figure 2.33 DC-10-10 Flight Test: PNLT Directivity to illustrate Effects of Flap
Deflection Angle on Airframe Noise From Landing Configuration.
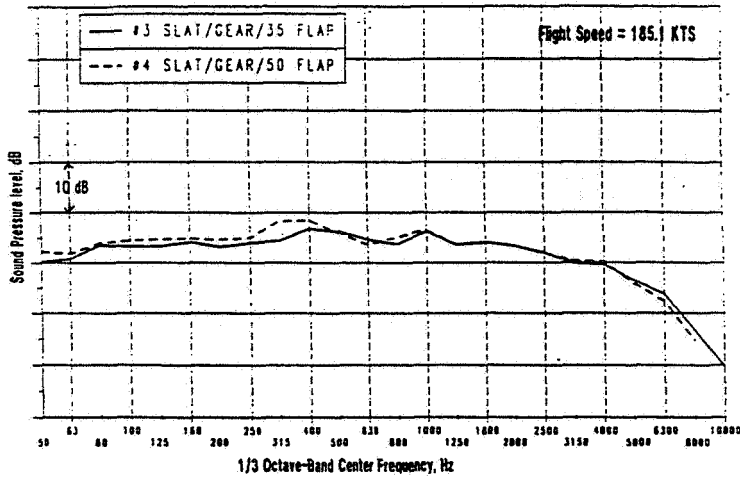
Figure 2.34 DC-10-10 Flight Test: One-Third-Octave SPL To Illustrate Effects Of Flap
Deflection Angle On Airframe Noise From Landing Configuration, 60 Degrees
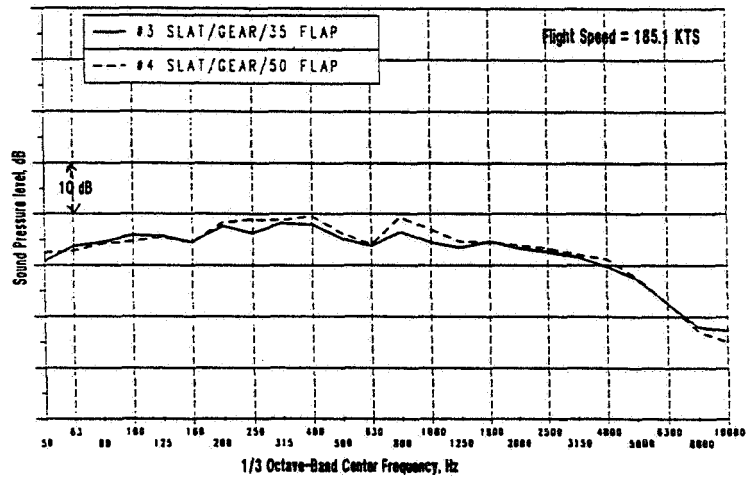
Figure 2.34 (continued) DC-10-10 Flight Test: One-Third-Octave SPL To Illustrate Effects Of Flap
Deflection Angle On Airframe Noise From Landing Configuration, 90 Degrees
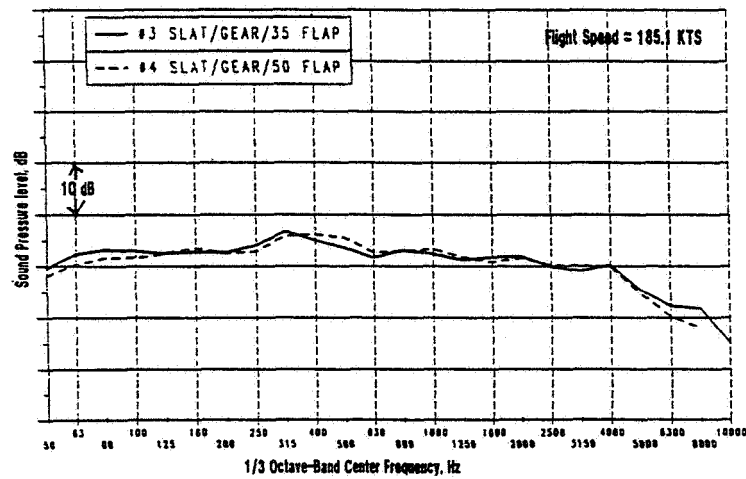
Figure 2.34 (concluded) DC-10-10 Flight Test: One-Third-Octave SPL To Illustrate Effects Of Flap
Deflection Angle On Airframe Noise From Landing Configuration, 120 Degrees
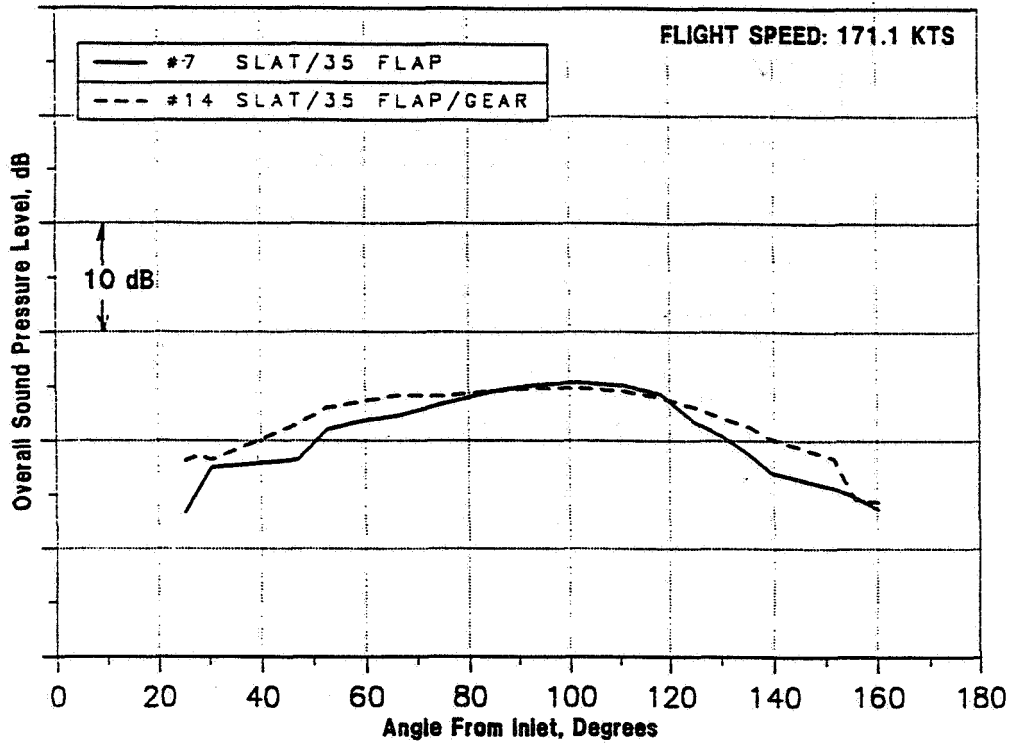
Figure 2.35 DC-10-10 Flight Test: OASPL Directivity to illustrate Landing Gear Effects On Airframe Noise From Flap/Slat Deployed Configuration
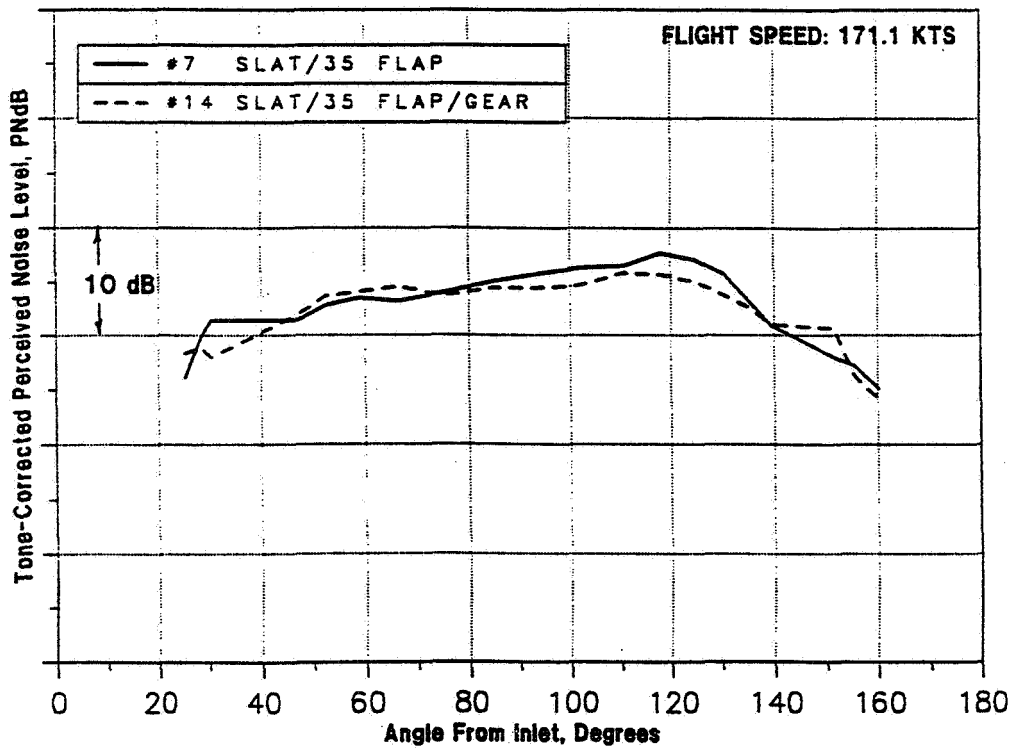
Figure 2.36 DC-10-10 Flight Test: PNLT Directivity to illustrate Landing Gear Effects On Airframe Noise From Flap/Slat Deployed Configuration

54

Figure 2.37 DC-10-10 Flight Test: One-Third-Octave SPL To Illustrate Landing Gear Effects On
Airframe Noise From Flap/Slat Deployed Configuration, 60 Degrees

Figure 2.37 (continued) DC-10-10 Flight Test: One-Third Octave SPL To Illustrate Landing Gear Effects On
Airframe Noise From Flap/Slat Deployed Configuration, 90 Degrees

Figure 2.37 (concluded) DC-10-10 Flight Test: One-Third-Octave SPL To Illustrate Landing Gear Effects On
Airframe Noise From Flap/Slat Deployed Configuration, 120 Degrees

B-737 Scale Model Airframe Noise
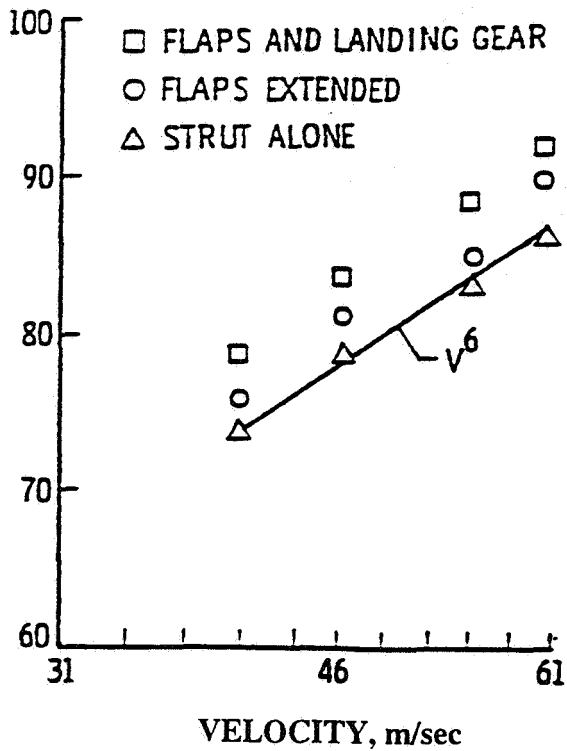
Figure 3.1 Velocity Dependence of OASPL (Ref.4)
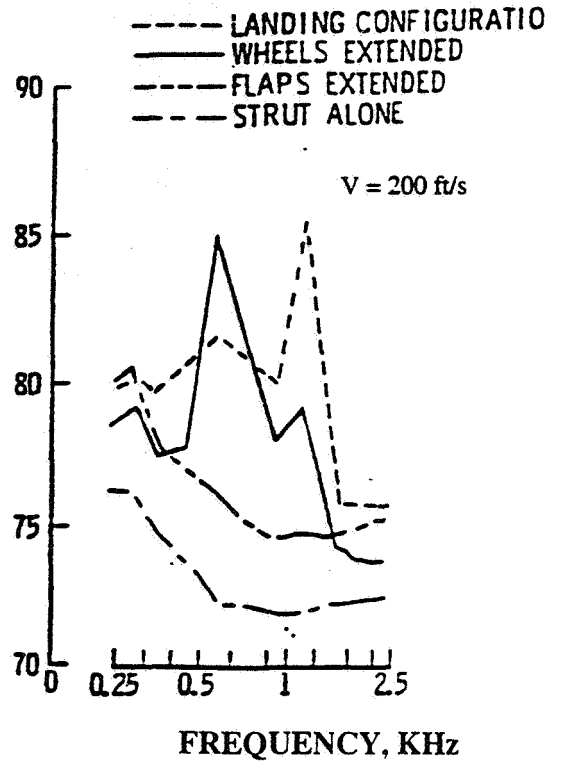
Figure 3.2 One-third-octave SPL spectra for various configurations (Ref.4)
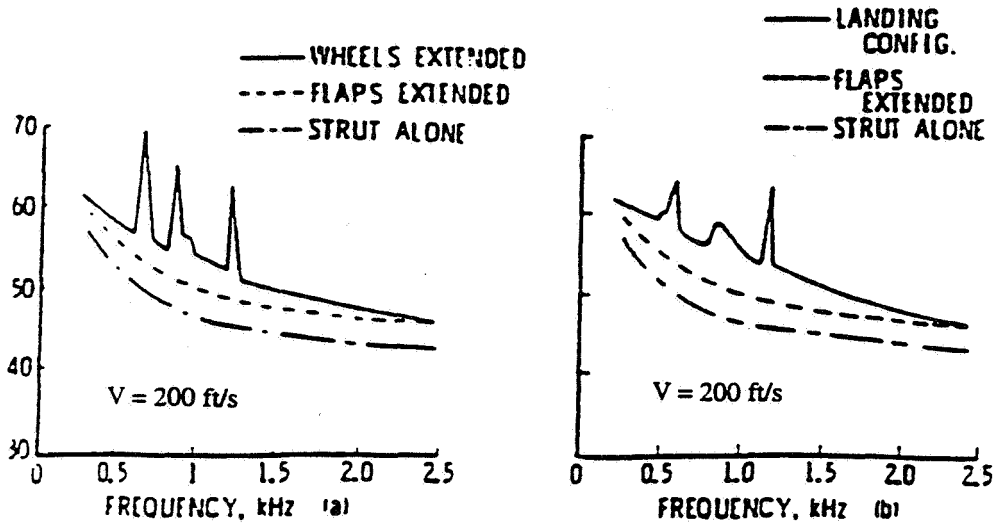
Figure 3.3 Narrowband SPL spectra for various configurations (Ref.4)

B-747 Scale Model Airframe Noise
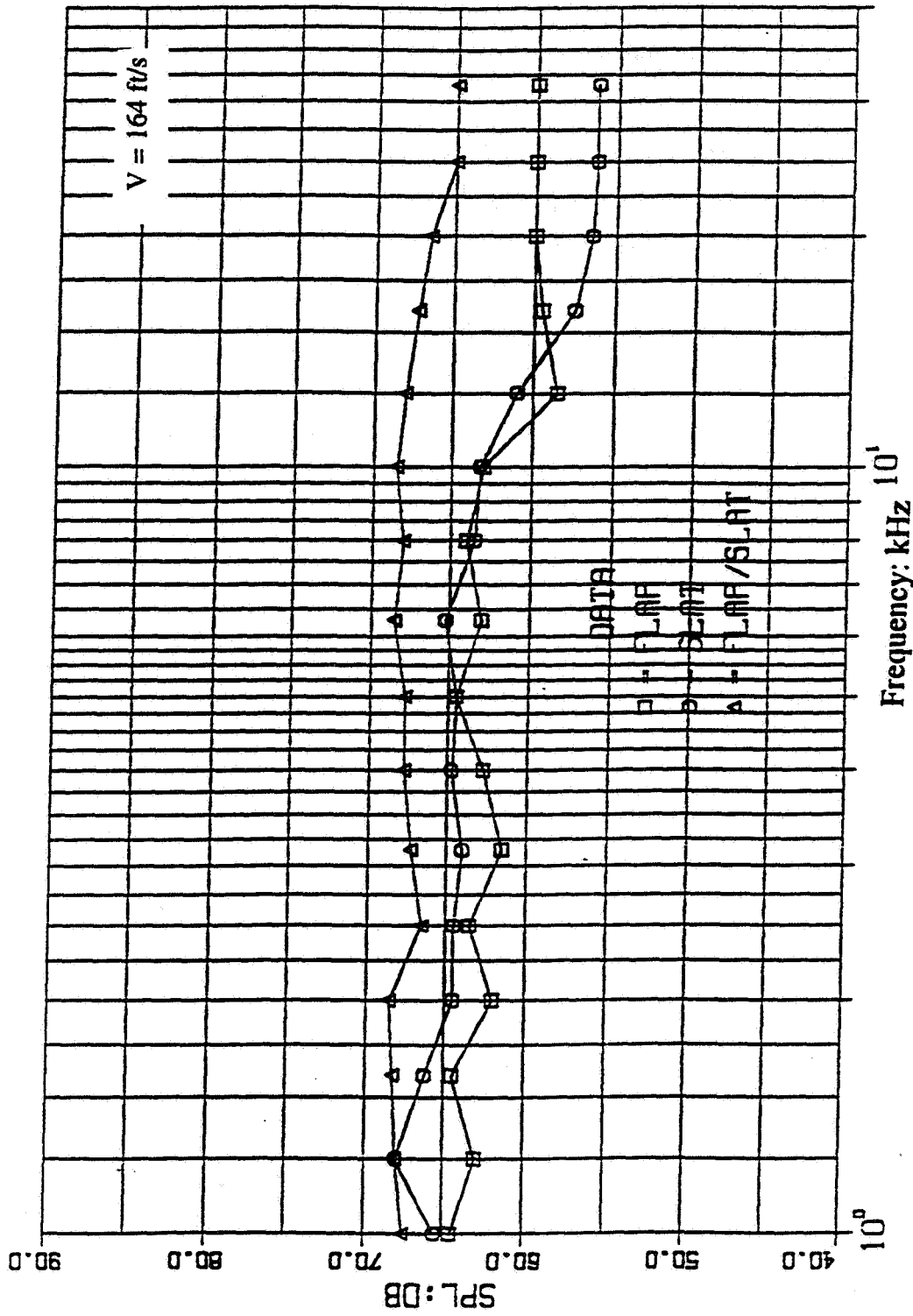
Figure 3.4   One-third-octave SPL spectra to illustrate interactions between slat and flap (Ref. 5)

B-747 Scale Model Airframe Noise
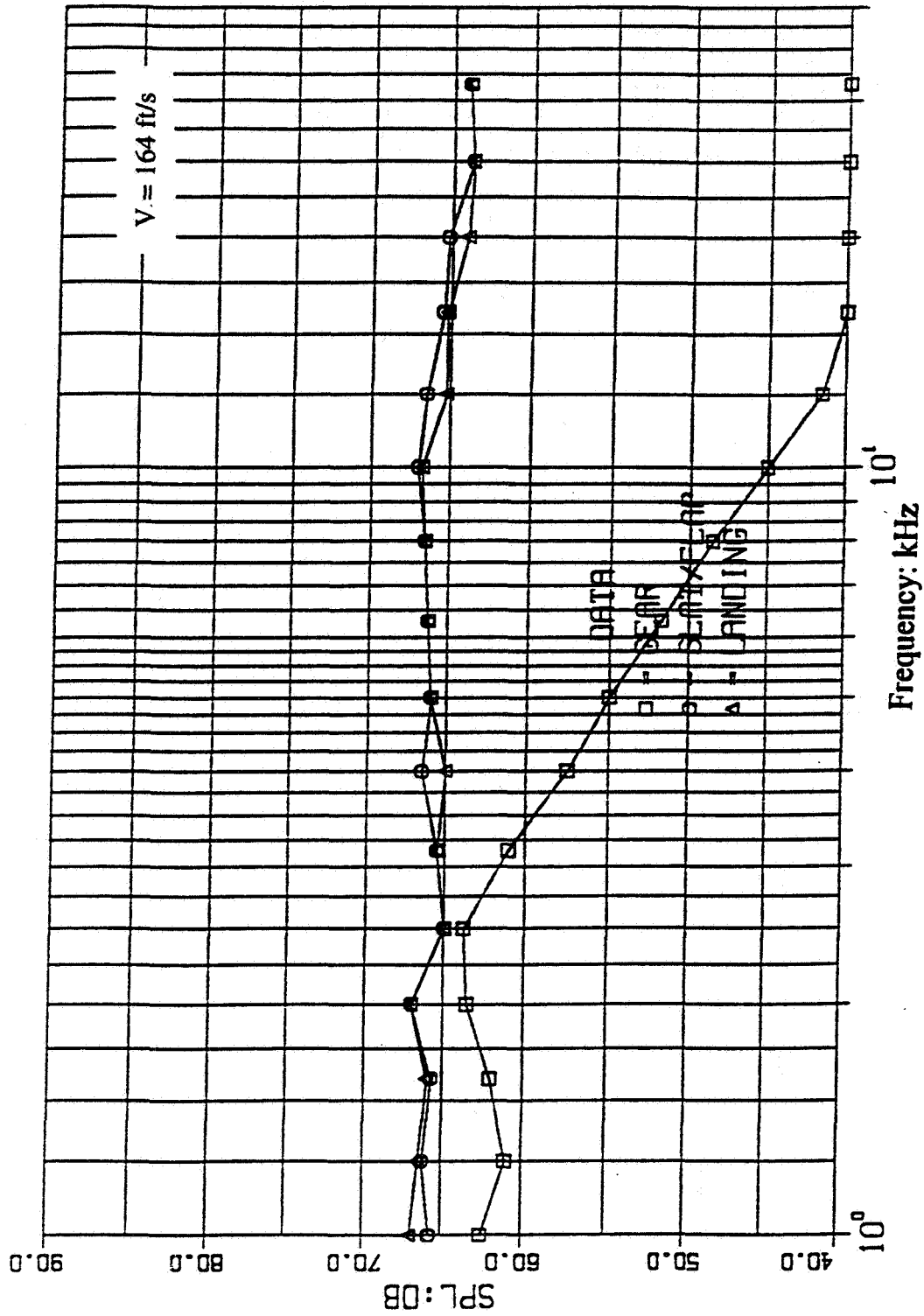
Figure 3.5 One-third-octave SPL spectra to illustrate gear effects on the airframe noise for the landing configuration (Ref. 5)

58
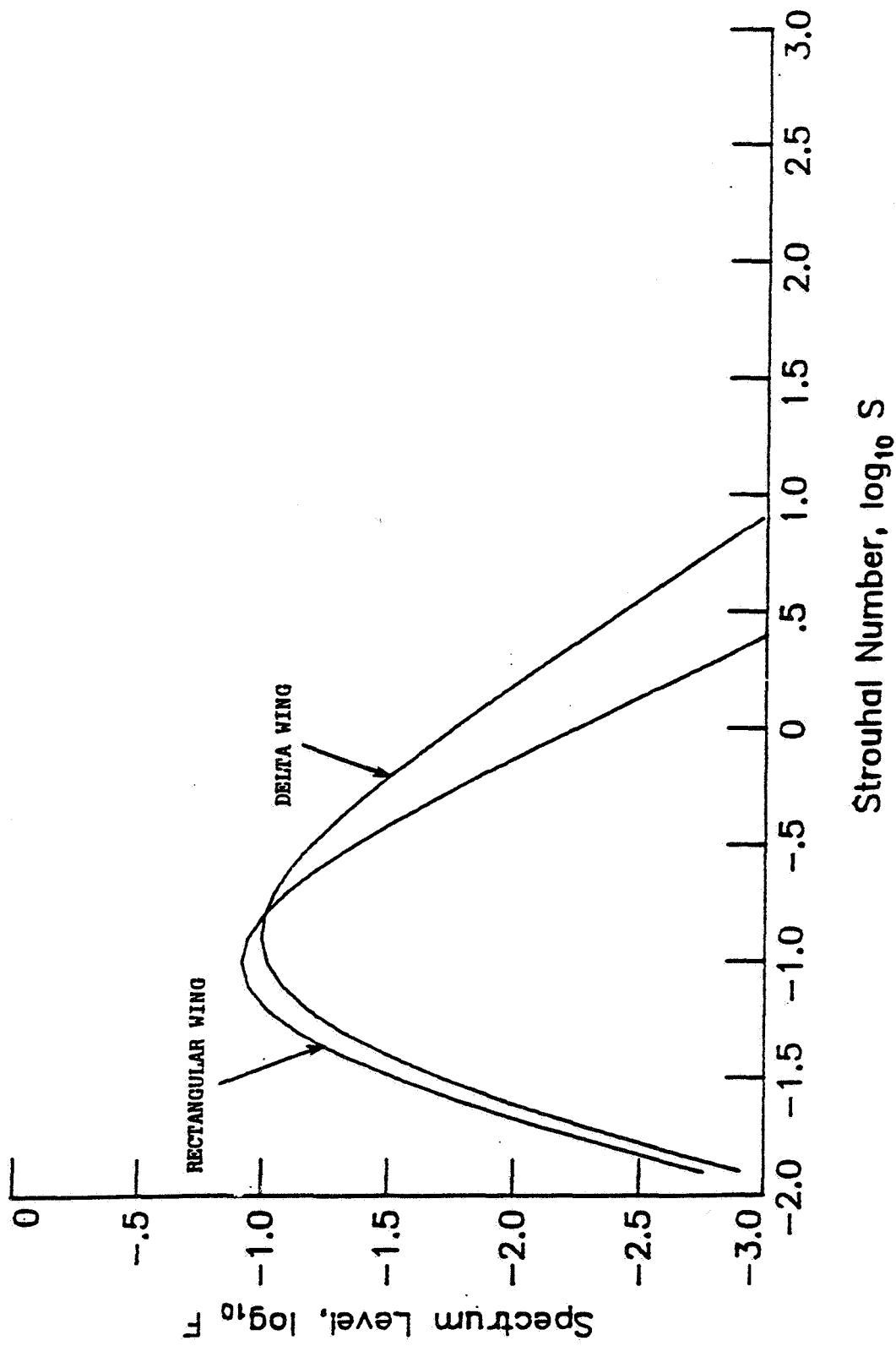
Figure 4.1 Spectrum level for clean wing, horizontal tail, and vertical tail trailing-edge noise.

(Zorumski, W.E., "Aircraft Noise Prediction Program Theoretical Manual," NASA TM 83199, 1982)

DELTA WING

RECTANGULAR WING

Strouhal Number, $\log_{10}$ S
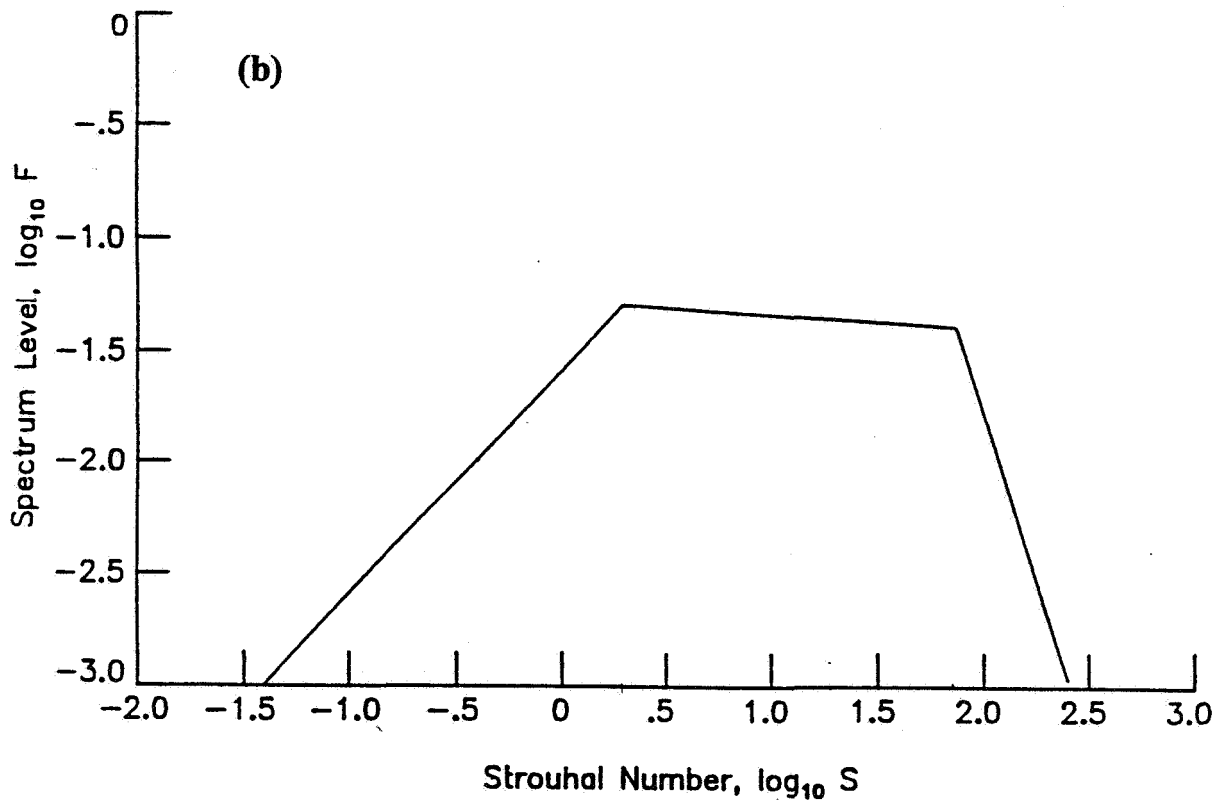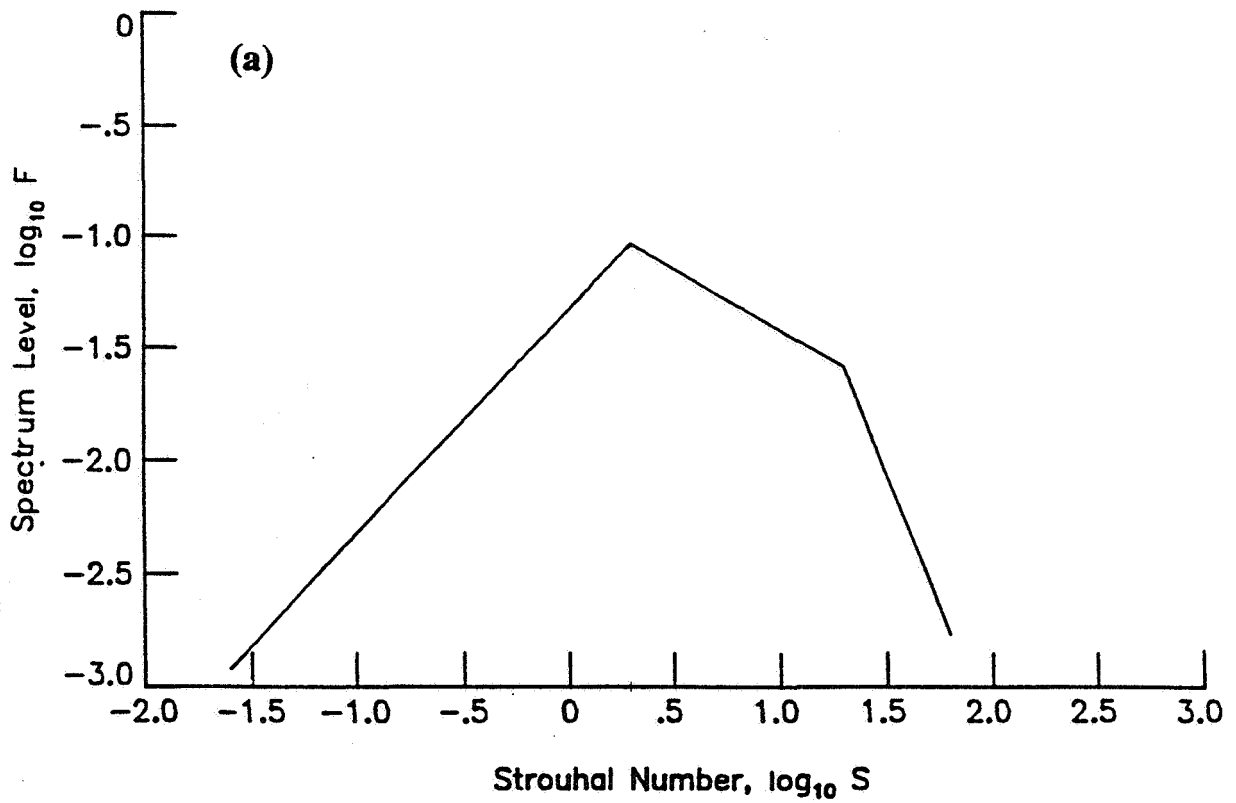
Spectrum Level, $\log_{10}$ F

Figure 4.2 Spectrum level for a) single and double slotted, b) triple slotted trailing-edge flap noise (Zorumski,W.E.,"Aircraft Noise Prediction Program Theoretical Manual," NASA TM 83199,1982)
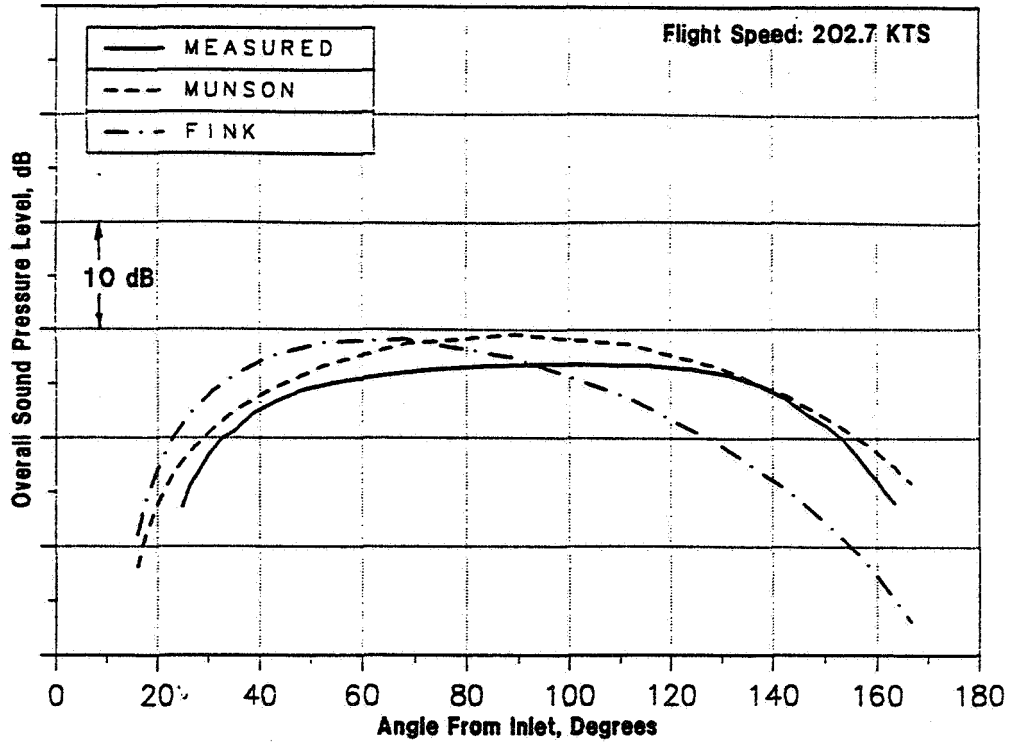
Figure 5.1 DC-9-30 Flight Test: OASPL Directivity Comparison:
Clean Configuration
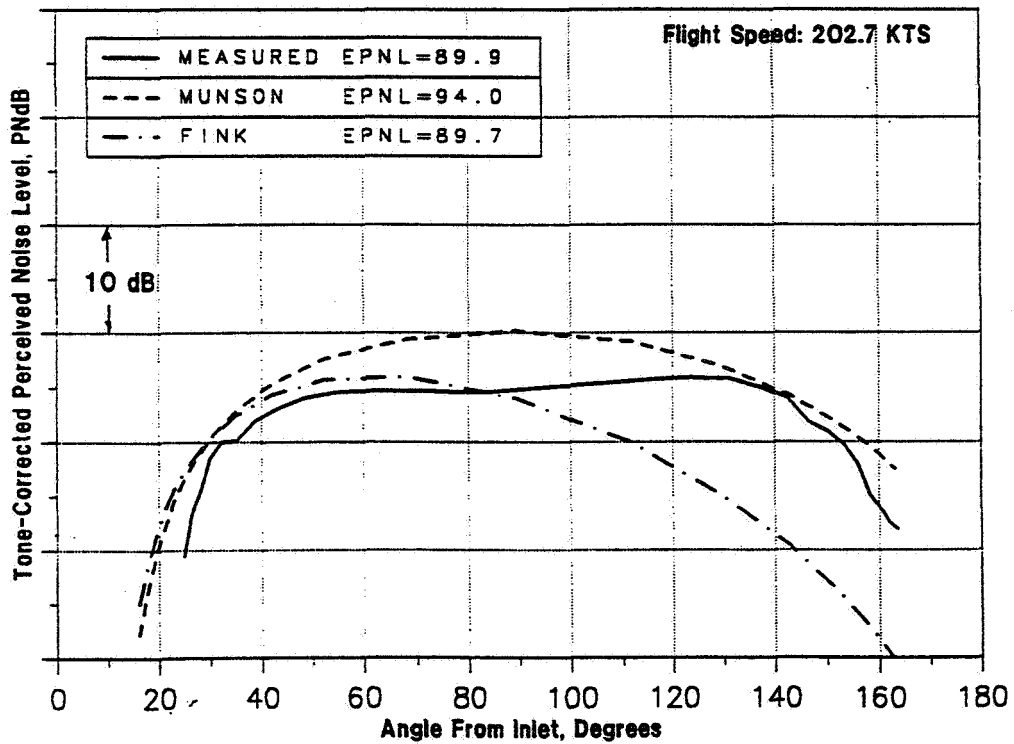
Figure 5.2 DC-9-30 Flight Test: PNLT Directivity Comparison:
Clean Configuration
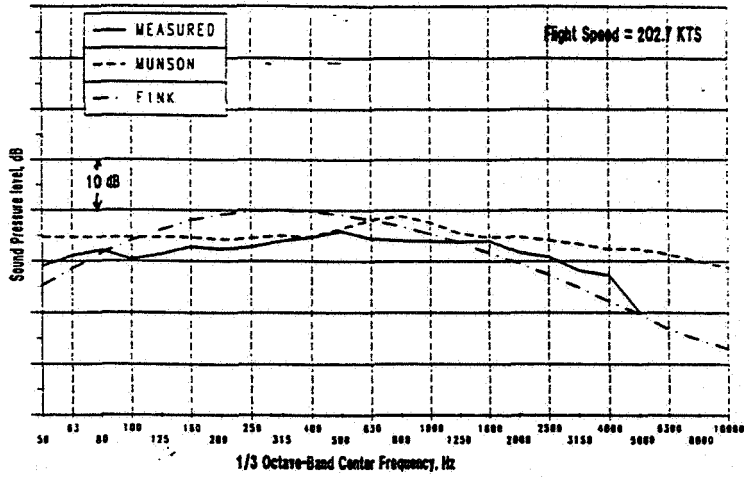
Figure 5.3 DC-9-30 Flight Test One-Third-Octave SPL Comparison:
Clean Configuration, 60 Degrees
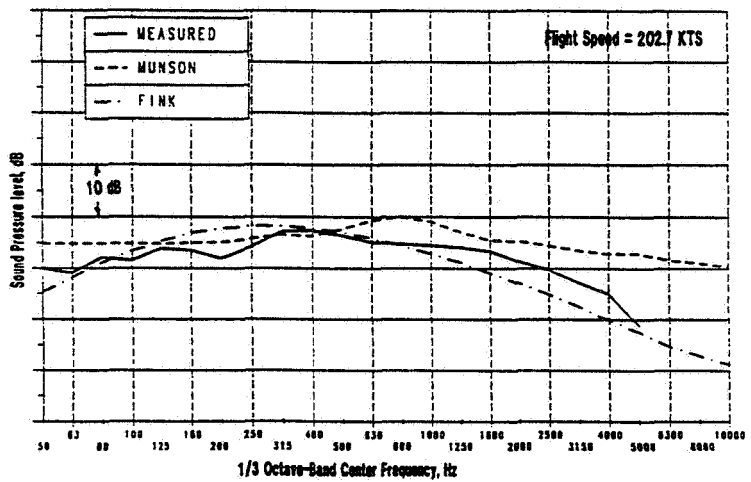
Figure 5.3 (continued) DC-9-30 Flight Test One-Third-Octave SPL Comparison:
Clean Configuration, 90 Degrees
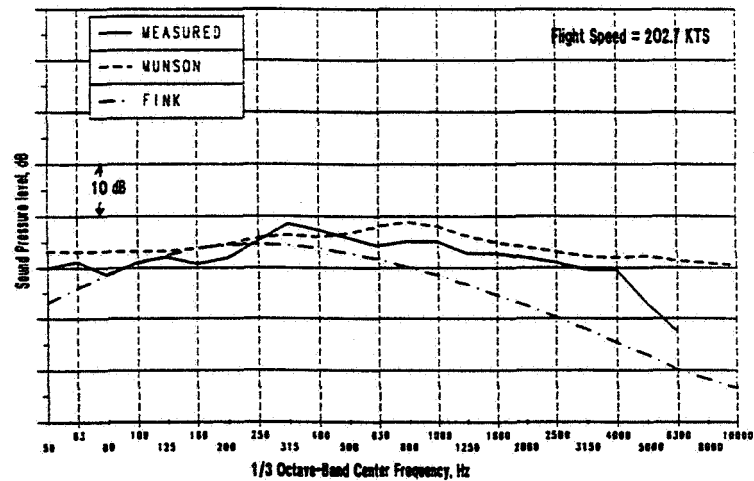
Figure 5.3 (concluded) DC-9-30 Flight Test One-Third-Octave SPL Comparison:
Clean Configuration, 120 Degrees
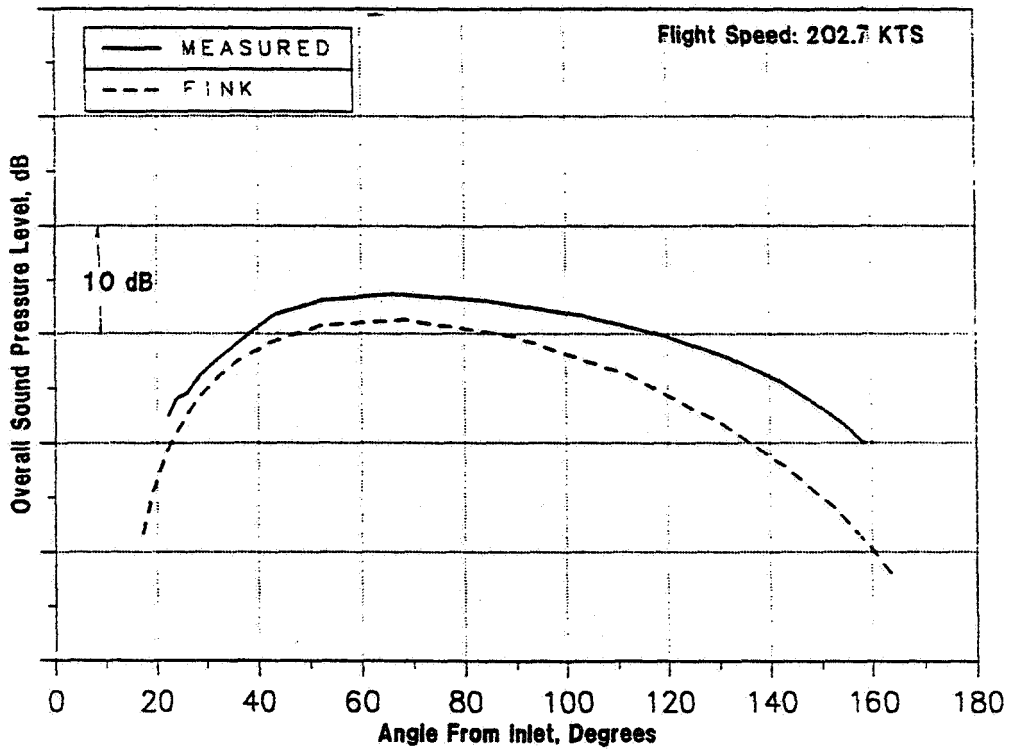
Figure 5.4 DC-9-30 Flight Test: OASPL Directivity Comparison:
Slat Deployed Configuration
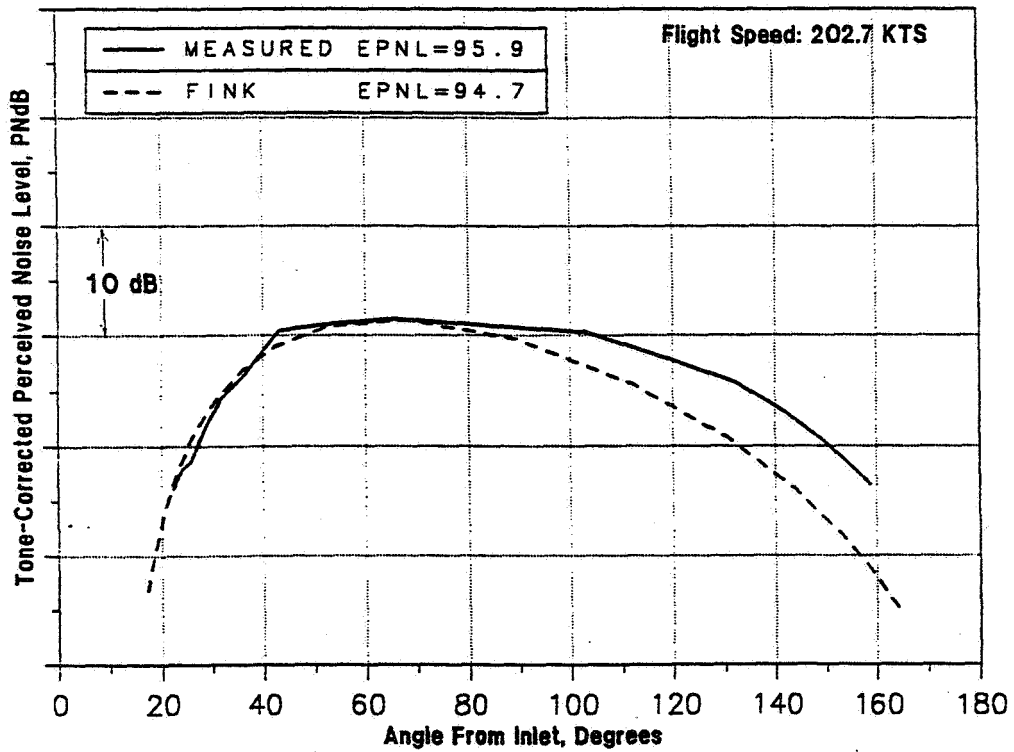
Figure 5.5 DC-9-30 Flight Test: PNLT Directivity Comparison:
Slat Deployed Configuration

63
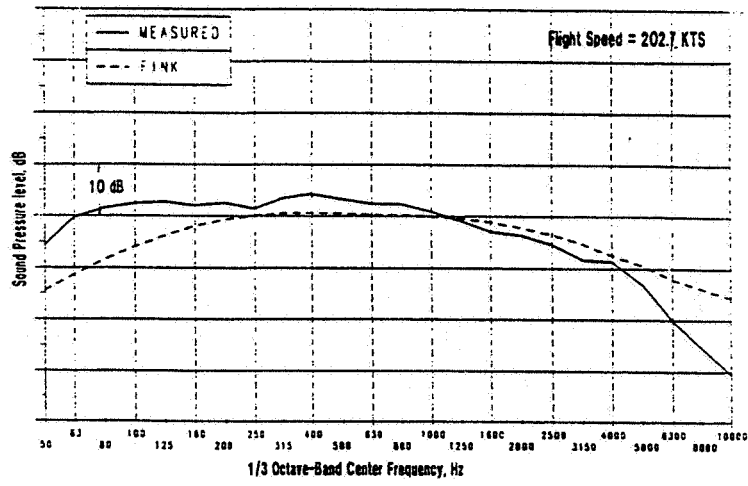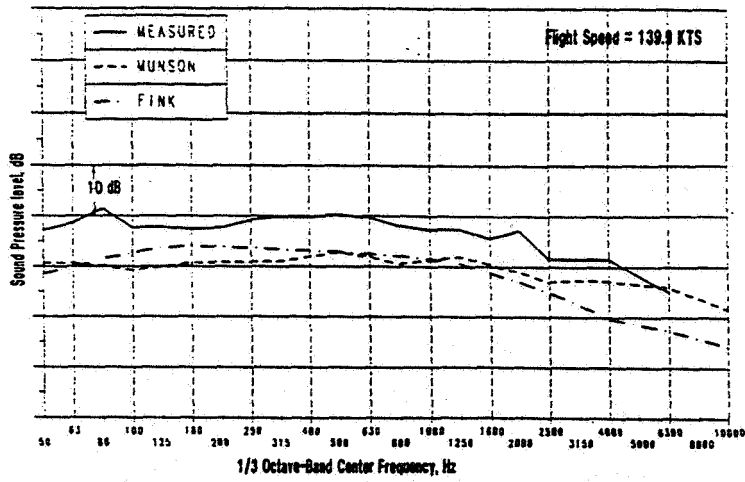
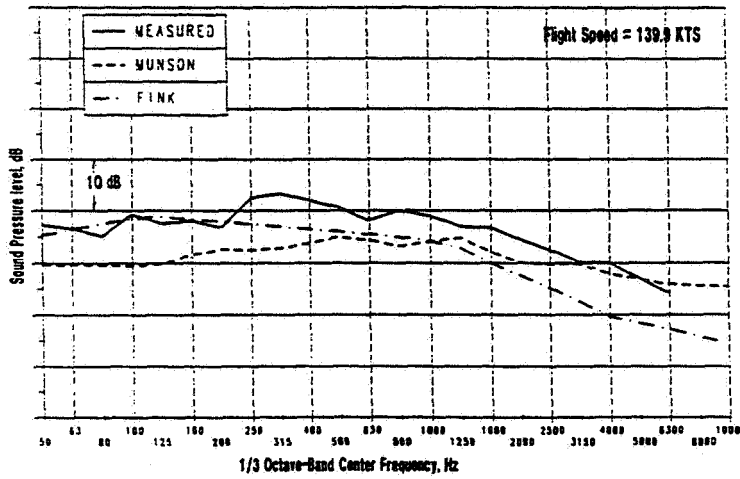Figure 5.6 DC-9-30 Flight Test: One-Third-Octave SPL Comparison:
Slat Deployed Configuration, 60 Degrees
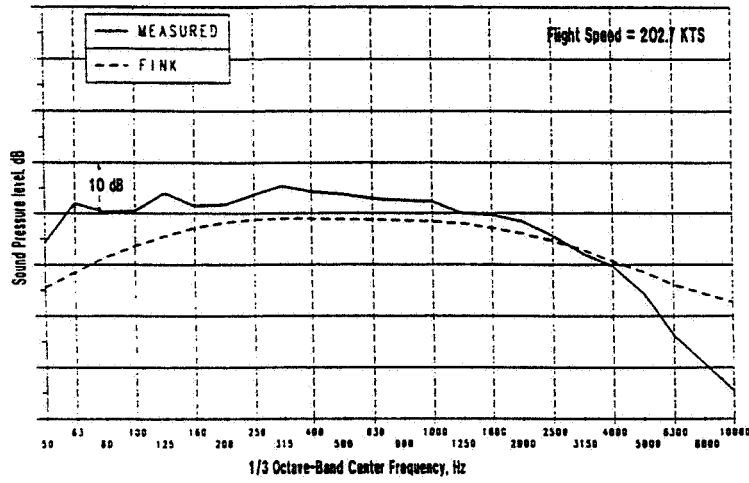
Figure 5.6 (continued) DC-9-30 Flight Test: One-Third-Octave SPL Comparison:
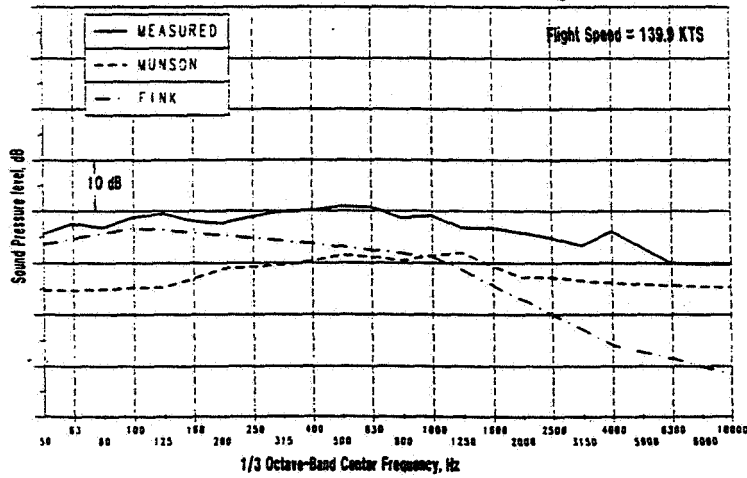Slat Deployed Configuration, 90 Degrees
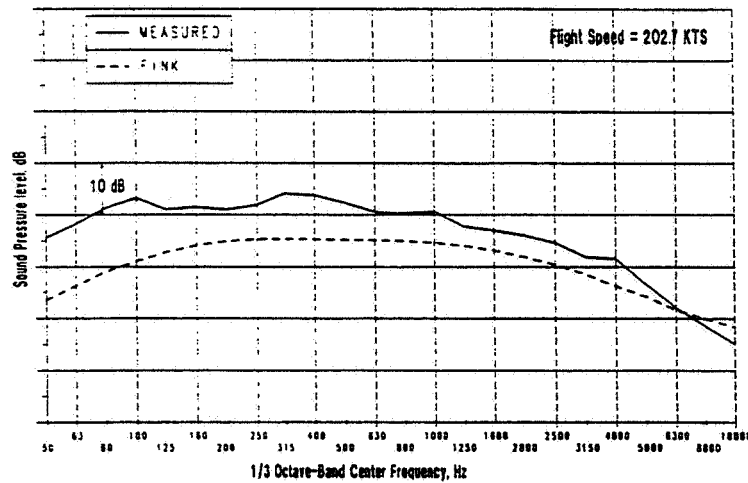
Figure 5.6 (concluded) DC-9-30 Flight Test: One-Third-Octave SPL Comparison:
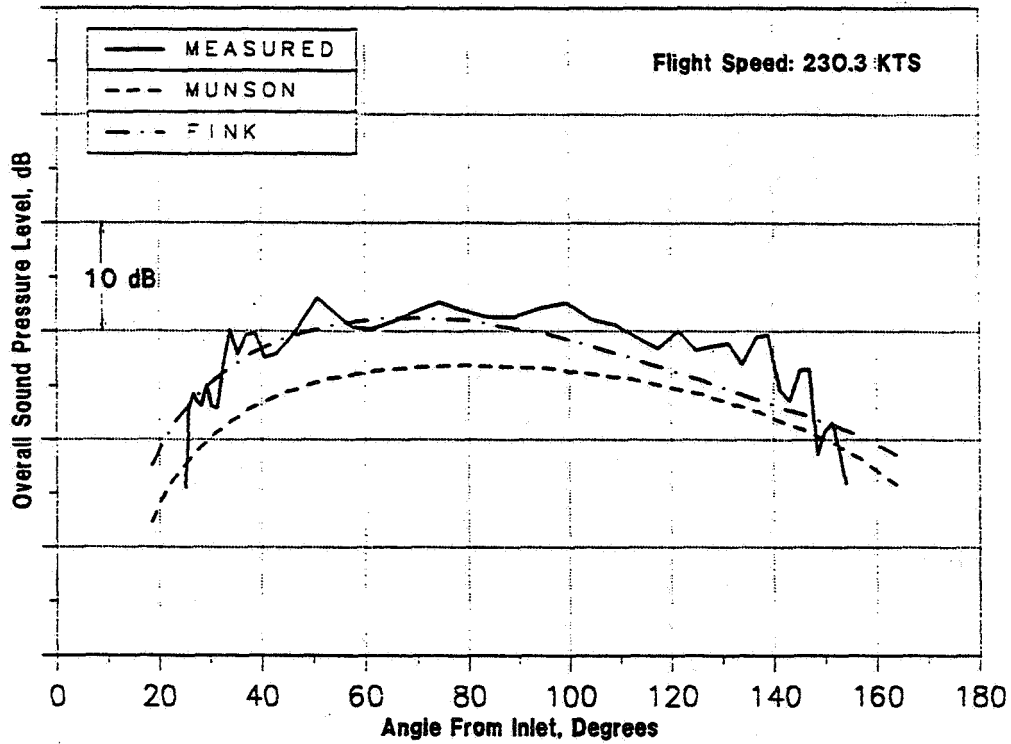Slat Deployed Configuration, 120 Degrees

64
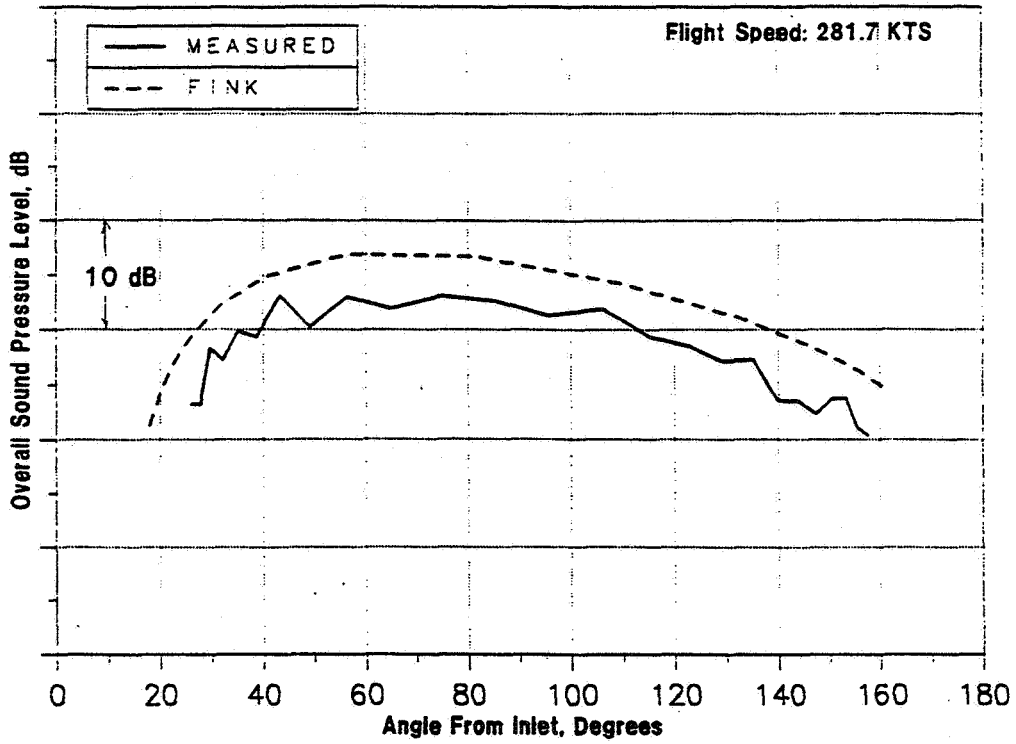
Figure 5.7 DC-9-30 Flight Test: OASPL Directivity Comparison:
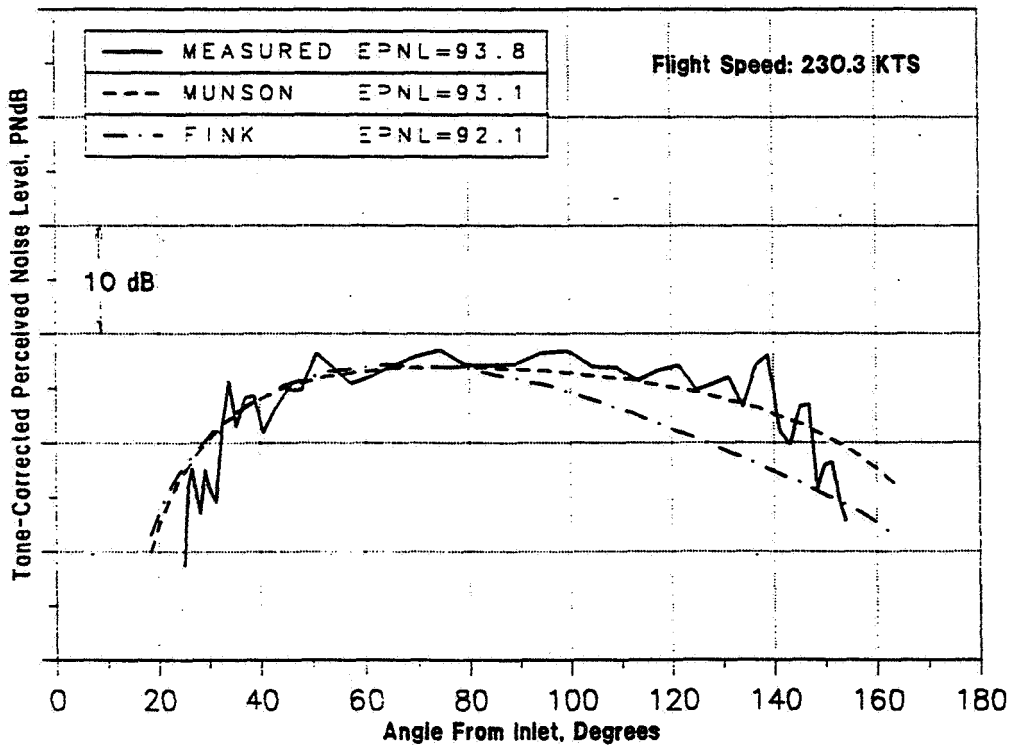**Landing Gear Deployed Configuration**
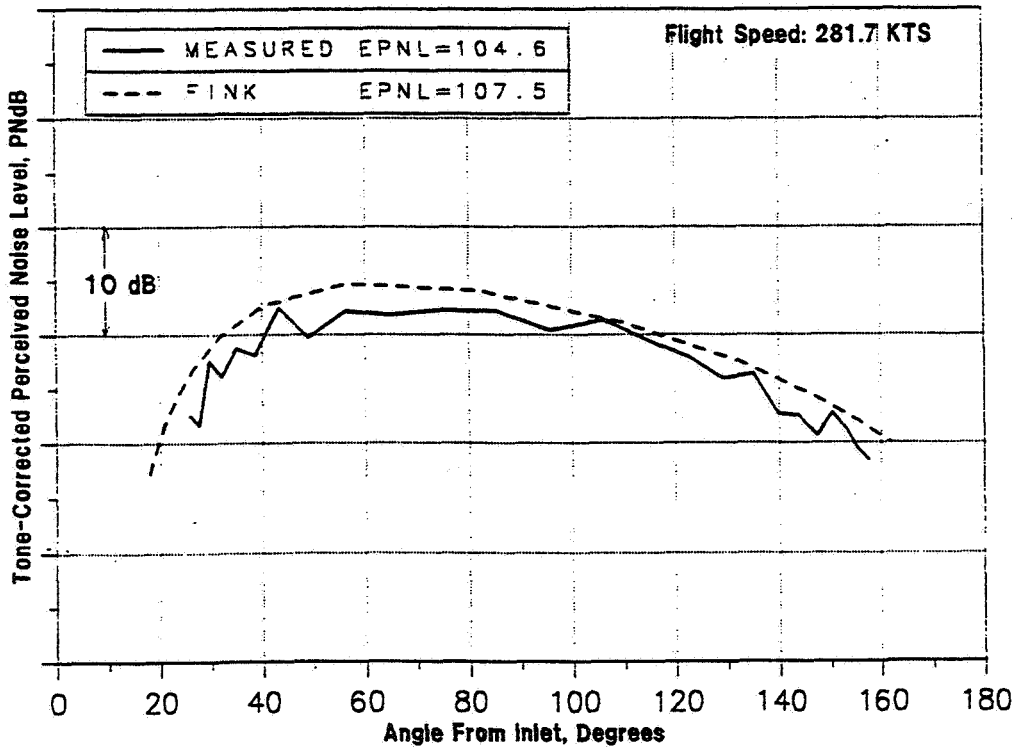
Figure 5.8 DC-9-30 Flight Test: PNLT Directivity Comparison:
Landing Gear Deployed Configuration
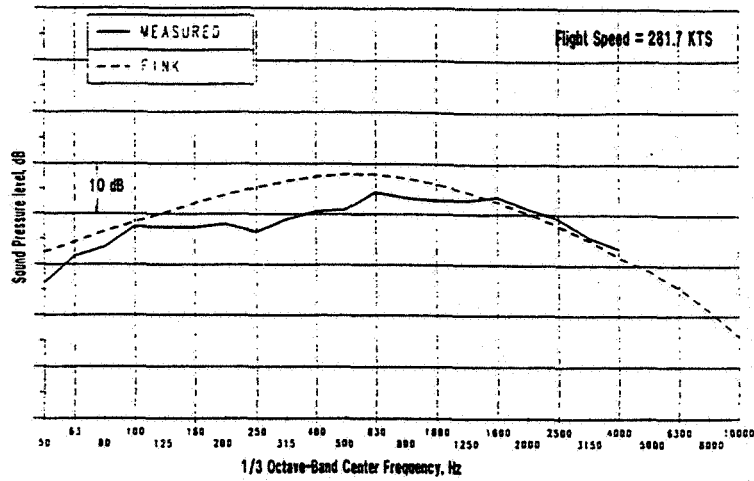
Figure 5.9 DC-9-30 Flight Test: One-Third-Octave SPL Comparison:
Landing Gear Deployed Configuration, 60 Degrees
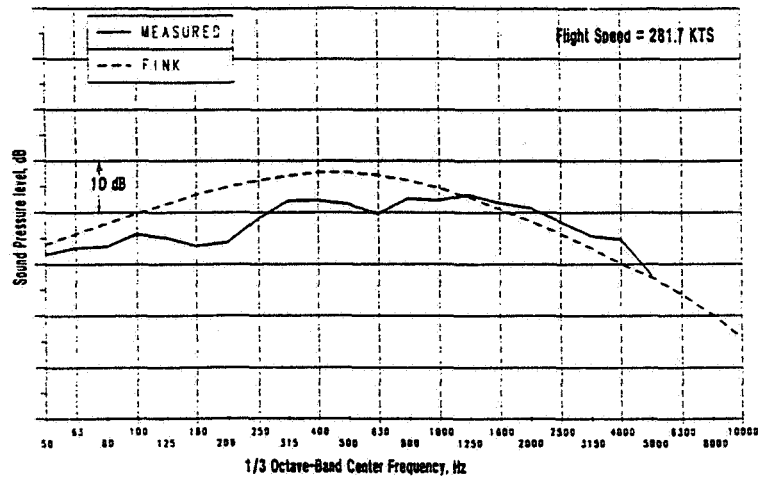
Figure 5.9 (continued) DC-9-30 Flight Test: One-Third-Octave SPL Comparison:
Landing Gear Deployed Configuration, 90 Degrees
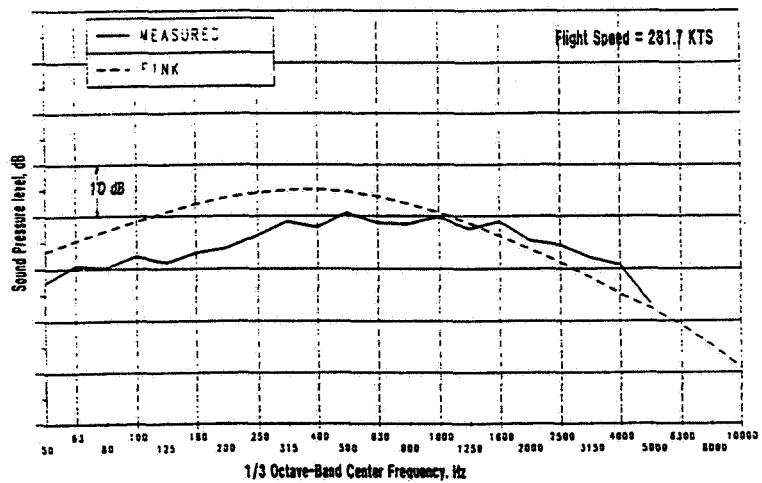
Figure 5.9 (concluded) DC-9-30 Flight Test: One-Third-Octave SPL Comparison:
Landing Gear Deployed Configuration, 120 Degrees

66
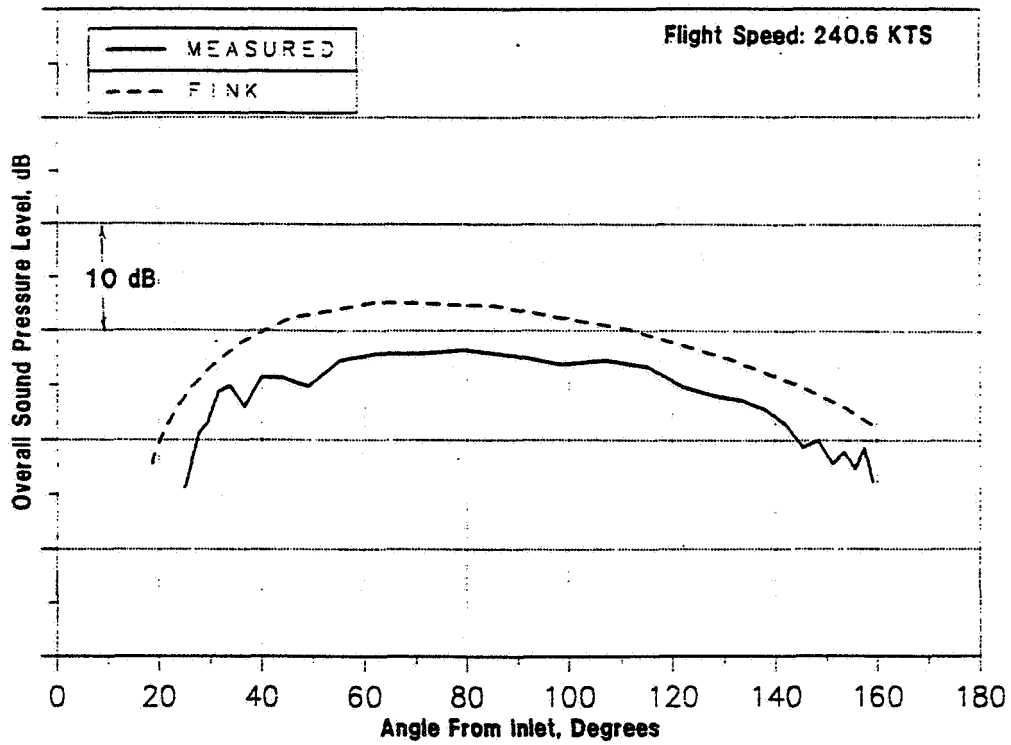
**Figure 5.10 DC-9-30 Flight Test: OASPL Directivity Comparison:
Landing Gear And Slat Deployed Configuration**
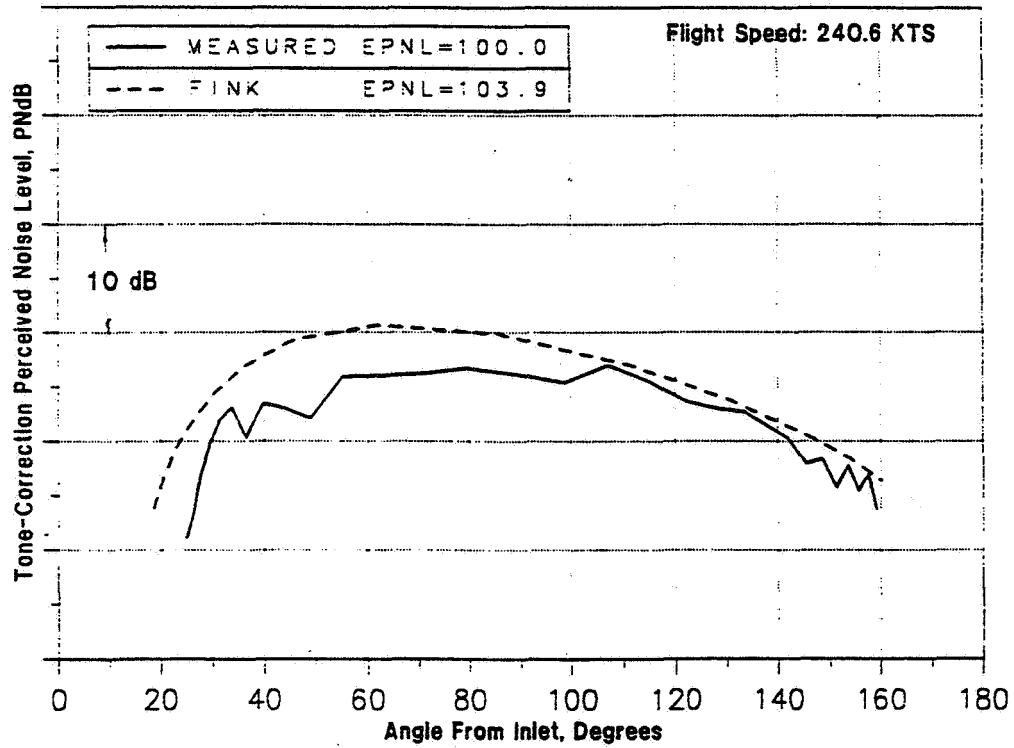
**Figure 5.11 DC-9-30 Flight Test: PNLT Directivity Comparison:
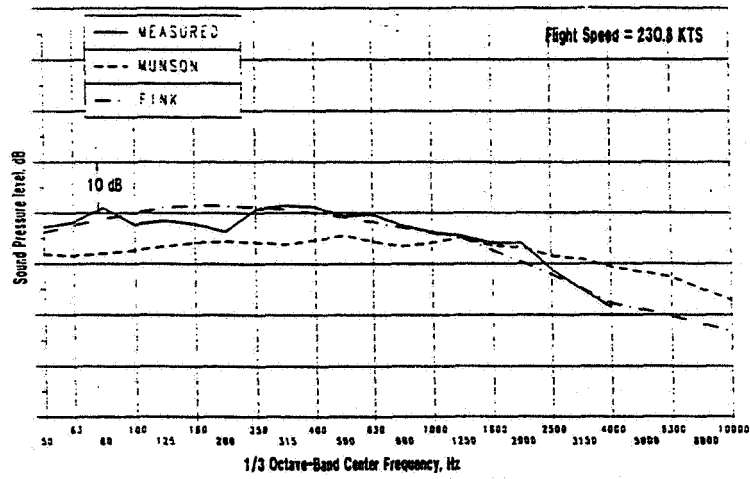Landing Gear And Slat Deployed Configuration**
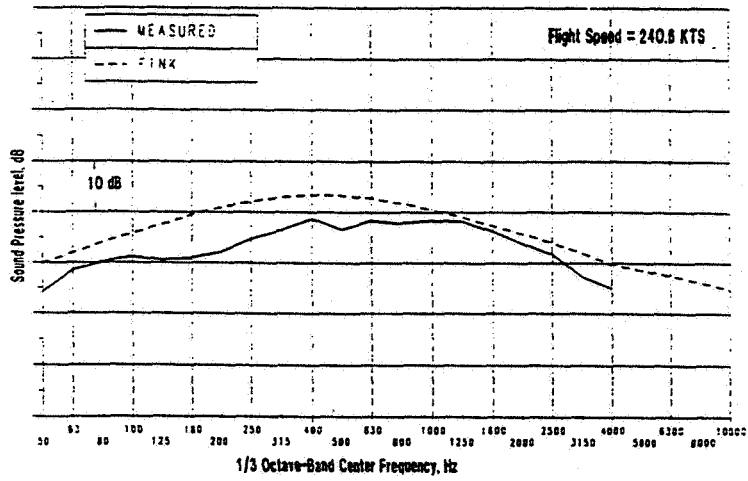
Figure 5.12 DC-9-30 Flight Test: One-Third-Octave SPL Comparison:
Landing Gear And Slat Deployed Configuration, 60 Degrees
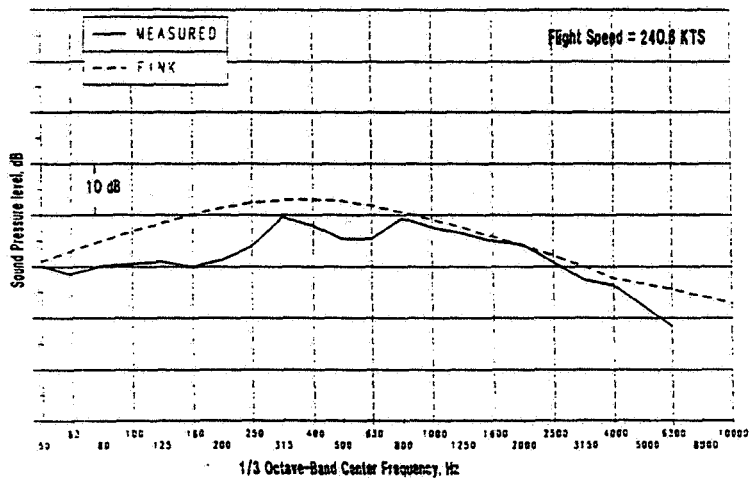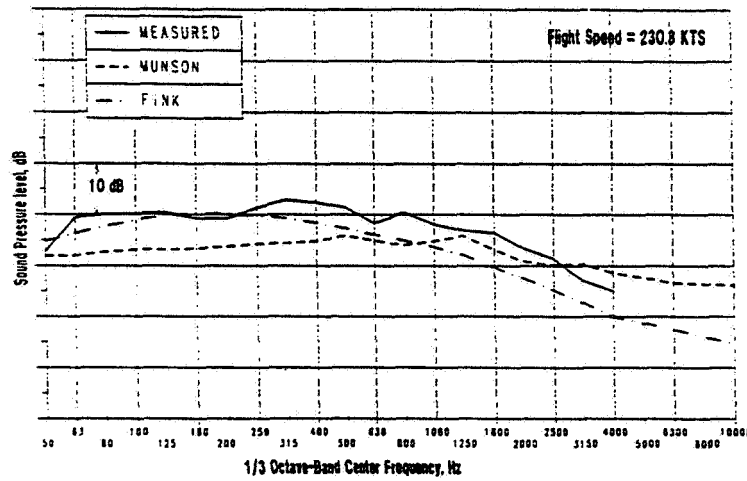

Figure 5.12 (continued) DC-9-30 Flight Test: One-Third-Octave SPL Comparison:
Landing Gear And Slat Deployed Configuration, 90 Degrees
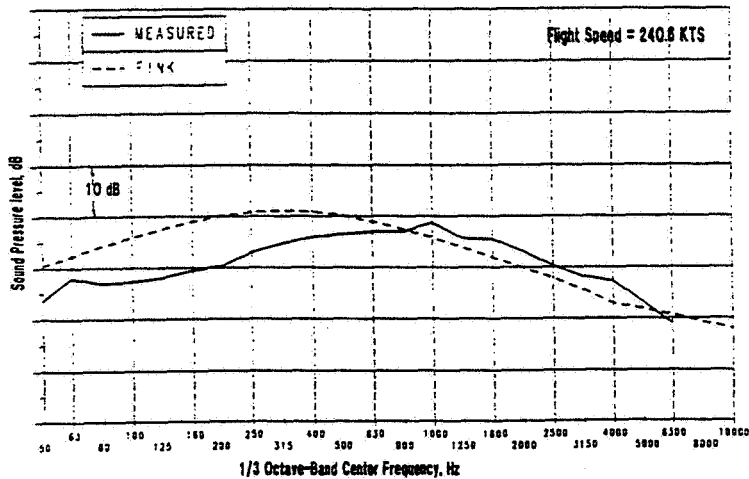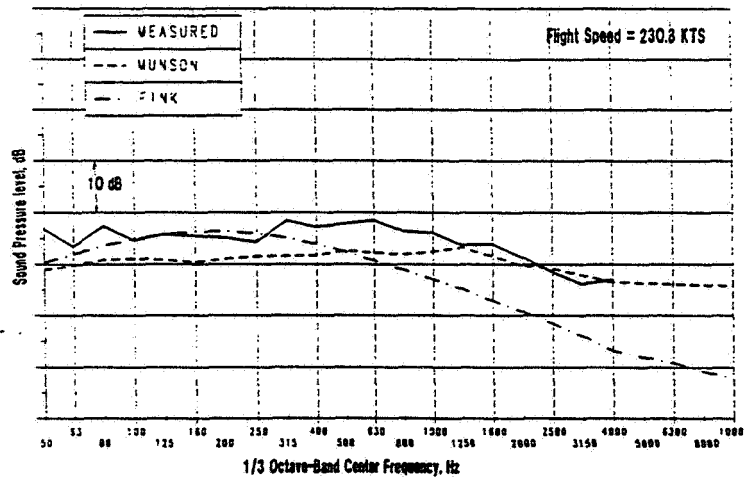

Figure 5.12 (concluded) DC-9-30 Flight Test: One-Third-Octave SPL Comparison:
Landing Gear And Slat Deployed Configuration, 120 Degrees

68
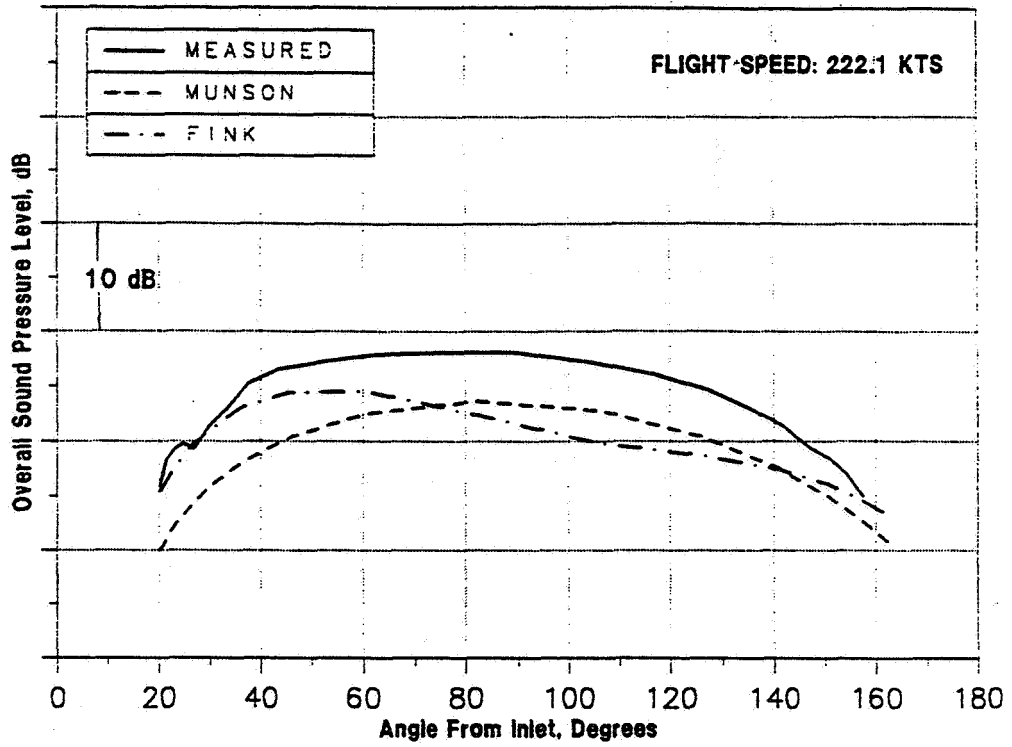
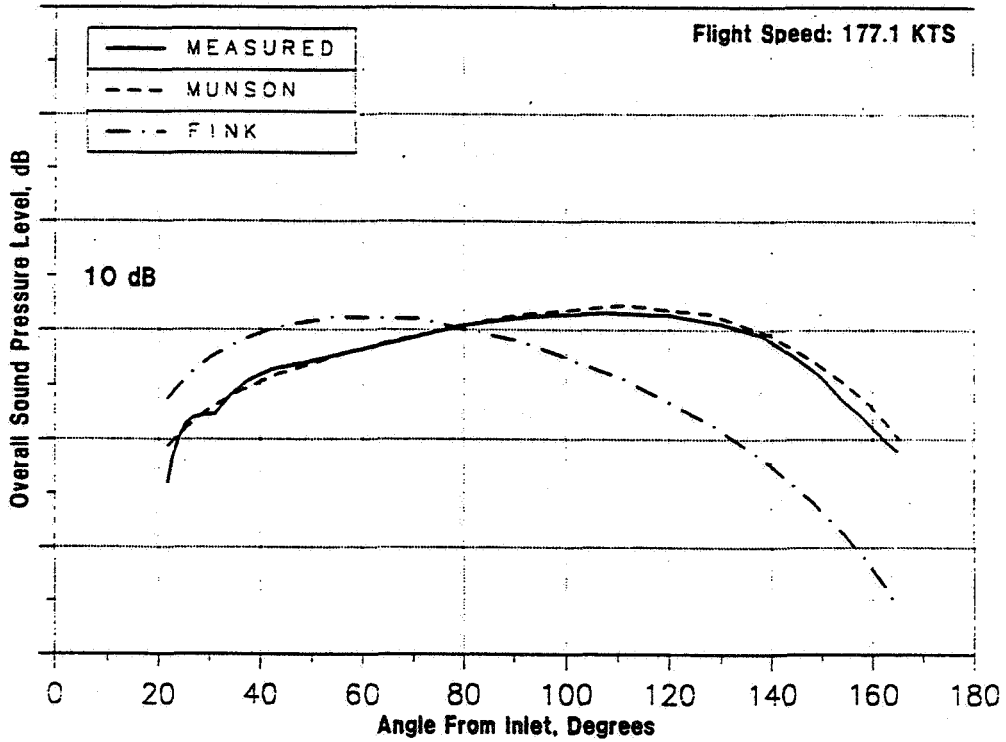**Figure 5.13 DC-9-30 Flight Test: OASPL Directivity Comparison:**
Slat And 20 Degrees Flap Deployed Configuration
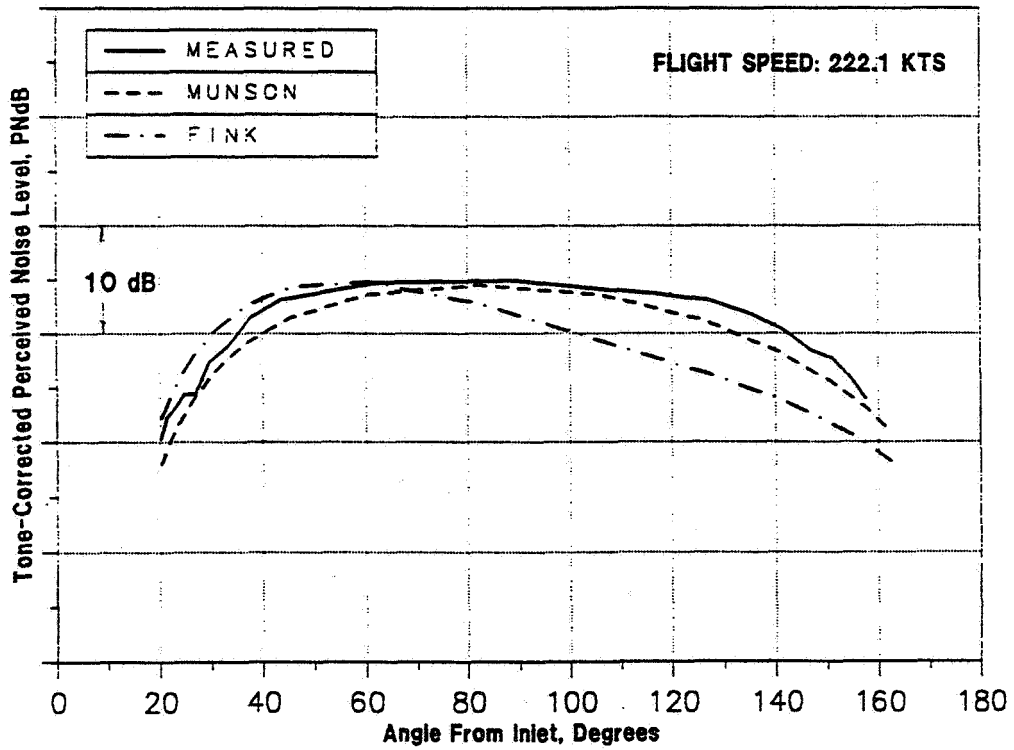
Figure 5.14 DC-9-30 Flight Test: PNLT Directivity Comparison:
Slat And 20 Degrees Flap Deployed Configuration

69
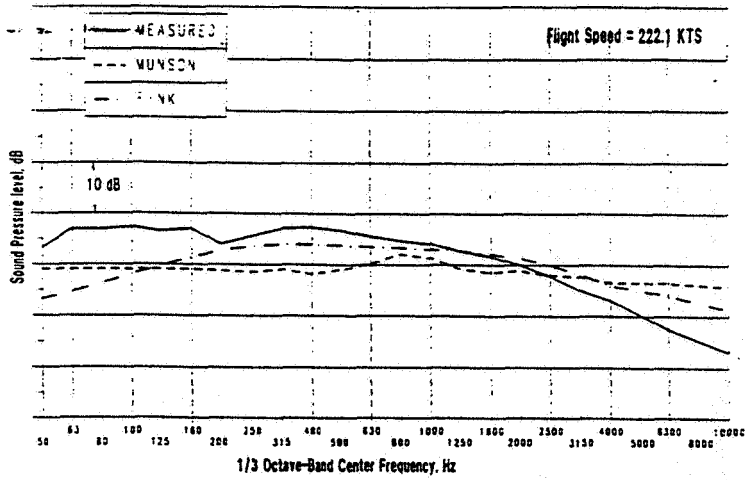
Figure 5.15 DC-9-30 Flight Test: One-Third-Octave SPL Comparison:
Slat and 20 Degrees Flap Deployed Configuration, 60 Degrees
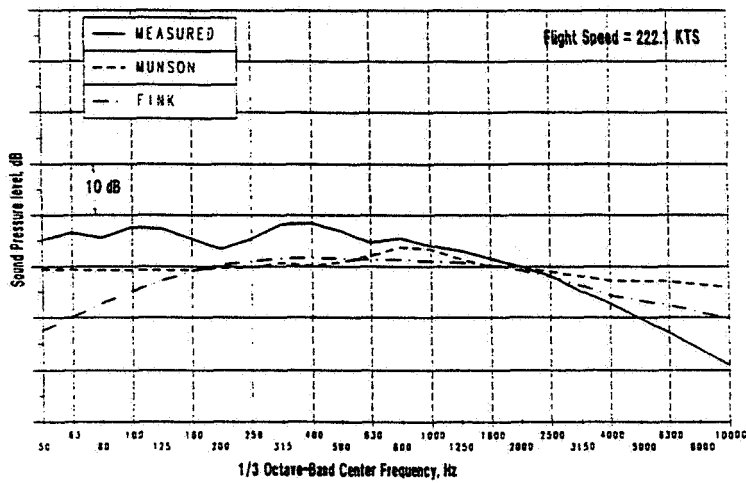
Figure 5.15 (continued) DC-9-30 Flight Test: One-Third-Octave SPL Comparison:
Slat and 20 Degrees Flap Deployed Configuration, 90 Degrees
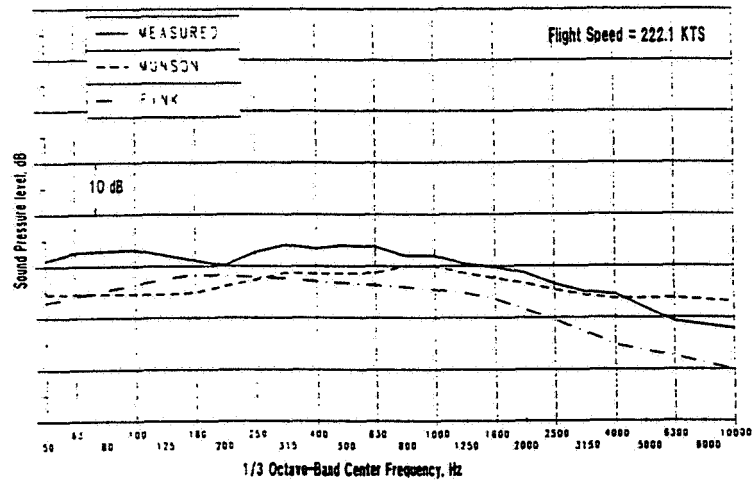
Figure 5.15 (concluded) DC-9-30 Flight Test: One-Third-Octave SPL Comparison:
Slat and 20 Degrees Flap Deployed Configuration, 120 Degrees
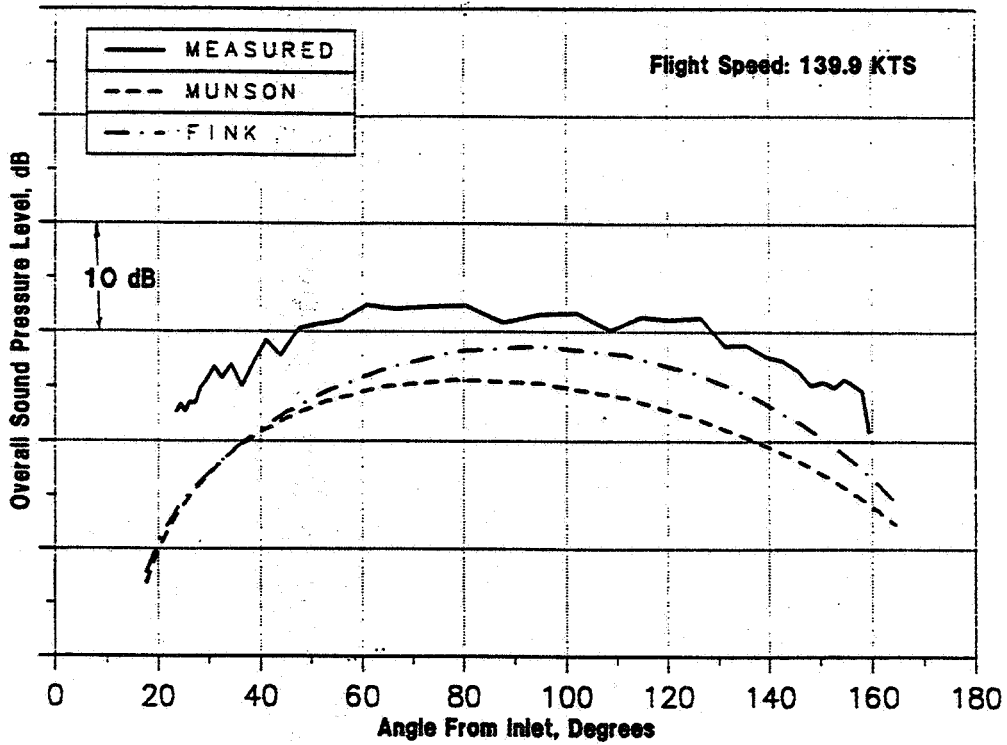
**Figure 5.16 DC-9-30 Flight Test: OASPL Directivity Comparison:
Slat And 50 Degrees Flap Deployed Configuration**
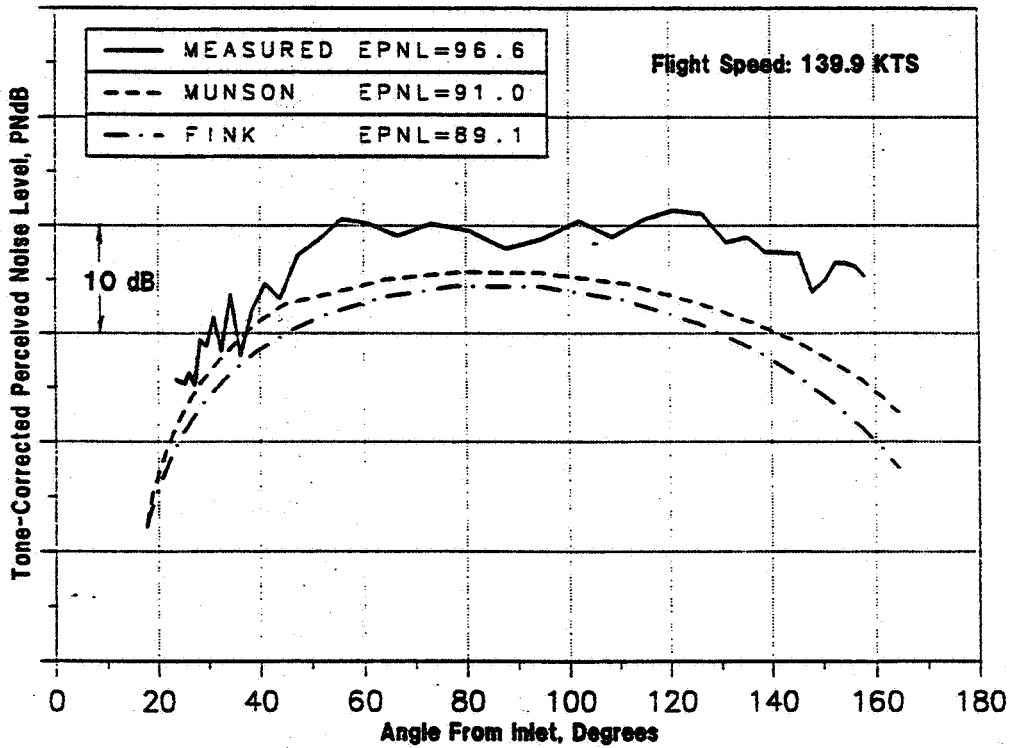
**Figure 5.17 DC-9-30 Flight Test: PNLT Directivity Comparison:
Slat And 50 Degrees Flap Deployed Configuration**

Figure 5.18 DC-9-30 Flight Test: One-Third-Octave SPL Comparison: Slat and 50 Degrees Flap Deployed Configuration, 60 Degrees

Figure 5.18 (continued) DC-9-30 Flight Test: One-Third-Octave SPL Comparison: Slat and 50 Degrees Flap Deployed Configuration, 90 Degrees
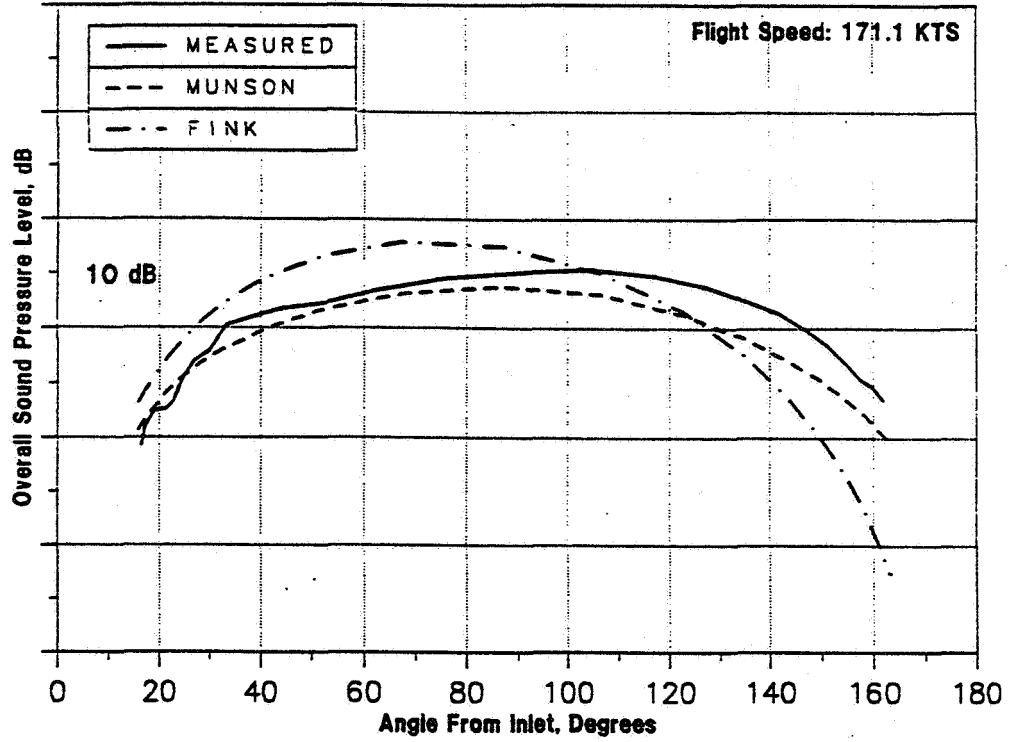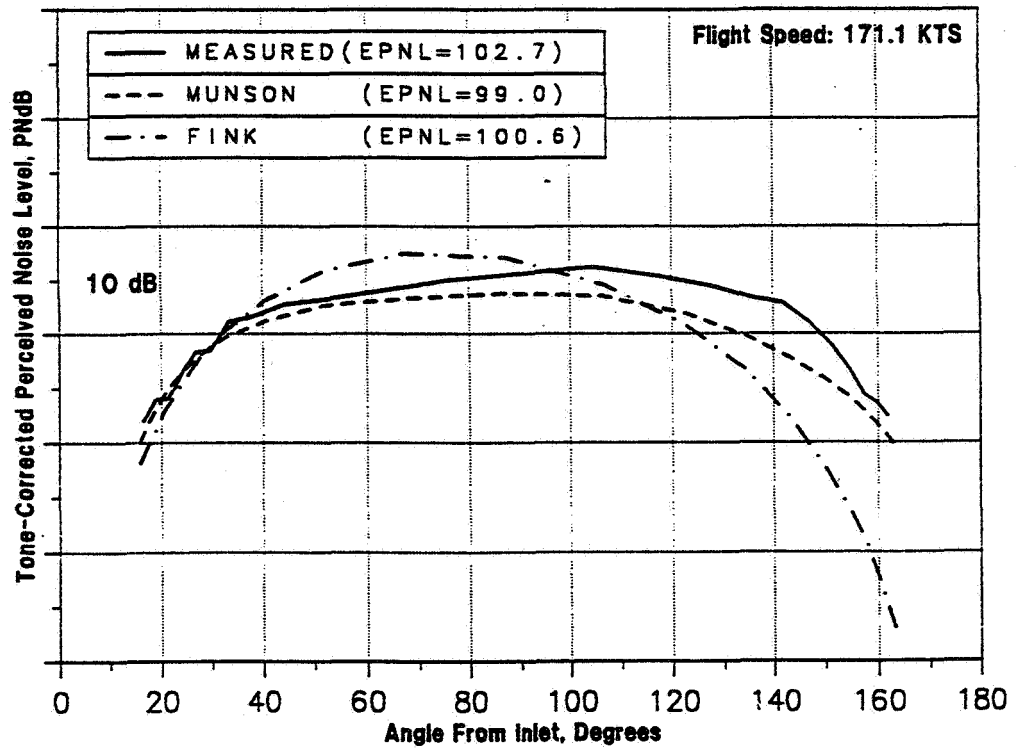

Figure 5.18 (concluded) DC-9-30 Flight Test: One-Third-Octave SPL Comparison: Slat and 50 Degrees Flap Deployed Configuration, 120 Degrees

72

Figure 5.19 DC-9-30 Flight Test: OASPL Directivity Comparison:
Slat, Landing Gear And 50 Degrees Flap Deployed Configuration

Figure 5.20 DC-9-30 Flight Test: PNLT Directivity Comparison:
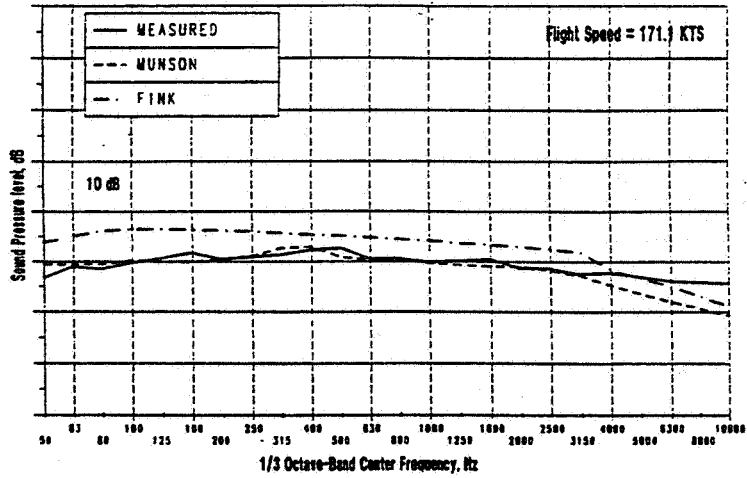**Slat, Landing Gear And 50 Degrees Flap Deployed Configuration**

73

Figure 5.21 DC-9-30 Flight Test: One-Third-Octave SPL Comparison:
Slat, Landing Gear And 50 Degrees Flap Deployed Configuration, 60 Degrees
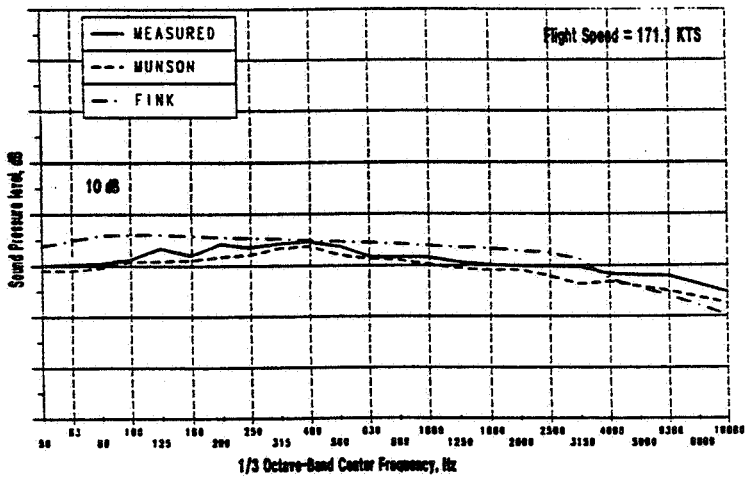

Figure 5.21 (continued) DC-9-30 Flight Test: One-Third-Octave SPL Comparison:
Slat, Landing Gear And 50 Degrees Flap Deployed Configuration, 90 Degrees
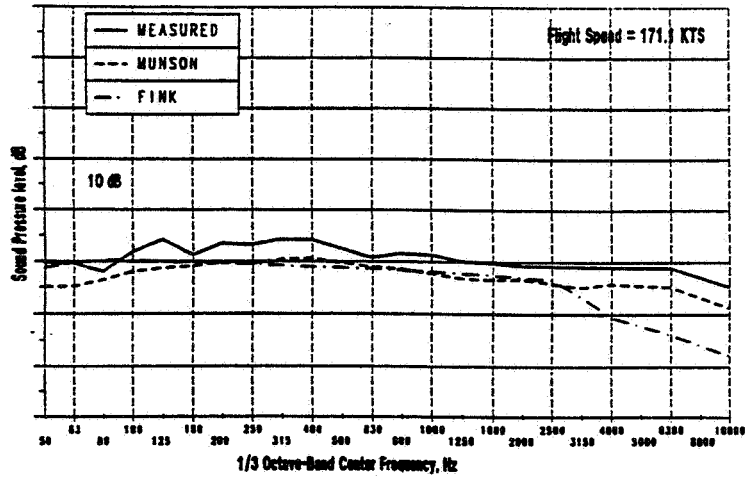

Figure 5.21 (concluded) DC-9-30 Flight Test: One-Third-Octave SPL Comparison:
Slat, Landing Gear And 50 Degrees Flap Deployed Configuration, 120 Degrees

74

Figure 5.22 DC-10-10 Flight Test: OASPL Directivity Comparison: Clean Configuration
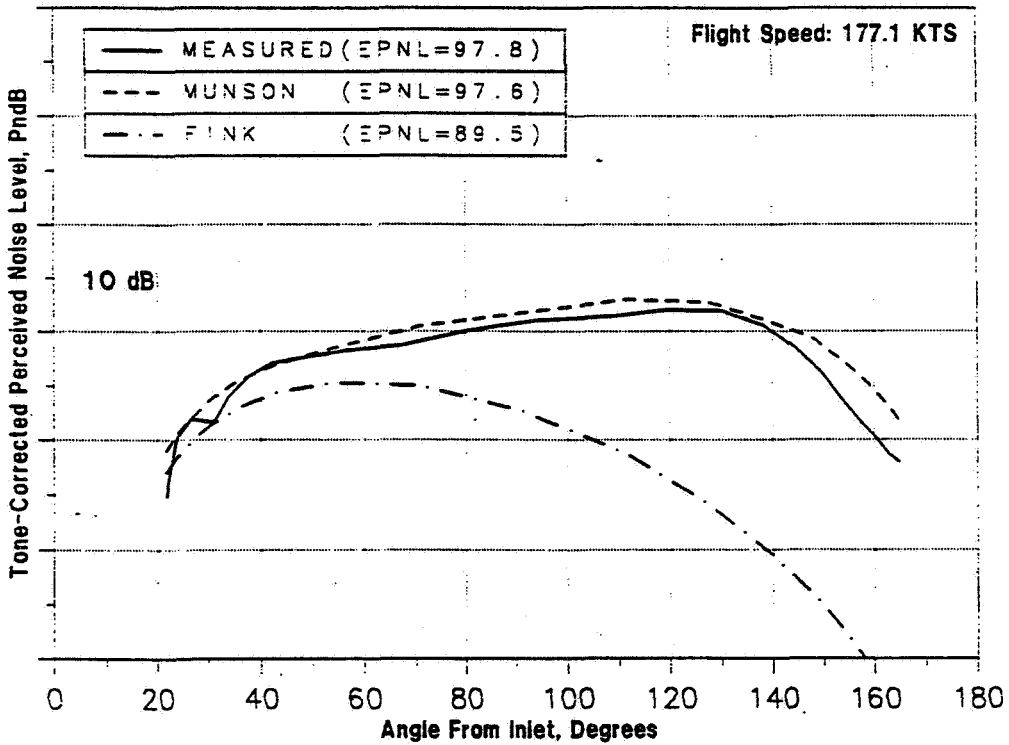
Figure 5.23 DC-10-10 Flight Test: PNLT Directivity Comparison: Clean Configuration
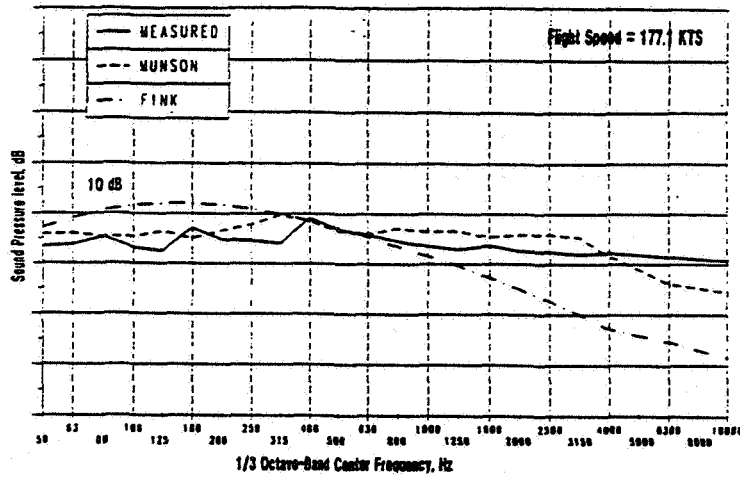
Figure 5.24 DC-10-10 Flight Test: One-Third-Octave SPL Comparison:
Clean Configuration, 60 Degrees
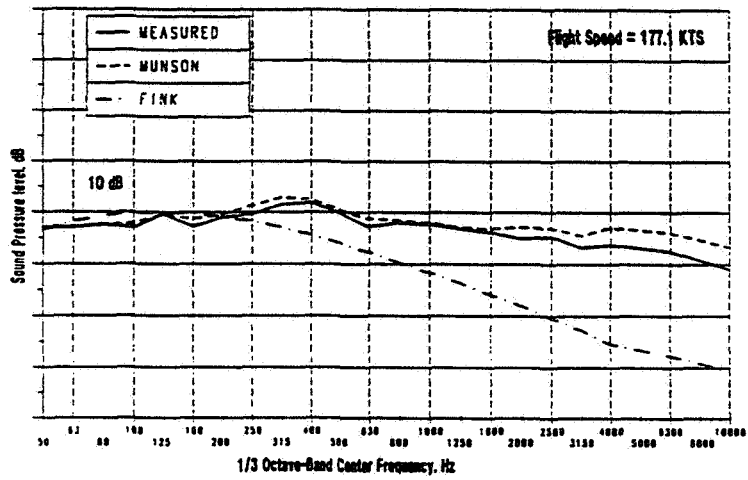
Figure 5.24 (continued) DC-10-10 Flight Test: One-Third-Octave SPL Comparison:
Clean Configuration, 90 Degrees
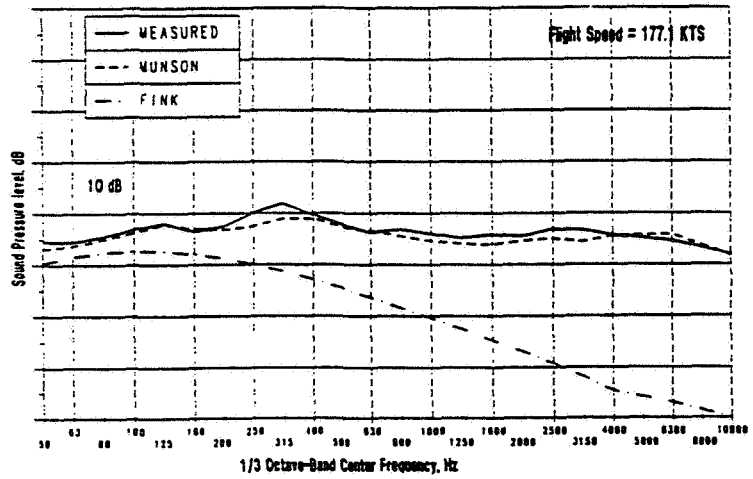
Figure 5.24 (concluded) DC-10-10 Flight Test: One-Third-Octave SPL Comparison:
Clean Configuration, 120 Degrees

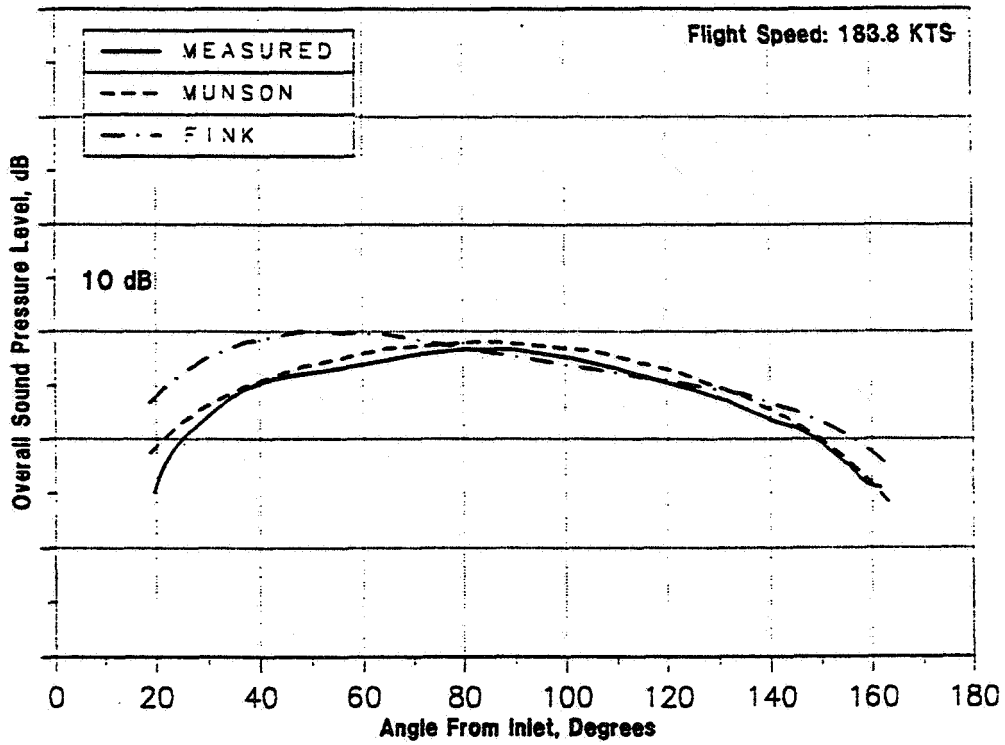**Figure 5.25 DC-10-10 Flight Test: OASPL Directivity Comparison:
Slat and 35 Degrees Flap Deployed Configuration**

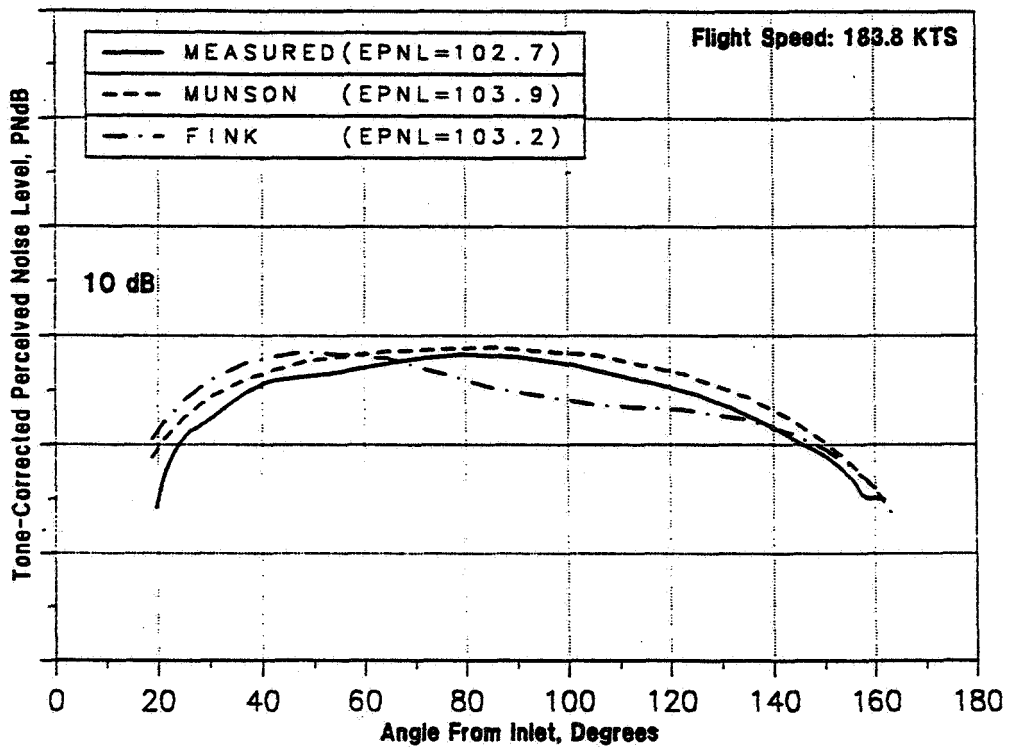**Figure 5.26 DC-10-10 Flight Test: PNLT Directivity Comparison:
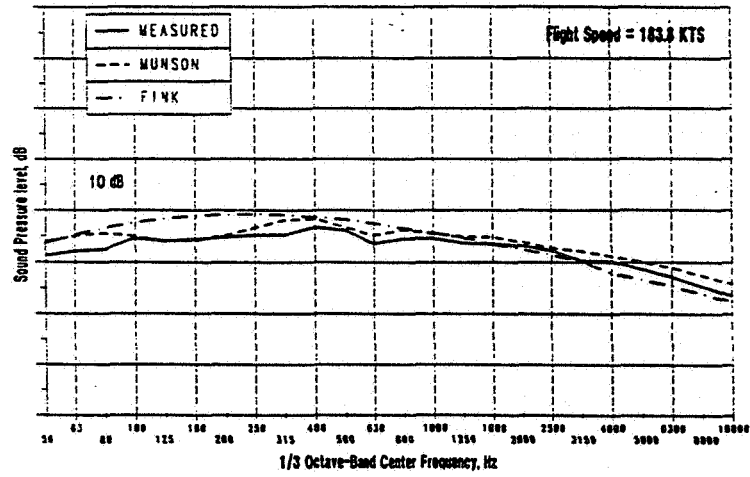Slat and 35 Degrees Flap Deployed Configuration**

Figure 5.27 DC-10-10 Flight Test: One-Third-Octave SPL Comparison:
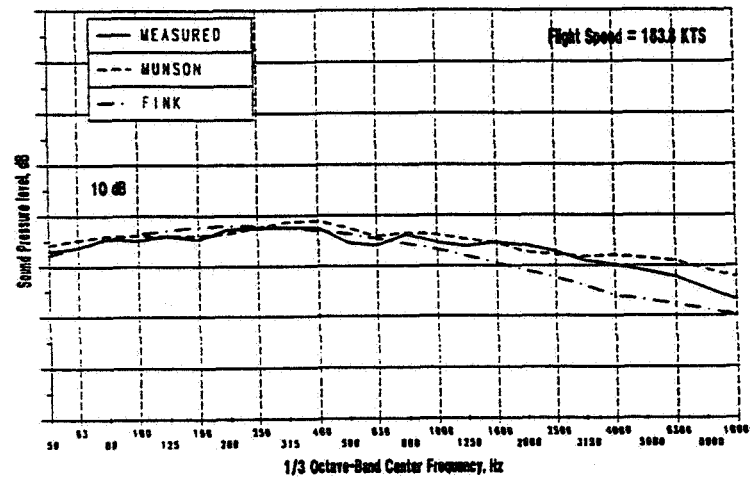Slat and 35 Degrees Flap Deployed Configuration, 60 Degrees

Figure 5.27 (continued) DC-10-10 Flight Test: One-Third-Octave SPL Comparison:
Slat and 35 Degrees Flap Deployed Configuration, 90 Degrees

Figure 5.27 (concluded) DC-10-10 Flight Test: One-Third-Octave SPL Comparison:
Slat and 35 Degrees Flap Deployed Configuration, 120 Degrees

78

Figure 5.28 DC-10-10 Flight Test: OASPL Directivity Comparison:
Slat, Landing Gear and 35 Degrees Flap Deployed Configuration

Figure 5.29 DC-10-10 Flight Test: PNLT Directivity Comparison:
Slat, Landing Gear and 35 Degrees Flap Deployed Configuration

Figure 5.30 DC-10-10 Flight Test: One-Third-Octave SPL Comparison:
Slat, Landing Gear and 35 Degrees Flap Deployed Configuration, 60 Degrees

Figure 5.30 (continued) DC-10-10 Flight Test: One-Third-Octave SPL Comparison:
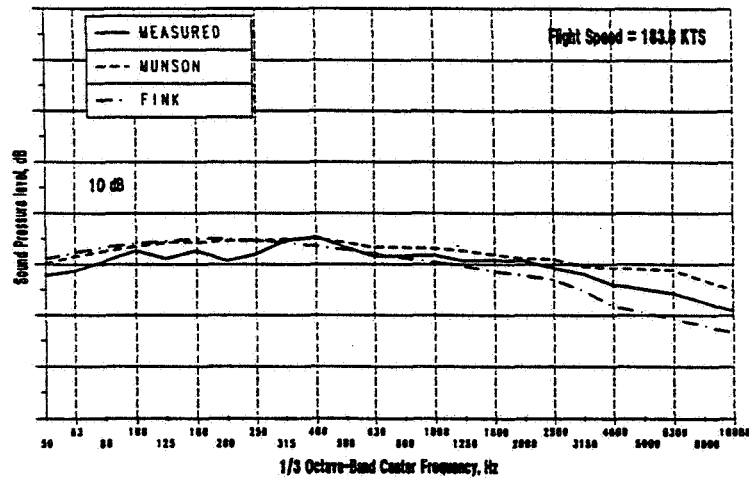Slat, Landing Gear and 35 Degrees Flap Deployed Configuration, 90 Degrees

Figure 5.30 (concluded) DC-10-10 Flight Test: One-Third-Octave SPL Comparison:
Slat, Landing Gear and 35 Degrees Flap Deployed Configuration, 120 Degrees
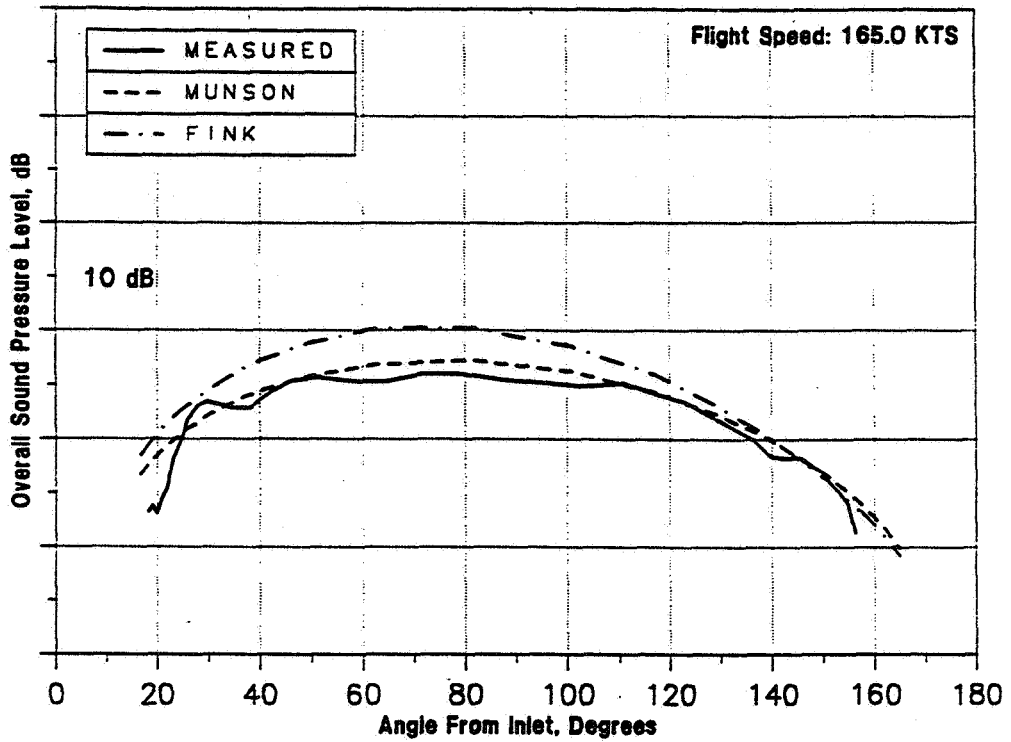
**Figure 5.31   DC-10-10 Flight Test: OASPL Directivity Comparison:
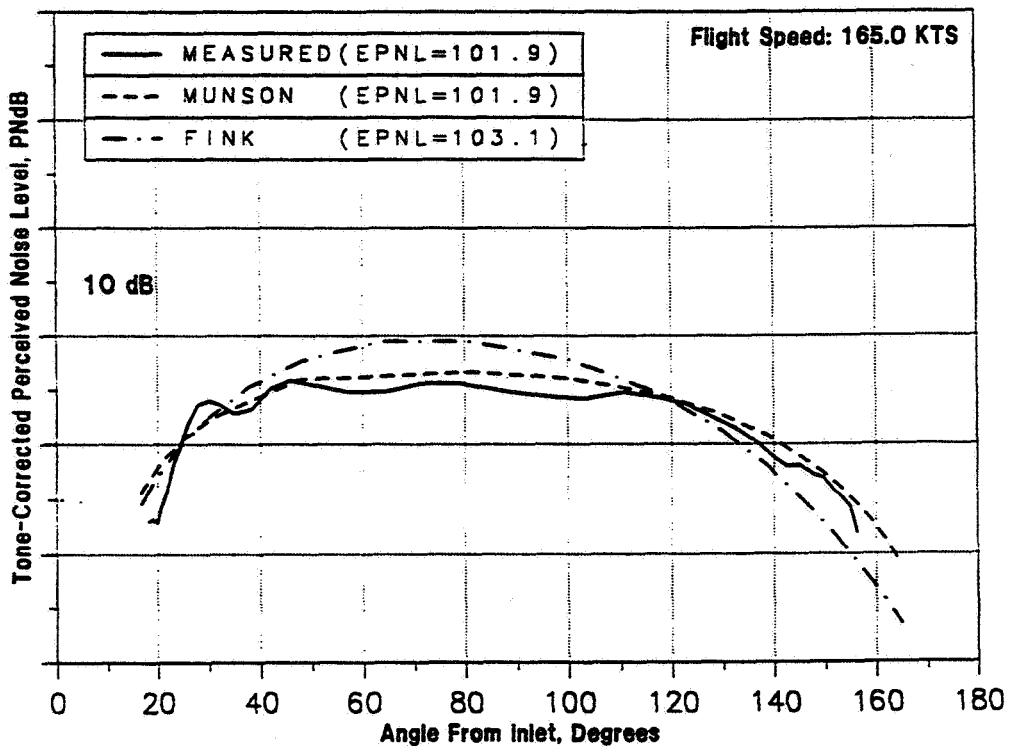Slat, Landing Gear and 50 Degrees Flap Deployed Configuration**

**Figure 5.32   DC-10-10 Flight Test: PNLT Directivity Comparison:
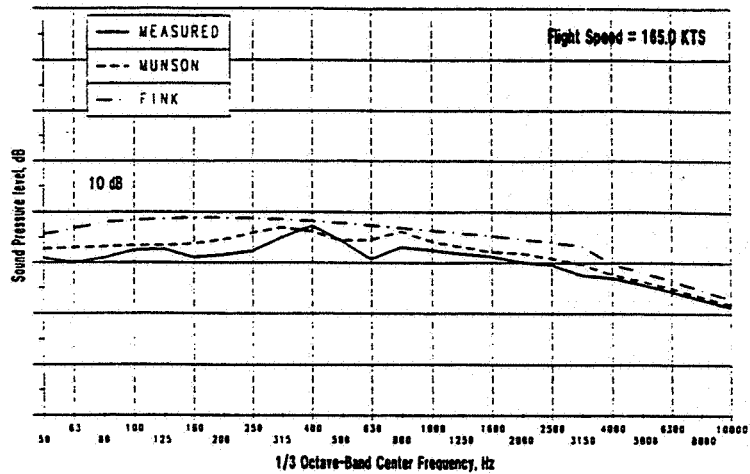Slat, Landing Gear and 50 Degrees Flap Deployed Configuration**

81

Figure 5.33 DC-10-10 Flight Test: One-Third-Octave SPL Comparison:
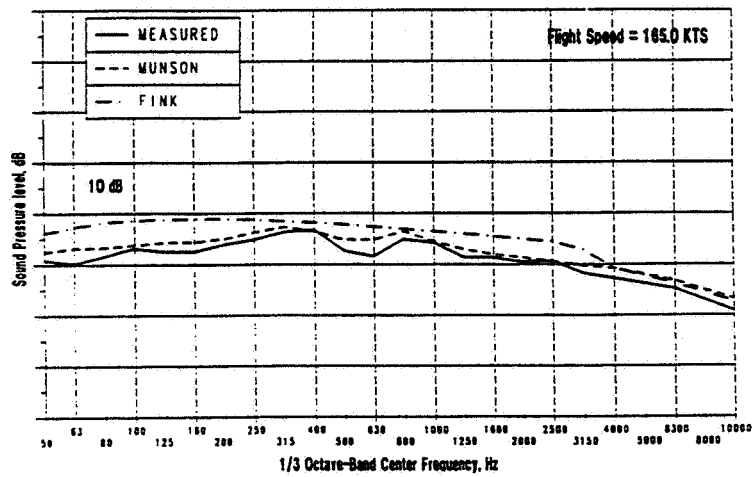Slat, Landing Gear and 50 Degrees Flap Deployed Configuration. 60 Degrees

Figure 5.33 (continued) DC-10-10 Flight Test: One-Third-Octave SPLComparison:
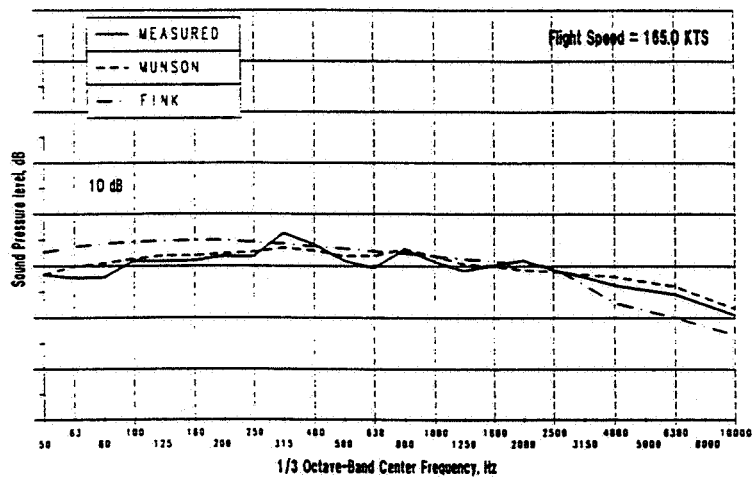Slat, Landing Gear and 50 Degrees Flap Deployed Configuration. 90 Degrees

Figure 5.33 (concluded) DC-10-10 Flight Test: One-Third-Octave SPLComparison:
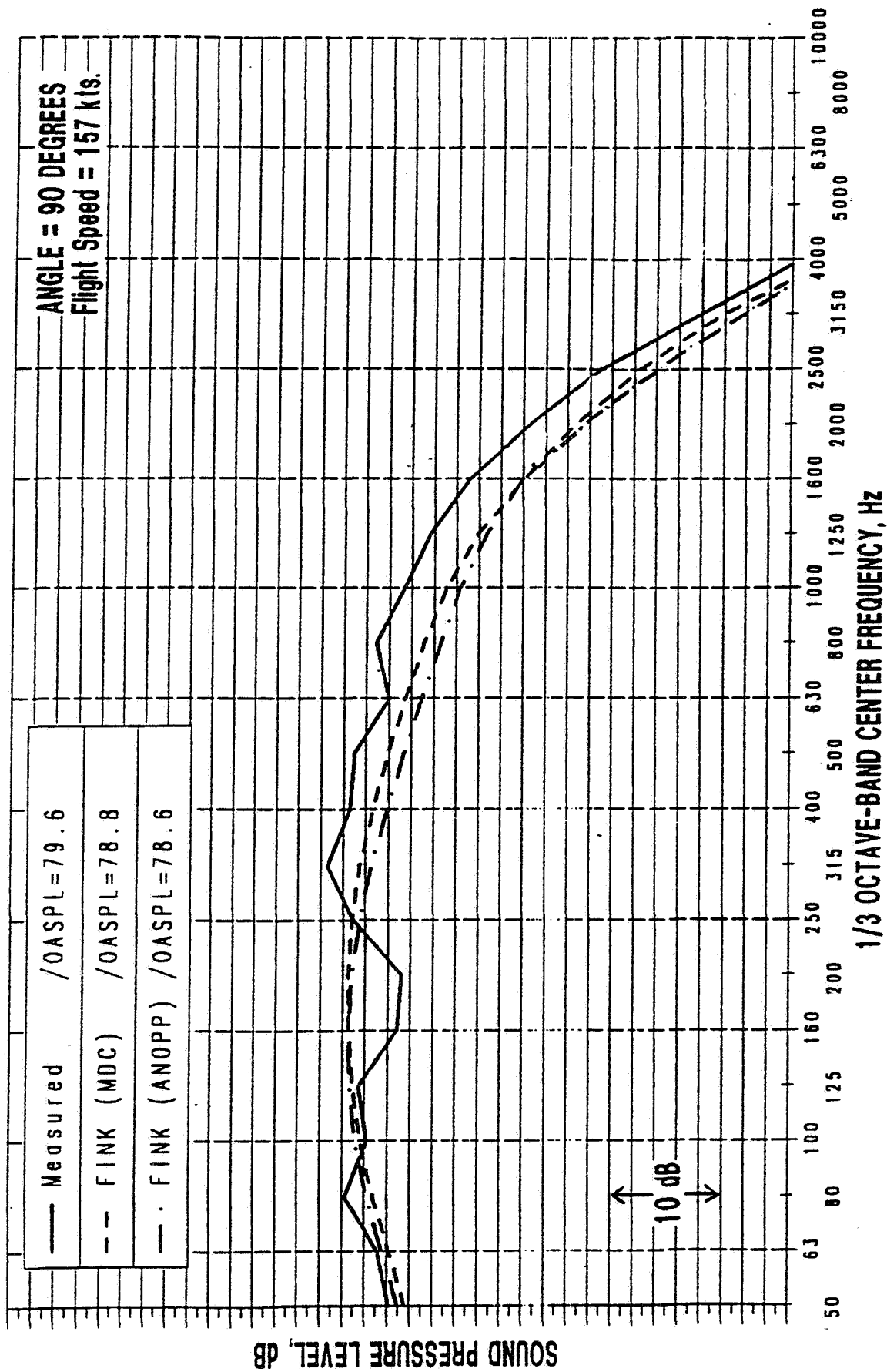Slat, Landing Gear and 50 Degrees Flap Deployed Configuration. 120 Degrees

Figure A.1 One-Third Octave SPL Data vs Prediction Comparison: Slat, 50° Flap and Landing Gear Deployed, Flight Speed 157 kts, $\theta = 90°$
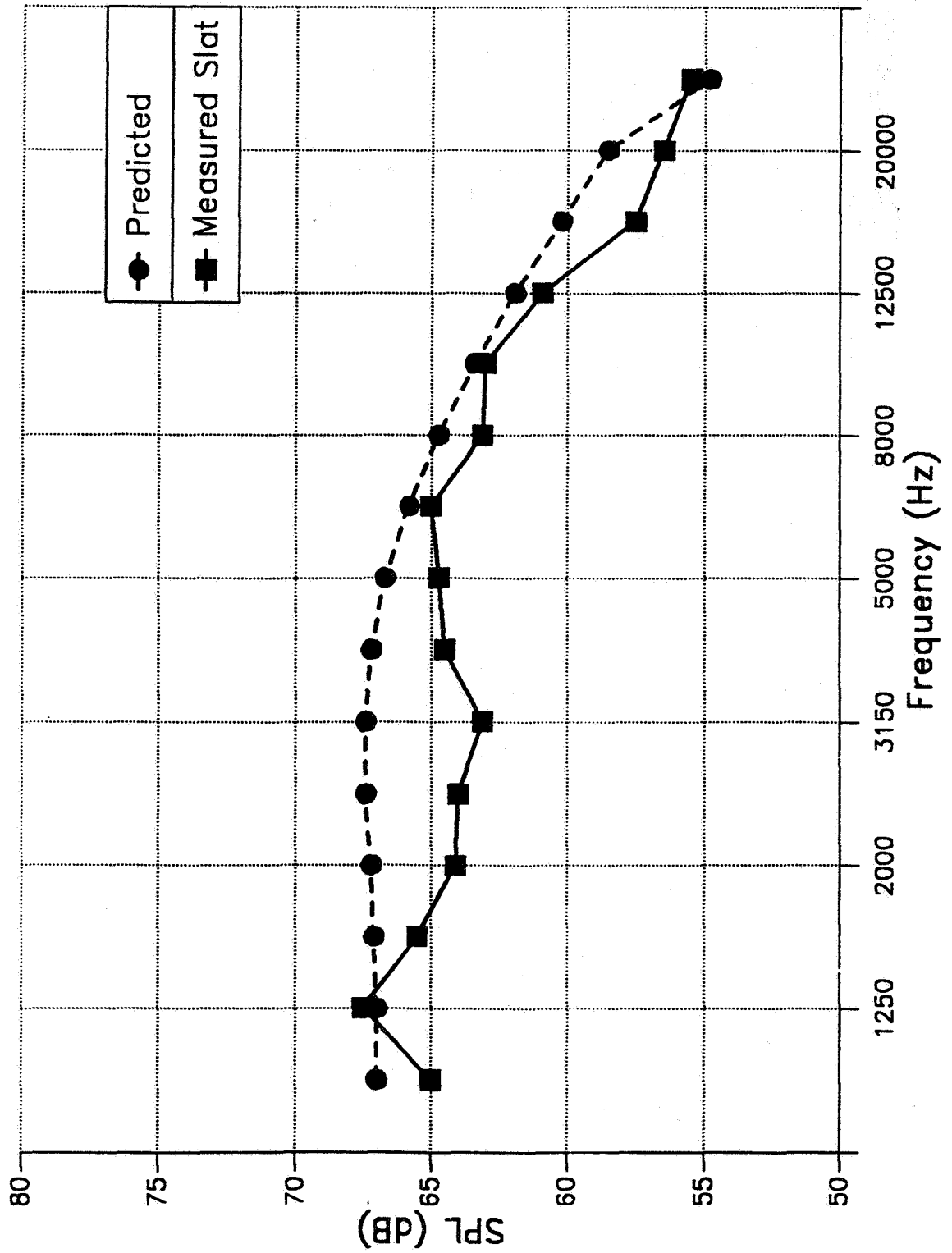
B747 3% Scale Model -vs- Prediction

Figure A.2 One-Third Octave SPL Data vs Prediction Comparison: Slat Deployed, Tunnel Speed 50 m/s, $\theta = 90^{\circ}$

B747 3% Scale Model −vs− Prediction

Figure A.3 One-Third Octave SPL Data vs Prediction Comparison: 30° Flap Deployed, Tunnel Speed 50 m/s, θ = 90°

B747 3% Scale Model -vs- Prediction
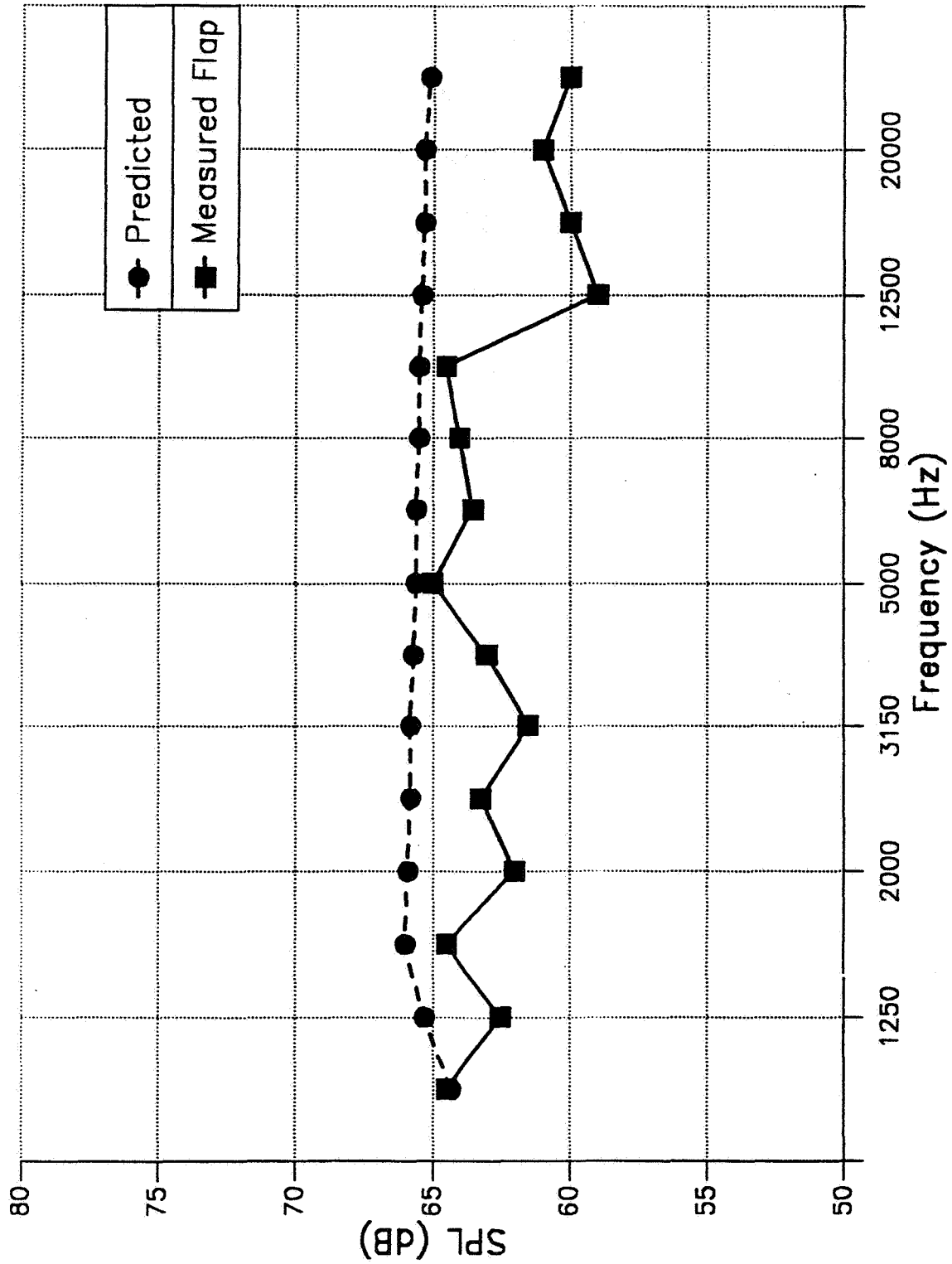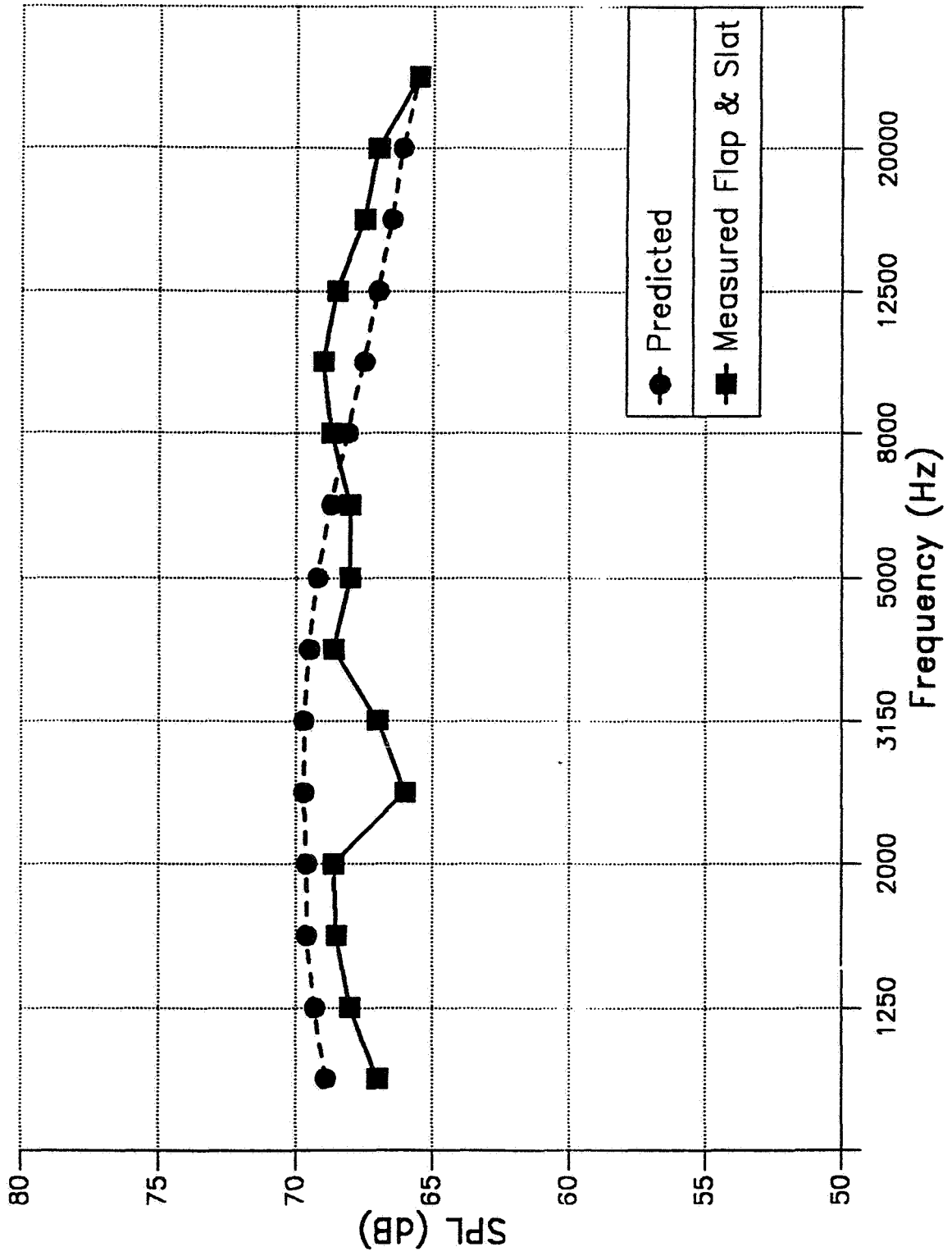

Figure A.4 One-Third Octave SPL Data vs Prediction Comparison: 30° Flap and Slat Deployed, Tunnel Speed 50 m/s, $\theta = 90^\circ$
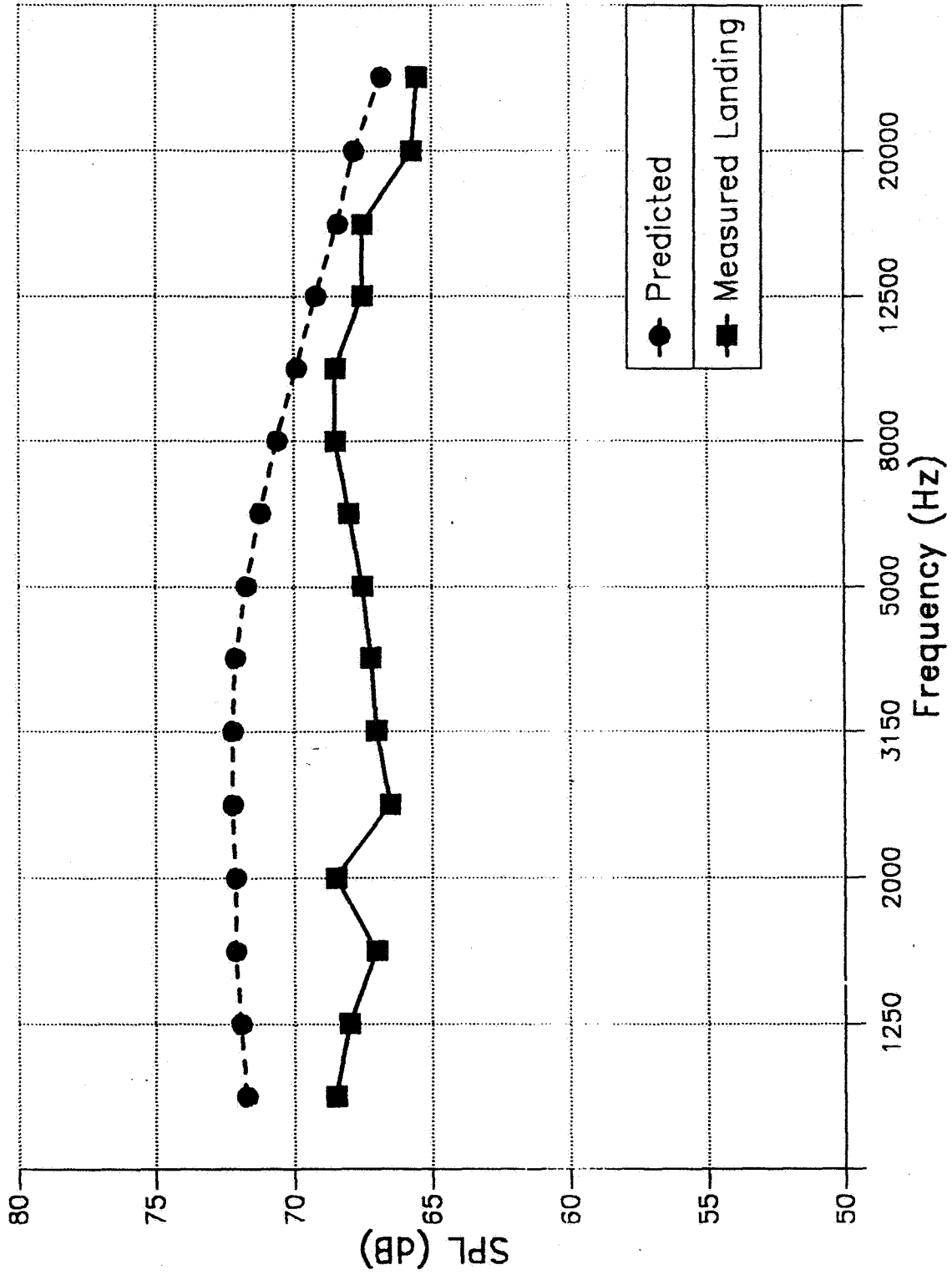
B747 3% Scale Model -vs- Prediction

Figure A.5 One-Third Octave SPL Data vs Prediction Comparison; 30° Flap, Slat and Landing Gear Deployed, Tunnel speed 50 m/s, $\theta = 90°$

REPORT DOCUMENTATION PAGE

Public reporting burden for this collection of information is estimated to average 1 hour per response, including the time for reviewing instructions, searching existing data sources, gathering and maintaining the data needed, and completing and reviewing the collection of information. Send comments regarding this burden estimate or any other aspect of this collection of information, including suggestions for reducing this burden, to Washington Headquarters Services, Directorate for Information Operations and Reports, 1215 Jefferson Davis Highway, Suite 1204, Arlington, VA 22202-4302, and to the Office of Management and Budget, Paperwork Reduction Project (0704-0188), Washington, DC 20503.

1. AGENCY USE ONLY (Leave blank)	2. REPORT DATE October 1995	3. REPORT TYPE AND DATES COVERED Contractor Report

4. TITLE AND SUBTITLE

Airframe Noise Prediction Evaluation

5. FUNDING NUMBERS

C NAS1-20103
TA 4
WU 538-03-13-03

6. AUTHOR(S)

Kingo J. Yamamoto, Michael J. Donelson,
Shumei C. Huang, and Mahendra C. Joshi

7. PERFORMING ORGANIZATION NAME(S) AND ADDRESS(ES)

McDonnell Douglas Aerospace - Transport Aircraft
Long Beach, California 90846-0001

8. PERFORMING ORGANIZATION REPORT NUMBER

CRAD-9310-TR-0129

9. SPONSORING/MONITORING AGENCY NAME(S) AND ADDRESS(ES)

National Aeronautics and Space Administration
Langley Research Center
Hampton, VA 23681-0001

10. SPONSORING/MONITORING AGENCY REPORT NUMBER

NASA CR-4695

11. SUPPLEMENTARY NOTES

Langley Technical Monitor: Michelle G. Macaraeg
Final Report - Task 4

12a. DISTRIBUTION/AVAILABILITY STATEMENT

Unclassified - Unlimited
Subject Category 71

12b. DISTRIBUTION CODE

13. ABSTRACT (Maximum 200 words)

The objective of this study is to evaluate the accuracy and adequacy of current airframe noise prediction methods using available airframe noise measurements from tests of a narrow body transport (DC-9) and a wide body transport (DC-10) in addition to scale model test data. General features of the airframe noise from these aircraft and models are outlined. The results of the assessment of two airframe prediction methods, Fink's and Munson's methods, against flight test data of these aircraft and scale model wind tunnel test data are presented. These methods were extensively evaluated against measured data from several configurations including clean, slat deployed, landing gear deployed, flap deployed, and landing configurations of both DC-9 and DC-10. They were also assessed against a limited number of configurations of scale models. The evaluation was conducted in terms of overall sound pressure level (OASPL), tone corrected perceived noise level (PNLT), and one-third-octave band sound pressure level (SPL).

14. SUBJECT TERMS

Airframe Noise; Prediction Model; DC-9; DC-10;
Fink, Munson; OASPL; PNLT; SPL

15. NUMBER OF PAGES
91

16. PRICE CODE
A05

17. SECURITY CLASSIFICATION OF REPORT Unclassified	18. SECURITY CLASSIFICATION OF THIS PAGE Unclassified	19. SECURITY CLASSIFICATION OF ABSTRACT	20. LIMITATION OF ABSTRACT